To the Dean of Graduate Studies: **Dr. Saundra DeLauder:**

The members of the committee approved the dissertation of **JALAAL A. HAYES** as presented on June 17, 2015. We recommend that it be accepted in partial fulfillment of requirement for the degree of Doctor of Philosophy in Applied Chemistry.

_____Department_____Date _____
Advisor

_____Department_____Date _____
Member

_____Department_____Date _____
Member

_____Department_____Date _____
Member

_____ Department _____ Date_____
Member

APPROVED

_____College _____Date _____
Graduate Coordinator

_____College _____Date _____
Dean, College of Mathematics, Natural Science, and Technology

_____College _____Date _____
Dean of Graduate Studies and Research

THERMODYNAMIC AND KINETIC STUDIES OF ALKALI METAL DOPED-LITHIUM AMIDE-MAGNESIUM HYDRIDE HYDROGEN STORAGE SYSTEM

BY

JALAAL A. HAYES

A DISSERTATION

Submitted as a partial fulfillment of the requirements for the Doctor of Philosophy degree in the Applied Chemistry Graduate Program of Delaware State University

DOVER, DELAWARE
August 2015

DEDICATION

I would like to dedicate this dissertation research to God and to my late grandfather, Mr. William Henry Deloatch. In addition, I would like to dedicate this to my family for their moral support through my academic journey.

To Saint Elmo Brady, the first African American male to receive his PhD in chemistry, I thank you for showing me that achieving this prestigious degree is possible.

To Dr. Percy Lavon Julian, the second African American male to receive his PhD in chemistry and become one of the best synthetic chemist of the 21st century making several discoveries in his field.

Finally, I would like to thank Dr. Jesse Ernest Wilkins, Jr., the greatest mathematician and engineer that inspired to begin this journey as a young man. Throughout my journey, you have shown me the way on how to deal with the struggles and challenges of being a young research scientist achieving milestones to put a dent in the STEM (Science, Technology, Engineering, and Mathematics) universe.

ACKNOWLEDGEMENTS

I would like to thank my research and dissertation advisor, Dr. Andrew J. Goudy (a member of the Academy of Science) for the opportunity to be a part of a renewable energy revolution in the Center for Hydrogen Storage at Delaware State University. He has assisted me greatly throughout this journey from reading and writing journal articles, working on instruments, and presenting at conferences around the world. I would also like to send gratitude for the support from my colleagues that have worked and taught me various methods in the lab as well: Tolulope Durojaiye, Adeola Ibikunle, Tope Sabitu, Samuel Orefuwa, Esosa Iriowen. I thank Dr. Hongwei Yang for giving me tips on solving any challenges that occurred in the laboratories. I also would like to thank Ms. Leida Sanchez, the budget analyst for the Hydrogen Storage Center, for the strong words of encouragement and creating a warm environment to allow me to grow not only as a scientist but as a person as well throughout this journey towards my doctorate degree. I also would like to acknowledge and thank my committee members for assisting me to complete the partial fulfillment for the doctorate degree. Finally, I would like to thank the Department of Chemistry as well as Delaware State University for having me attend this great institution as well as U.S. Department of Energy and Department of Transportation for funding this research study.

THERMODYNAMIC AND KINETIC STUDIES OF ALKALI METAL DOPED-LITHIUM AMIDE-MAGNESIUM HYDRIDE HYDROGEN STORAGE SYSTEM

JALAAL A. HAYES

Faculty Advisor: Dr. Andrew Goudy

ABSTRACT

In recent years, complex metal hydrides have been widely studied as promising hydrogen storage materials. These complex metal hydrides may include the following: $LiBH_4/MgH_2$, $Ca(BH_4)_2$, $Ca(BH_4)_2/MgH_2$ and many others. The $2LiNH_2/MgH_2$ system has been recognized as an attractive system for hydrogen storage. However, there is a need to focus on the following factors: increase the reaction rate of hydrogen with this system, prevent the emission of ammonia, and lower the desorption temperatures.

In a previous study, alkali metal hydride catalysts (KH and RbH) have been added to the $2LiNH_2/MgH_2$ system and their effects on desorption temperatures and dehydriding rates have been compared. Thermodynamic and kinetic studies have shown RbH to be the best catalytic additive for the $2LiNH_2/MgH_2$ system so far. Kinetics studies were done at constant pressure thermodynamic driving forces. The results showed that the RbH doped mixture desorbed hydrogen about twice as fast as the KH doped mixture

as and about 60 times faster than the un-catalyzed mixture. However, no absorption studies were done

Throughout this dissertation research, alkali metal hydrides (KH, RbH, and CsH) and their thermodynamic properties in the operating temperature range of 140-180 degrees Celsius will be discussed and compared at 180 degrees Celsius to determine if these systems can operate at low temperatures required by United States Department of Energy. At lower temperature pressure composition isotherms, the weight percent of hydrogen decreased. However, the ΔH for absorption and desorption studies have remained similar compared to previous studies done by Goudy and colleagues. Activation energies for absorption studies and desorption were achieved. As expected, activation energy values for absorption were less than the values for desorption studies.

Kinetic results were also conducted at lower temperature range from 160-180 degrees Celsius. For the first time, absorption kinetics at constant thermodynamic driving force has been conducted in this dissertation study. For each alkali metal-doped system, the absorption kinetic study has been shown that it is twice as fast as desorption kinetic studies for each temperature. For modeling studies, it shows that all the systems undergo a diffusion-controlled process. It is still confirmed that $1.9LiNH_2+1.1MgH_2+0.1RbH$ is still the fastest system compared to the other doped lithium amide-magnesium hydride hydrogen storage system.

Cycling studies were done to test the durability of the doped- systems over time for practical applications. RbH-doped system showed that for each cycle that the mid-

plateau for absorption and desorption formed a hysteresis up to 70 cycles. The other two systems remained the same.

TABLE OF CONTENTS

LIST OF TABLES

Page

LIST OF FIGURES

CHAPTER 1

INTRODUCTION

1.1 Why Hydrogen? - A Short History

Before research and developmental studies of hydrogen energy and storage became the subject of significant interest in more contemporary times, there had been a concern or disbelief as to whether or not hydrogen would ever be considered a renewable or potential alternative energy source in the near future for human civilization. The idea of a hydrogen economy originated on November 27, 1820 by the Reverend William Cecil.[1] He presented a speech on the element hydrogen and how it could be used in combustion engines eliminating the problem of pollution in the natural environment with greenhouse emissions. Due to the disbelief of Reverend Cecil's concept in his day, his vision had not been pursued until more than a century later.[1]

During the 1930s and 1940s, it was reported that scientist Rudolf Even created an engine that ran on a mixture of hydrogen and other petroleum compounds.[1,2] During the revival of interest in hydrogen during the seventies, the focus on the potential of creating a hydrogen economy began to increase since fossil fuels had been proven to be a finite energy source. In addition, environmental pollution caused by fossil fuels emerged as a major societal concern. Consequently, researchers and scientists formed an organization whose primary mission is to provide research reports on the theoretical and experimental findings regarding hydrogen energy research. That organization is the International

Association of Hydrogen Energy. In 1975, the International Association of Hydrogen Energy created special publication called the International Journal of Hydrogen Energy. The International Journal of Hydrogen Energy journal is still published and widely used today.[1,2]

Since the seventies, various research and development studies began to emerge regarding hydrogen energy research and potential usage throughout the world. Though it is the smallest element in the chemical world, research has demonstrated that it is the most abundant in the universe as well.[1.2]

1.1.1 Hydrogen Benefits

Hydrogen as a potential source of energy can provide significant societal benefits. Other than its abundance in the universe, research studies have demonstrated that it is a very powerful energy source as well. According to the United States Department of Energy (DOE), hydrogen is three times more powerful than the standard petrochemicals used to power automotive vehicle engines and many other applications as well.[3] Another significant benefit is it's very clean fuel quality. When hydrogen is burned in the presence of oxygen, it produces water (either gas or liquid state). Though it may be explosive due to thermal expansion, the by-product will be 99.9 percent clean water in the air which is very environmentally sound to the larger environment. Moreover, hydrogen can be used for other applications if found to be a potential solution for the societal energy crisis. Contingent on the pace of research and developmental progress as a usable energy source, a robust hydrogen economy may begin to take shape

and rapidly expand into commercialization for various societal uses. In the United States, the main target for the use of hydrogen energy will be for automotive applications.[1-2, 3-8] However, other applications of hydrogen energy can be used for stand-alone systems such as houses, mobile phones, hybrid grid systems and many other energy dependent systems. [9-14]

1.1.2. Hydrogen Challenges

Although hydrogen has the potential to become a major asset in the energy market, there are still some concerns with recent challenges that it faces as a viable commercial energy source. Though hydrogen is abundant, it can be extracted in various forms. Based on the current research literature, hydrogen is not yet available for the use freely. Currently, the only way to obtain the potential energy carrier is through methods such as electrolysis and steam methane reformation. Since the 1970s, scientists have developed various experimental procedures for extracting and producing the necessary hydrogen for the targeted energy production that they sought. In a later part in this chapter of this, we will discuss further methods.[14-93]

The burning of hydrogen gas produces clean water; however other dangerous compounds can potentially emit CO_2 and various pollutants. As an example, hydrogen fuel cells such as solid oxide have been studied for potential commercial applications for the near future. In findings throughout various research studies[7-8], poisonous sulfur emission can sometimes occur while hydrogen is being used. That finding has been determined to be a potential hazard because it is contributing to greenhouse gas

emissions. Consequently, those processes add to the existing problem of greenhouse gas emissions rather than minimize or solve the problem. As a result, scientist are continuing their investigations to find ways to prevent sulfur emissions while hydrogen is being used in a fuel cell.[7-8]

Another significant downside is the fact that hydrogen research and development is lagging behind other energy sources economically. Further development of hydrogen as an energy source will be limited if it is not economically viable and commercially feasible. Those are two major factors that are necessary to speed up the development of new applications for the energy market. Based on the previous views of former United States Department of Energy Secretary Steven Chu, there was a policy to push for mainly electric cars, solar panels for homes, automotive applications, and more recently the production of methane gas for the energy market.[3] In order for the hydrogen economy to garner energy market share, research and development efforts must accelerate the movement towards the next stage of commercial viability.

Recently, General Motors[65], Toyota[66], Honda[67], and Ford[68] have established targeted goals for the release of the first-generation of hydrogen-fuel cars in the year 2015. Though this could be a great start, more efficient studies such as better materials for hydrogen storage and production still need to be achieved. That is necessary in order to pave the way toward the commercialization stage for many other applications other than just on-board applications.

1.2 Hydrogen Energy Production

Hydrogen energy as a potential major source of energy production has been studied extensively in the United States and in other nations.[1-43] Existing published research reports indicate that there are various methods that have contributed to hydrogen energy production. In this current dissertation, the focus will be on two methods that produces nearly 99% of clean hydrogen: 1) steam methane reformation and 2) electrolysis.

1.2.1 Steam methane reforming

According to the various publications and research, steam methane reforming (SMR) is a widely used for hydrogen production. Steam methane reforming is the process in which methane (CH_4) is mixed with water to produce hydrogen gas and carbon monoxide.[5] The process is considered highly endothermic which is why high temperature is needed to operate and conduct the SMR process. A benefit of steam methane reforming process is that it is a cost-effective process. The reason is because the hydrogen is easily attainable from the methane and water which are highly abundant in the United States. Therefore, the method is highly used for industrial processes.[69] Although it is cost-effective, there are some disadvantages to this hydrogen production process. One of the main disadvantages is that it produces carbon monoxide as a byproduct. This is considered dangerous for the environment. Another disadvantage is the usage of fossil fuels for this method. The main goal for using hydrogen as an energy source is to replace

fossil fuels for less greenhouse gas emission and using this method is not advantageous towards this goal.

1.2.2 Water Splitting/ Electrolysis

Electrolysis, commonly known as water splitting, is another widely known method for producing hydrogen. The process is basically splitting water molecules (H_2O) into hydrogen and oxygen (O_2) using electrical current directly on the water from a power source such as a battery.[70] Based on Figure 1.1, a redox reaction is occurring where oxygen is being oxidized on the left side of the apparatus whereas the hydrogen molecules are being reduced forming H_2.The advantage of producing hydrogen in this matter is that it is 100 percent clean compared to steam reforming. The disadvantage of this method is that is not cost-feasible for commercial applications. Research studies suggested that solar energy can be an effective way to drive the cost down of producing hydrogen for this particular process.[70]

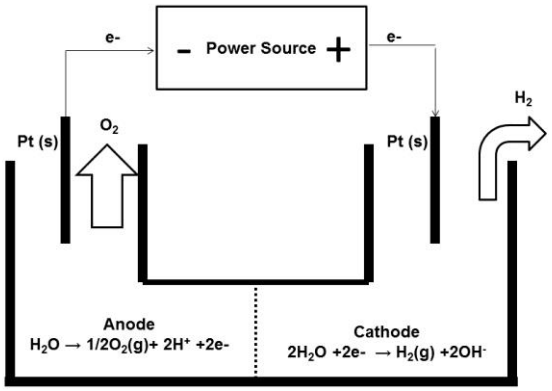

Figure 1.1 Schematic Diagram of Electrolysis

1.3 Hydrogen Storage

There have been various approaches pursued in the search for a more efficient method to store this chemical element. The need for storage is similar to storage needs for fossil fuels today. DOE is concerned with finding more efficient storage methods in order to use hydrogen energy for future use particularly for mobile applications.[9-14,16] Based on the existing research literature, there are two major types of storage materials for hydrogen: chemically bound (chemisorption) [9-14,16] storage and physically bound (physisorption)[17-24] storage. Further discussion will focus on chemisorption storage.[9-14,16]

1.3.1 Thermodynamic Properties

Thermodynamic properties of hydrogen storage materials are based on the changes of absorption and desorption of hydrogen within the materials.[84] According to existing theoretical studies, the hydrogen comes in the alpha (beginning) phase of the storage material. When hydrogen is desorbed from the material, it transitions from the alpha (α) phase to the beta (β) phase, or the product phase. The transition occurs at a change in pressure and constant temperature. The measurement of these transitions can be demonstrated through pressure-composition-temperature isotherms and also from van't Hoff plots.[25-26] Pressure-composition-temperature (PCT) isotherms demonstrate the hydride desorption and absorption transition of hydrogen from a storage material.[25] The fundamental concept of these analyses is to determine the heat of absorption and desorption of the storage materials that is also designated as ΔH. **Figure 1.2** presents a typical PCI plot of a typical metal hydride storage material. The alpha phase starts at the

beginning of both x and y-axis whereas the beta phase is further along in the plot. The point at which alpha and beta phases are at equilibrium are at a plateau region of the plot represented as α+β.[70] The pressure-composition-temperature isotherm will be further discussed in the methodology section as well as the van't Hoff plots.[25]

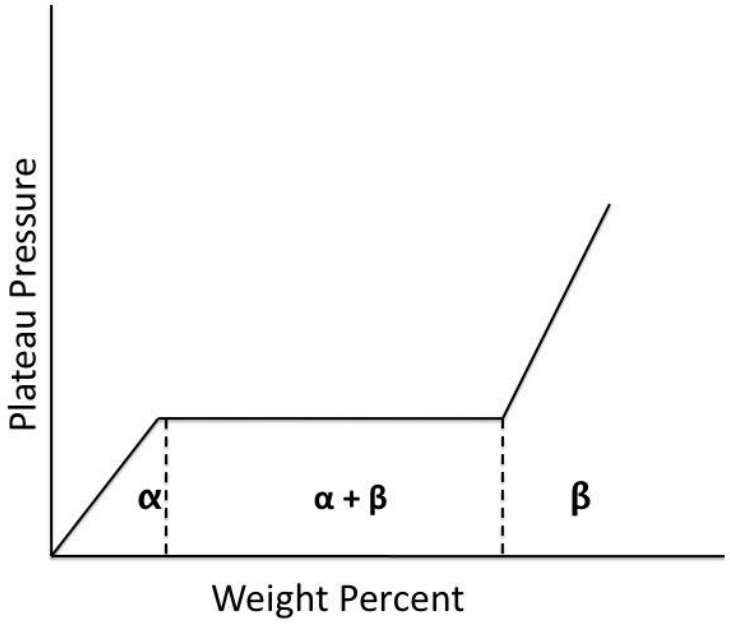

Figure 1.2. Example of a Pressure-Composition Isotherm

1.3.2 Kinetic Properties

The kinetic properties demonstrate how fast or slow hydrogen can be absorbed and desorbed from its hydrogen storage material.[25,83] This property can be measure primarily on the Sievert's apparatus which is based on the existing research literature at this point. In addition, experimental procedures and analyses will be discussed throughout the current dissertation. [25-28]

1.3.3. DOE Standards for on-board hydrogen storage applications

In discussing chemisorption and physisorption storage materials, the United States Department of Energy has standards that each system must follow in order to become potential hydrogen storage materials in the future. **Table 1.1** contains the standards that have been established in various published literature sources regarding hydrogen storage materials. The expected year for having the materials with these standards is 2015.[3] By that time, the hydrogen market should begin to emerge, then paving the way for mass production and further applications.[3]**Figure 1.3** shows a schematic of a hydrogen-powered vehicle.

Thermodynamics	30kJ/mol <ΔH< 60kJ/mol
Temperature	60°C-120°C
Kinetics	Absorption/Desorption: Less than 5 minutes for 5 kg for on-board application
Cycle Stability	Greater than 500 Cycles
Weight Percent	6 wt%

Table 1.1. US Department of Energy Standards for hydrogen storage materials (especially for chemisorption materials)[3]

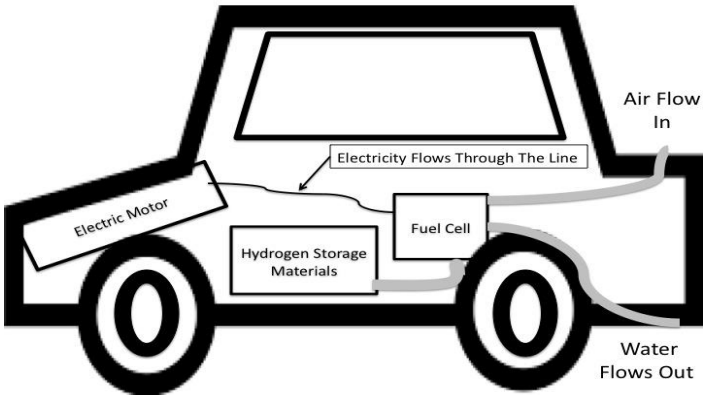

Figure 1.3. H_2 Storage on-board application for automotives.

1.3.3.1. Other Applications

Recently, more applications for hydrogen energy have been proposed due to the fact that it is a clean carrier of energy. However, the probability of significant commercial applications will not occur before 2020 according to the US Department of Energy. From the chemically bound hydrogen storage materials, metal amides have demonstrated that they will have the most promise due to their limited weakness as compared to other chemically bound structures.[9-14,16] If researchers develop other ways to control the ammonia from constant reversibility of reactions from storage, then that will be another potentially promising hydrogen storage material.[9-14,16] For physisrption, the more promising material is carbon nanotubes. The primary reason is the simplicity of adding the necessary additives in order to increase adsorption and desorption capacities of hydrogen.[17-24]

1.4. Physisorption and Its Systems

Physisorption (or physically bound) is a process of storing the hydrogen gas into the pores of the hydrogen storage materials.[17-24] This type of storage process consists of binding the hydrogen to the compound by Van der Waals forces in order for it to be absorbed and released quickly from the system. As a result, reversibility and faster kinetics can serve as a great advantage for the physically bound process.[17-24] Current hydrogen storage materials: metal organic frameworks (MOFs) and carbon nanotubes (CNTs) will be discussed in more detailed in the succeeding section.

1.4.1. Metal-Organic Frameworks

Metal organic frameworks (MOFs) are crystalline materials that have micro pores that absorb gases particularly hydrogen. The discovery of this storage material was made by Yaghi et al in 1995.[19,24] The structure of MOFs include organic polymers, which are interconnected with metal linkers. **Figure 1.4** presents examples of some of the MOFs that have been used and can be used for potential hydrogen storage.[24] Other than its primary characteristics, its strengths and weaknesses will be further discussed in terms of use as a hydrogen storage material for the future. [17-24]

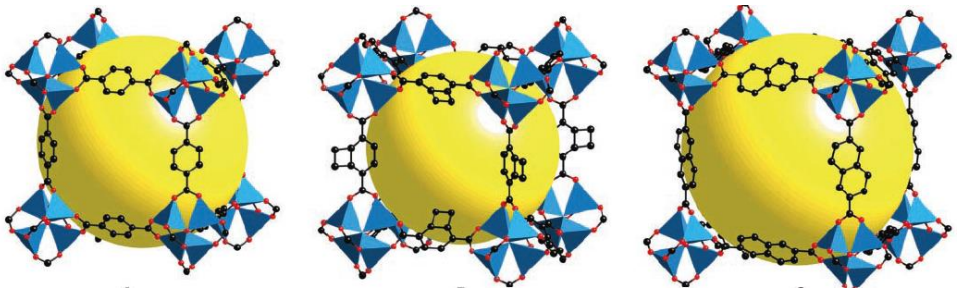

Figure 1.4 MOFs that are known to be used in hydrogen storage (L-R MOF-5, MOF-6, and IR-MOF 8).[24]

The major advantage of MOFs is the high surface area that adsorbs a large amount of hydrogen on the surface of the material. As an example, MOF-5 and Cu-BTC produce a higher storage capacity than other carbon materials at 0.6 MPa.[9] The storage capacity reflects the large surface area that is accompanied with that MOF. Another distinct advantage is the high porosity of the hydrogen materials. For example, many metal-organic frameworks such as MOF-5 have high pore diameters for hydrogen to be stored according to Hirscher et al.[45]

However, one of MOFs shortcomings is storage at low temperatures (i.e. cryogen temperature). Based on the existing research literature, hydrogen adsorption and desorption is mostly conducted between temperature levels of 20-120 K, which is lower than room temperature (298 K). [17-19,45] Another significant shortcomings is the low weight percent of hydrogen that is released from MOFs. Based on findings from other research investigations, the average weight percent that is released from metal organic frameworks is 1.4 wt% -2.5 wt% which does not meet the existing DOE standard which is 6-9 wt% for hydrogen release and desorption.[17-19,45]

1.4.2. Carbon Nanotubes

Carbon nanotubes (CNTs) are carbon molecules that are microporous with nanotubular structures.[20-23] There are four types of carbon nanotubes which are: single-walled carbon nanotubes, double-walled carbon nanotubes, multi-walled carbon nanotubes, and coiled carbon nanotubes.[20] Single-walled (SWNTs) are nanotubes that only contain one wall of pores on its surface. Double-walled (DWCNTs) consists of two walls that are concentrically thick on the nanotubes for increased porosity for gases. Multi-walled (MWCNTs) are similar to DWCNTs. However, they have more walls concentrically attached and are very thick inside the tubular structure. Coiled carbon nanotubes (CCNTs) are quite unique. The structure of coiled carbon nanotubes consist of cylindrically-shaped walls.[22,24] **Figures 1.5-1.8** present the structures of classified carbon nanotubes.[81] Iijima et al discovered those carbon molecules in 1991.[18-22] That discovery was very important because of its potential use for hydrogen storage. Consequently, strengths and weaknesses for the current research will be discussed further in this section.

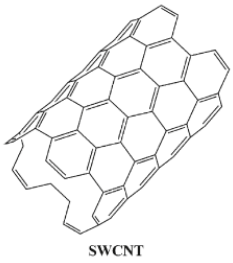

Figure 1.5. SWCNTs[71]

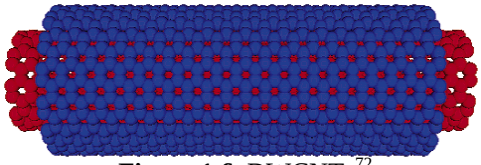

Figure 1.6. DWCNTs[72]

Figure 1.7. MWCNTs[73]

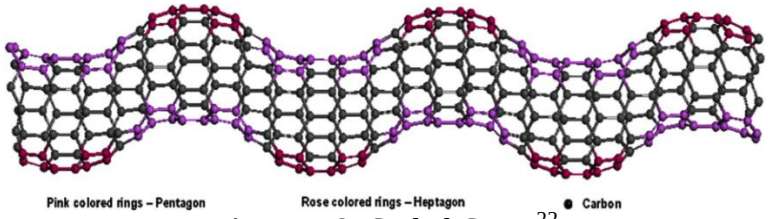

Figure 1.8. Coiled CNTs[22]

Strengths of carbon nanotubes are similar to the metal-organic frameworks discussed previously regarding hydrogen energy.[22] One strength is the low density of the material. Another strength is the large surface area on the CNTs. [18,22,71-73] For example, Gayathri et al demonstrated that the ring-coiled structure (known as Y-configuration) of a sample could absorb up to 6.8 wt% hydrogen due to its large surface area.[22]

A weakness or shortcoming of the latter hydrogen material is the need for transitional metals to increase adsorption. Wu et al used palladium (Pd) to increase the adsorption for hydrogen from 4 wt% to about 4.5 wt%, which is 0.5wt% closer to DOE's goal for hydrogen storage. [23] Another shortcoming of the CNTs is the need for activating agents due to the high stability of the compound.[22-23, 71-73] For example, in order to

increase the adsorption with the Pd, Wu et al used potassium hydroxide, KOH, in order to activate/ destabilize for proper experiments. [23]

1.5. Chemisorption and Its Systems

Chemically bound storage or chemisorption is a process in which hydrogen is adsorbed and desorbed within the storage material. Over the years of numerous hydrogen storage material research investigations, various useful ways have been found for storing hydrogen chemically. **Figure 1.9** presents the materials used for the study that occurred in this research area. Most of these chemisorption systems are mainly composed of lightweight, complex metal hydride systems.[9-16] That observation is represented on the far left barrel of one-tenth in **Figure 1.9**. Of the existing complex metal hydride systems, the following three chemical storage materials will be discussed further: borohydrides, alanates, and metal amides.

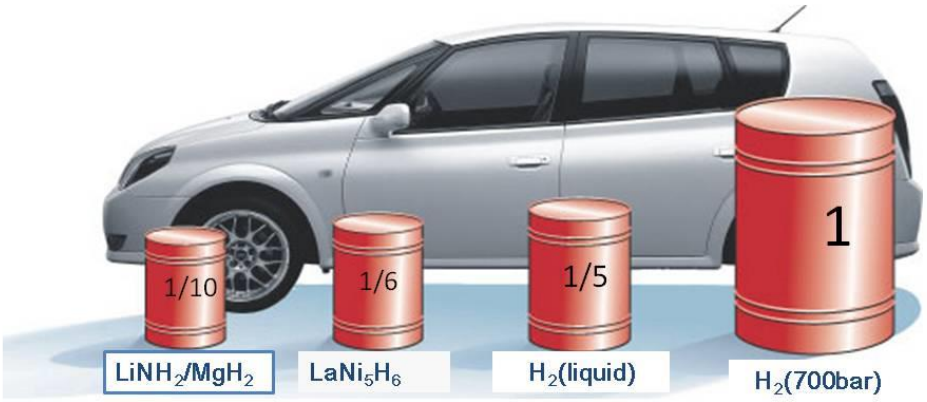

Figure 1.9. Proposed materials that have been observed over the years for potential hydrogen storage applications include automotive applications.[33]

1.5.1. Alanates

Alanates are metal hydrides that are composed of aluminum bonded to hydrogen (Al-H_4) and are bonded to a certain metal (particularly alkali metals).[14,75,86] In 1997, Bogdanovic et al discovered alkali metals as a potential use for hydrogen storage with the compound sodium alanate.[14,75] The advantages of those hydrogen storage materials are that they are stable and can hold a hydrogen capacity of 5.5 wt%. [75] In addition, complex hydride systems can release hydrogen in a two-step process (**Equations 1.1 and 1.2**).[14]

$3NaAlH_4 \leftrightarrow Na_3AlH_6 + 2Al + H_2$ (Eq.1.1)

$Na_3AlH_6 \leftrightarrow NaH + Al + 3/2H_2$ (Eq.1.2)

The disadvantage of that system is the inability to destabilize the compound to achieve DOE's goal of 6-9 wt% of hydrogen. Like the complex borohydride systems, researchers have found additives, along with a destabilizing agent, which magnesium hydride (MgH_2) might destabilize the compound thus releasing and absorbing hydrogen at a faster rate. Dathar and Mainardi have explored titanium additives for $NaAlH_4$. They concluded that the stability for the release of hydrogen was lowered to 43 kJ/mol.[75] Also, Jun Lu et al have explored the destabilization of $LiAlH_4$ for the release of hydrogen. [14]

However, another shortcoming was the reversibility factor of the alanates. Based on the existing research literature, alanates can reabsorb hydrogen from 300 °C-500 °C which more recent research investigations are attempting to modify.[14,25,86] Jun Lu et al used a method called "cycling" in an attempt to increase stability of the alanate sample. They achieved a constant 6.9 wt% for the total sample, which explained the effect of no variation of storage occurring on that sample.[14]

1.5.2. Borohydrides

Borohydrides are of major interest for the hydrogen storage research efforts due to the chemical properties of these particular systems. **Equation 1.3** presents a decomposition of potential storage material magnesium borohydride releasing hydrogen.[76] These chemical properties consist of lightweight systems, bond stability between boron and hydrogen, and contain the capacity of hydrogen up to 13.6 wt%-18.3 wt% of hydrogen in its initial state.[10-14] However, the reactions are slow and the systems release hydrogen at higher temperatures. There are various additives that have been

suggested in order to potentially lower the activation energy needed to destabilize borohydrides. By destabilizing borohydrides, more hydrogen is released at lower temperatures and absorbed from the complex system.[6-10, 40]

$$Mg(BH_4)_2 \rightarrow MgB_2 + 4H_2 \qquad \text{(Eq.1.3)}$$

Goudy et al have experimented with destabilizing a lithium borohydride system with the compound calcium hydride (CaH_2). The calcium hydride compound lowers the original temperature of the borohydride system from 600°C to a range of 400°C-500°C.[9] Though this method has been used, an additive of titanium chloride is still required to improve the kinetics of the reactions.[9] Also, Newhouse and co-workers observed some destabilization of magnesium borohydride with the addition of titanium (III) fluoride and scandium (III) chloride. The destabilization allows for the magnesium hydride system to produce faster kinetics in desorbing the hydrogen.[29]

Another method that has been explored by researchers is the use of different additives.[12-13] Different additives have served as catalysts to release 6-9 wt% of hydrogen from the compound at a faster rate than without the additive. Based on the existing research literature,[12-13]most additives are composed of transitional metal oxides or transitional metal halides. One of the main catalysts that is used for the improvement of the hydrogen storage properties is titanium additive. Mao et al used titanium additives to improve the hydrogen release and adsorption rate of sodium borohydrides.[12] Also, Vajo

et al experimented with two to three percent of titanium chloride, which improved the destabilization of lithium borohydride from the original complex system.[13]

1.5.3 Ammonia Borane

Recently, there have been lightweight hydrogen systems that are being considered by the US Department of Energy. Based on the structure, ammonia borane has been demonstrated to be a hybrid between the borohydride system and the amide system. According to Rassat et al, ammonia borane met and exceeded the required hydrogen storage weight capacity (11 wt %) to approximately 13-16 wt% hydrogen capacity.[30,87] **Equation 1.4** presents the reaction of ammonia borane undergoing the release of hydrogen. There are methods of producing hydrogen from ammonia borane: hydrolysis and thermolysis. The hydrolysis method involves mixing the ammonia borane with water thus having a soluble and aqueous storage form of ammonia borane to produce hydrogen.[30] Thermolysis is a process in which the temperature or another thermodynamic change in the system would allow for the release of a particular substance (in case hydrogen). In focusing on solid-state systems, thermolysis will be the main focus of further review.[30-32]

$$NH_3BH_3 \rightarrow 1/x\ (NH_2BH_2)_x + H_2 \qquad \text{(Eq. 1.4)}$$

According to Hwang et al, at three temperature ranges, ammonia borane has been observed theoretically to release hydrogen. These temperature ranges are 90-117 ˚C, 150-

170 ˚C as well as temperatures greater than 500 ˚C.[31] According to the US Department of Energy's on-board hydrogen requirements, the first temperature range is most suitable for the PEM fuel cell (**Figure 1.1**) and for mobile applications. Findings of recent research publications indicate that they had focused their studies on how to improve the ammonia borane hydrogen storage system.[87] Duman and Ozkar discovered ruthenium (III) acetylacetonate as a catalyst for the ammonia borane system.[32] Those results indicate that the thermodynamics and kinetics had been determined. For the kinetic data, it was demonstrated that the system released hydrogen by a first-order reaction. This means that the catalyst acts readily when the hydrogen is released from the ammonia borane system. As for the thermodynamics, the activation energy dropped 48 kJ/mol.

Although there have been improvements and more are being developed in the systems, there are still some major shortcomings that present significant concerns for the ammonia borane system. The first significant shortcoming is the operating temperature. For a full release of hydrogen, the operating temperature must exceed 280 ˚C. In addition, the reversibility of the system must be increased more too. According to more current studies in the research literature, the reaction demonstrates that ammonia borane can only produce hydrogen with irreversible reactions. There is the potential that further experimental studies can solve the latter shortcoming by focusing on the development of a method to increase the reversibility of the system. If successful, such a method will become a major advancement for hydrogen storage.[30-32,87]

1.5.4. Metal Amides

In more recent years, improved methods for hydrogen storage have been studied extensively. As was previously discussed regarding magnesium hydride to borohydrides, complex lightweight materials have been used for on-board hydrogen storage.[89] However, in 2002 and 2004, P.Chen et al discovered new lightweight materials that appeared to be better candidates for hydrogen storage applications.[33] Those materials are the metal amides. Metal amides are metals that are bonded to amide anions in the formation of M-N-H where "M" represents the metal contained in the compound. The composition of metal amides is the reason that they are major candidates for use with hydrogen. Their lightweight structure and the low temperature of 200°C for releasing and absorbing hydrogen are better than borohydrides which release hydrogen at 400 -500°C after destabilization.[33,89] Lithium amide was the first metal amide that was studied.[33] Afterwards, studies of other hydrogen storage materials made of metal amides have emerged too. Those newer materials have been widely studied for other potential applications too. In the next section, discussion will be focused on the following: lithium amide, lithium amide/lithium hydride and their catalytic effects, lithium amide/magnesium hydride and catalytic effects thermodynamically and kinetically.[33-46]

1.5.4.1 Lithium amide

As was previously stated, lithium amide was the first of the metal amides developed in special organic chemical investigations. Before hydrogen storage, lithium

amide was used in organic chemistry reactions for reduction purposes. However, it was discovered that this material was suitable for use as a hydrogen storage material by PChen in 2002.[33] Lithium amide was found to release at least 10.5 wt% of hydrogen as compared to the predecessor hydrogen systems.[33]

1.5.4.2 Lithium amide/lithium hydride ($LiNH_2$/LiH)

Based on a 2002 study that was published in Nature, P. Chen et al assumed that lithium amide could be combined with lithium hydride for a complex hydrogen storage system.[33] **Equations 1.5 and 1.6** present the basis for the reaction of the lithium amide/lithium hydride. With these equations, the researchers observed that a stable compound Li_3N was formed. Evidence has been presented indicating that this compound is a key compound for producing a reaction. By producing a reaction, that reaction enables the system to be cycled multiple times with the weight percent of 6.5 wt%. For this particular system, there are two types that have been studied: $LiNH_2$/LiH and $2LiNH_2$/LiH. In this section, both of these types will be discussed further along with the progression of catalytic improvements.[33]

$$LiNH_2 + LiH \rightarrow Li_2NH + H_2 \qquad \text{(Eq.1.5)}$$

$$Li_2NH + LiH + H_2 \rightarrow Li_3N + 2H_2 \qquad \text{(Eq.1.6)}$$

1.5.4.3 $LiNH_2$/LiH (Li-N-H system)

Based on the existing research literature, findings demonstrated that the lithium amide/lithium hydride has generated major interest. During preparation, a10% excess of

the lithium hydride was used to suppress the release of ammonia during repeatable analysis and cycling of the system. **Equations 1.5 and 1.6** present the basis for the reactions of lithium amide and lithium hydride. In the desorption reaction, the final product of that system is lithium nitride, Li_3N. Also in the existing research literature, lithium nitride has generated significant interest when it was utilized with hydrogen. Scientists have suggested that lithium nitride can store the same amount of hydrogen as lithium amide. Although investigations have provided evidence that lithium amide has more significant potential for use than the alanates, there remain some improvements that must be made to the system. Specifically, lowering the temperature of the release of the hydrogen and increasing the rate of hydrogen as well.

Wang et al indicated that the Li-N-H system could desorb hydrogen at around 280 $^{\circ}C$.[40] However, those scientists conducted another study experimenting with transitional metal additives in order to solve the previous identified shortcomings. The transitional metal additives (titanium, chromium, iron, and nickel) have been useful in solving those problems. Based on their research, titanium was shown to be a great additive for lowering the enthalpy value -75 kJ/mol to -46.6 kJ/mol. Ichikawa et al also studied $TiCl_3$ as an additive for the $LiNH_2$-LiH system. Based on their findings, the small amount of $TiCl_3$ showed that the desorption temperature lowered from 400°C to 250°C. In addition, the emission of ammonia did not occur when compared to the un-doped system.[40]

Lamb et al discovered that pressure cycling can increase the performance of the $LiNH_2$/LiH system. The improvement of this system enabled an increase in the

reversibility of dehydriding and rehydriding to the 11wt% hydrogen criteria. The results in that study indicated that the addition of nitrogen gas to the lithium amide-lithium hydride system provided a more significant improvement as compared to cycling without the nitrogen gas. The primary reason for the improvement was that nitrogen gas along with the lithium metal (liquid state) formed Li_3N readily. Therefore, that result increased the capacity of the hydrogen in the system.[35]

Aguey-Zinsou et al worked with BN particles as additives to determine the effects on the Li-N-H systems.[36] Their results indicated that the improvement of the system was achieved by allowing the hydrogen to diffuse through the system at a faster kinetic rate than would occur in the system without the BN particles. Also, it was noted that the hydrogen was released at a lower temperature of 200 ˚C and under 7 hours as well.[36]

All of the aforementioned studies have provided evidence of various methods to improve the system. However, there were still some shortcomings that occurred. According to Cao et al, the systems still needed to meet or exceed the thermodynamics criteria required by DOE which are enthalpies in the range of 30 kJ/mol to 60 kJ/mol. The Li-N-H systems represent 66 kJ/mol and 88 kJ/mol which are clearly out of the range of the DOE standards. Some other limitations include metal amides that can also release ammonia into the environment while releasing hydrogen as well. Therefore, researchers have suggested that magnesium hydride must bond to this metal amide in order to limit the amount of ammonia that is released.[37]

1.5.4.4 Lithium amide/magnesium hydride ($LiNH_2/MgH_2$)

After the extensive research that has been conducted on the lithium amide/lithium hydride system, the findings suggest that lithium metal should be replaced with magnesium for various reasons. One of the reasons, according to the existing research literature, is that experimentally it can be demonstrated that magnesium hydride lowers the enthalpy (ΔH) value as compared to the lithium hydride compound. Research findings indicate that magnesium hydride is thermodynamically favorable for absorption and desorption compared to lithium hydride thus reflecting the low enthalpy value, which lowers the temperature also.[38] Similar to the previously discussed system, there are two types of this system along with potential catalytic improvements as well: 1:1 and 2:1. Based on the existing research literature, $2LiNH_2/MgH_2$ has provided evidence of a greater utility for hydrogen storage applications.[37]

1.5.4.5 $LiNH_2/MgH_2$ (Li-Mg-N-H system)

To solve the problem regarding the thermodynamics criteria, research findings suggest that partial replacement of the lithium metal in the LiH with the magnesium metal is a promising solution. Based on the density-functional theory (DFT) calculations, it has been demonstrated that magnesium hydride (MgH_2) was a more thermodynamically favored option. **Equations 1.7 and 1.8** present the reaction of the lithium amide and magnesium hydride in respect to the release of the hydrogen from the system.[37,40]

$$2LiNH_2+MgH_2 \rightarrow Mg(NH_2)_2 +2LiH \qquad \text{(Eq.1.7)}$$

$Mg(NH_2)_2 + 2LiH \leftrightarrow Li_2Mg(NH)_2 + 2H_2$ (Eq.1.8)

Based on these reactions, other research study findings indicate that it has lower operating temperatures and produces faster reaction rates as compared to the Li-N-H system. Zhang Xiong et al conducted an experimental and theoretical study comparing the Li-Mg-N-H system with the Li-Ca-N-H system.[38]. Those research findings indicated that the Li-Mg-N-H system had demonstrated that it would desorb at around 157 ˚C as compared to the Li-Ca-N-H system which desorbs at around 132 ˚C. However, findings also indicate that the Li-Mg-N-H has a better structural change as compared to the CaH_2 system.[38] In that study, pressure composition isotherm analysis indicated that the Li-Mg-N-H system also has higher hydrogen content as compared to the Li-Ca-N-H system. Other studies have also suggested that Li-Mg-N-H system has greater potential as a system of interest for hydrogen storage.[38,40]

Like other systems, the Li-Mg-N-H system also needs some vast improvements such as operating temperature, hydrogen weight capacity, and faster kinetics. Osborn et al first analyzed the behavior of 1:1 ratio of $LiNH_2/MgH_2$ hydrogen system.[39] Using X-ray diffraction and PCT isotherm analyses, they concluded that the system undergoing release of hydrogen also had released ammonia as well. Moreover, Durojaiye and Goudy have compared the 1:1 and the 2:1 system of lithium amide-magnesium hydride system.[42] Their results demonstrated that the 2:1 system performed better thermodynamically (temperature and enthalpy value, and hydrogen content) and kinetically (faster rate of

dehydrogenation) than the 1:1 system.[42] Therefore, the $2LiNH_2$ +MgH_2 system was considered to have a greater potential for hydrogen storage in the subfield of metal amides.

1.6 $2LiNH_2$ +MgH_2

With various considerations and suggestions of the $2LiNH_2/MgH_2$ hydrogen storage system, the suppression of ammonia was greater as compared to the 1:1 system. As was previously demonstrated, **Equations 1.7 and 1.8** presents the reaction of $2LiNH_2$/ MgH_2 system that had been used. However, because of environmental concerns, that shortcoming required significantly more improvement. Luo, Durojaiye, and many other researchers have suggested that adding an additional 10% excess of magnesium hydride would help solve this problem. However, significant shortcomings still remain. Those shortcomings consisted of lowering the temperatures, speeding up the kinetics, and increasing hydrogen content. Other researchers have suggested that using dopants and additives will help limit those shortcomings in a major way.

1.6.1 $1.9LiNH_2+MgH_2+0.1KH$ and other K-based additives

In observing this challenge, various researchers have suggested the use additives and catalysis as a way to significantly limit the ammonia along with treating the system thermodynamically and kinetically. P. Chen et al have discovered that potassium hydride, a light metal catalyst, would be a great catalyst that would improve the $1.9LiNH_2+MgH_2+0.1KH$ system.[14,42,91] Later, two research groups, Goudy and his research group and Lu and his research group discovered a way to limit the amount of

ammonia released in the air and lower the temperature.[14,42]. Their research methods included the design of a $2LiNH_2/MgH_2$ system along with 4-mol% excess of potassium hydride.[14,42] Both groups' results generated from the use of those research methods indicated that at around 200 °C, there were small amounts of emissions of ammonia released from the system.[14, 42]

Also, Li et al have focused their attention on potassium-based additives for the $2LiNH_2/MgH_2$ hydrogen storage system.[49] Based on their findings, they discovered that the catalyst of interest, KF produced a catalytic effect on the system after the system was re-hydrogenated at temperatures greater than 200 ˚C. Liang et al observed that KOH additive produced a significant improvement on the Li-Mg-N-H system.[34] Their results indicated that the KOH-doped system decreased the operating temperature by 74 degrees as compared to the un-doped system. In addition, the cycling stability of the system only decreased 0.002% within the 30 cycle study.[34]

1.6.2 $1.9LiNH_2 + MgH_2 + 0.1RbH$ and other Rb-based additives

Recently, Durojaiye et al[41] conducted another study on a novel system involving 3.3 mol% of rubidium hydride (RbH) as a destabilizing agent. In that study, RbH had to be synthesized using a process called mechanical ball milling. From the results presented in a recent paper, that system provided evidence that it was a better alternative because it produced a lower desorption temperature and faster kinetics as compared the previously studied potassium hydride- catalyzed system.[41]

After the introduction of RbH to the system, other researchers such as Li et al continued to investigate further utility of the Rb-based additives. Li et al first introduced RbF dopant to the $2LiNH_2/MgH_2$ system.[47] Based on their results, they observed that after milling RbF with the system, RbF reacted with LiH and formed RbH and LiF. The RbH demonstrated that the mixture had a major effect on lowering the desorption temperature and significantly increasing the desorption kinetics just as Durojaiye et al. demonstrated. However, the only concern reported was the decrease in weight percent in the PCT isotherms due to the molecular weight of RbF.[47]

Additionally, Li made a further discovery. He discovered that a more significant improvement on $2LiNH_2/MgH_2$ system could be realized with the addition of small amounts of RbH and KH.[48] Their results indicated that at 130 °C, the desorption kinetics produced with the RbH/KH-doped system was 43 times faster than the un-doped system. For thermodynamic studies, desorption operating temperature for the co-catalyzed system was approximately 40 degrees lower than the un-doped system as well.[48]

1.7 Motivation

Lithium amide-magnesium hydride systems have been found to be promising for hydrogen storage applications due to the low operating temperatures compared to other systems. A review of research studies in the existing research literature shows that the majority of the experiments were conducted at higher temperatures (above 200 °C). In addition, most of the studies done on the $2LiNH_2/MgH_2$ hydrogen storage system were dehydriding kinetic studies. Therefore, the current dissertation will focus on the thermodynamic and the kinetic properties of these alkali metal dopants and their effects on the $2LiNH_2/MgH_2$ system for both absorption and desorption studies

1.7.1 Goals of Current Research

The goals of the dissertation research are as follows:

- Investigate the probability of producing thermal stability between 30 kJ/mol $<\Delta H <$ 60kJ/mol at constant temperatures lower than 200°C.
- Investigate the probability of producing accelerated kinetics at constant temperatures lower than 200°C using suitable catalytic additives.
- Perform absorption studies for the alkali metal-doped systems for the first time at constant thermodynamic driving force.
- Determine the rate-limiting step for the kinetic data using kinetic modeling equations.
- Determine the maximum durability of the catalyzed system at temperatures lower than 200°C using cycling procedures.

CHAPTER 2

EXPERIMENTAL METHODS

This chapter will introduce and explain all of the necessary steps that were necessary in order to accomplish the goals of the current dissertation research study. In addition, extensive elaboration was provided in order to outline all of the specific procedures, materials, etc. that were central to the completion of all experiments described. Finally, the experimental section discusses the primary purpose, aim and significance of the current research study.

2.1 Chemicals That Were Used

Chemicals that were used for the current doctoral dissertation research study were purchased from Sigma Aldrich and Alfa Aesar. Using those chemicals, rubidium hydride and cesium hydride were prepared from 95 percent pure rubidium using a method described by Elensari et al[50] and a modified procedure by Durojaiye et al[41]. In section 2.1 of this chapter, that process is described further and discussed in detail. All samples were prepared in an argon-filled atmosphere provided by the glove box (**Figure 2.1**) and ball-milled by a Spex Mill/Mixer Shaker mill for two hours (120 mins) shown in **Figure 2.2**. Afterward, they were transferred to 10 ml glass vials and stored in an argon atmosphere glove box for further analyses that are described in the current study.[9,17]

Figure 2.1 Glove Box where all the samples were prepared in an argon atmosphere.

Figure 2.2 SpexMill/Mixer Shaker Mill used for preparing alkali-metal doped lithium amide-magnesium hydride hydrogen storage systems.

2.2 Synthesis of Rubidium Hydride and Cesium Hydride

According to Elansari et al, rubidium hydride and cesium hydride are not readily available. Therefore, those materials were synthesized in the laboratory.[50] In the beginning, approximately 4-5 g of rubidium metal/ cesium metal and ten10 mm titanium carbide balls were transferred into a titanium carbide vial. Afterwards, a pressurized lid was placed on the vial in order to secure the vial contents. Tightly securing the vial in that manner was necessary in order to prevent contamination.[41]

In the next step, hydrogen gas was added into the vial. In order to add hydrogen into the vial, the hydrogen was blown out of a tube that was connected to the Sievert's apparatus so that the tube would not have a buildup of atmospheric air. After the hydrogen gas flowed through, the tube was then connected to the lid on the vial. Once connected, the pressure added to the vial was ~90 psi-100 psi. After pressurization, the vial was transferred to the planetary mill (Fritsch pulverisette 7) which is presented in **Figure 2.3**. A diagram of the pressurization process is shown in **Figure 2.4** for clarification.

A rotation rate of 100 rpm was conducted for 15 minutes. During that process, the rotation rate was increased progressively by 25 rpm. In addition, the 15 minute milling time was kept constant until 250 rpm was achieved. That process was repeated three times by restarting from 100 rpm. At 250 rpm, a 12 hour milling period was set which included 36 cycles of 20 minutes of milling and 10 minutes of pause times. However, it should be noted that before the start of each milling cycle the vial was re-pressurized

between 90-110 psi. The lid of the vial was changed when 175 rpm was achieved because of the spread of rubidium metal onto the inside of the lid, which could prevent effective pressurization of the vial.[41]

After the 18 hour milling process was completed, the vial was re-pressurized then it was placed in an oven at 120^{o}C for 1 hour. Afterwards, a white powdered substance emerged at the end of the incubation process that was observed in the argon filled glove box. To determine that the RbH/ CsH had been synthesized, an X-ray analysis was conducted. The diffraction pattern was then compared with the x-ray pattern shown in the X' Pert Highscore database.[41,50]

Figure 2.3. Fritsch pulverisette 7 was used for reactive ball milling in synthesizing rubidium/ cesium hydride (RbH/CsH).

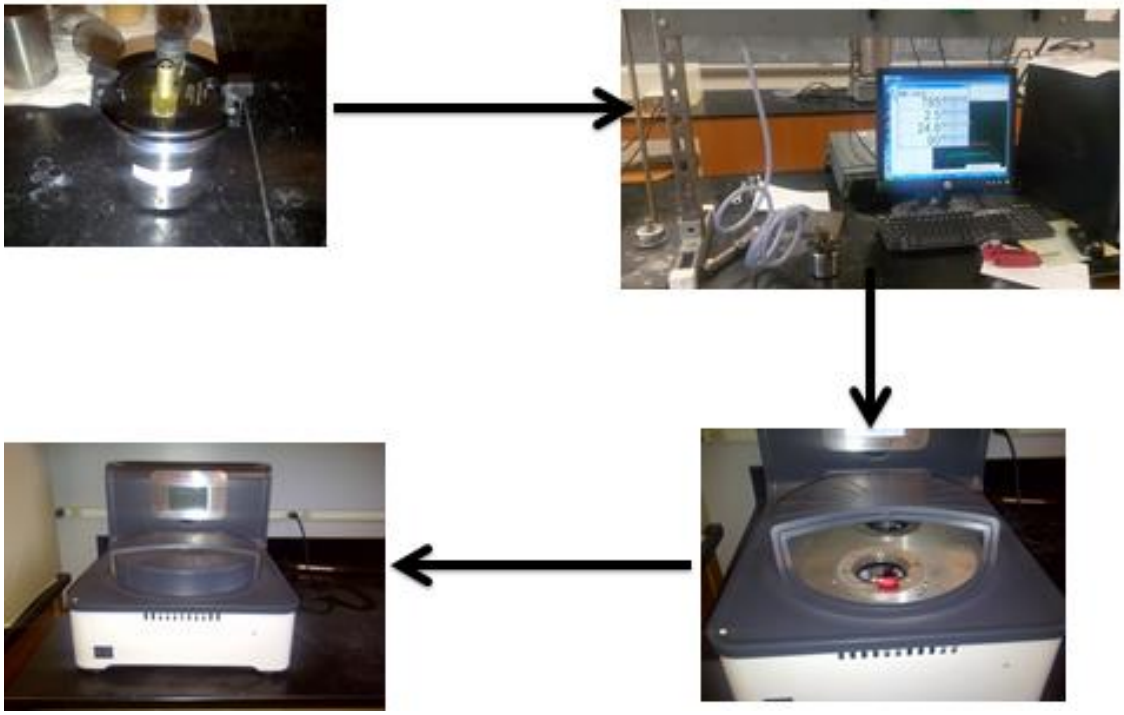

Figure 2 .4 The Process of hydrogen pressurization of the rubidium/cesium metal.

2.3 Powder X-Ray Diffraction

Based on the existing research literature, powder x-ray diffraction is a characterization technique used to identify the purity of materials, phase transitions, and structural properties of solid state materials.[39-42] **Figure 2.5** shows the X-ray Diffractometer model made by PANanalytical. The diffraction patterns produced from this instrument were used to determine lattice parameters. [34,41,44]

All analyses were conducted using copper K-alpha radiation. Also, samples were prepared in an argon-filled glove box and were sealed with a thin Kapton polymer film to

protect them from moisture and external contaminants. The Kapton film does not interfere with experimental scans from X-rays. For the sample stage scan, a razor was used to make certain that the sample was spread evenly over the dish.

Figure 2.5 X-Ray Diffractometer

2.4 Fourier Transform Infrared Spectroscopy (FTIR)

To measure the N-H vibrations of the undoped and doped materials, samples were measured by an FTIR instrument located at Delaware State University. That instrument is the IR Prestige-21 Fourier Transform Infrared Spectrophotometer model 8400S from the Shimadzu Corporation shown in **Figure 2.6**. Each sample was mixed with KBr at a ratio approximately 1:10. Then those mixtures were hand-ground into fine powder using an agate mortar and pestle in an argon filled glove box. The ground mixture was transferred to a pellet press holder and pressed at 13 kilopound per square inch (ksi) for ~ 1-2 min to form a pellet of ~12 mm in diameter and 0.5 mm in thickness. There was a brief exposure of sample pellets to air during hydraulic pressing and movement to the sample compartment of the spectrometer.[80]

Figure 2.6 IR Prestige - 21 Fourier Transform Infrared Spectrophotometer.

The FTIR spectrophotometer was powered on and the IR solution icon and the monitor were double clicked in order to open the software template. Sample information and other parameters needed such as measurement mode, number of scans and range were inputted. The background was measured first by clicking on the BKG (background) icon on the software. Once that background was run, the prepared pellet was carefully placed in the sample compartment and the sample measurement taken with the compartment closed. After 16 scans were accumulated, a final infra-red spectrum was produced. All sample measurements were taken under ambient conditions. Background measurement of air was obtained prior to each sample measurement. The background measurements were automatically subtracted from the sample measurement by the spectrometer.

2.5 Temperature Programmed Desorptions (TPD)/Pressure-composition isotherms (PCIs)

Before PCIs were conducted, a temperature-programmed desorption was completed. That experimental procedure exhibited the release of hydrogen from a fresh sample. TPDs were used to determine two primary factors that enabled further analyses: 1) the total amount of hydrogen each hydrogen system released and 2) the temperature at which the sample released hydrogen gas. Observing temperatures at which the hydrogen was released enabled the selection of potential temperatures for pressure-composition isotherms.

A potential hydrogen storage system would require thermostability (ΔH) in the range 30 kJ/mol to 60 kJ/mol based on DOE requirements. To measure the thermostability of each sample, pressure-composition isotherms were gathered. Once gathered, van't Hoff plots were calculated from the mid-plateau pressures. From those plots, an enthalpy value was calculated which described the thermostability of the KH-doped, RbH-doped and CsH-doped systems studied.[24] In previous research studies, pressure-composition isotherms were gathered at constant temperatures starting at 200°C and above.[41,43]

However, in the current research study, pressure-composition isotherms were gathered at temperatures below 200 °C. That process was designed to produce results that contained low plateau pressures experimentally. Based on data extrapolation, plateau pressures were collected around 80 °C that were based on theoretical calculations. However, for the current doctoral dissertation research study, the focus was primarily on the temperatures discussed in the temperature programmed desorption section of the current chapter. For the experimental data, a computer program called LabView was used to create experimental runs and collect the resulting data .[52-53]

For the experimental data, the LabView computer program was used to record experimental runs and collect the TPDs and PCIs data. The temperature range of isotherms was 150 °C-180 °C. As the temperatures became lower, the settling temperature programs were modified to record accurate and precise results.

Figure 2.7 Pressure Composition Isotherm Instrument by Advanced Materials Corporation (Pittsburg, PA)

2.5.1 Cycling

Figure 2.8 shows isotherms gathered for absorption and desorption for $LiNH_2/MgH_2$ catalyzed with KH.[43] However, kinetic and thermal stability have not been conducted on that system to date. To test the kinetic and thermal stability, cycling studies were conducted on the un-catalyzed, KH-catalyzed and RbH-catalyzed system.[4,12,42-43]

Experimental procedures for cycling have been conducted that were based on those conducted by Z. Dehouche and that research group.[27] The sample was prepared in a PCI sample chamber in an argon-filled glove box. The sample chamber was then

connected to the PCI instrument .The program used to conduct the temperature and PCI analyses was the Labview Software. That program begins with evacuation of the system for 1 hour at the desired temperatures stated in this study. The primary reason for that procedure is enable the sample to be fully "degassed" of hydrogen and argon. After that, the evacuation program is then conducted for 2 hours to ensure that a clean and activated surface exists for the hydrogen to interact with the complex system. Then hydriding and dehydriding is applied to the sample for 1 hour each and conducted 10 consecutive times. Finally, absorption and desorption studies of isotherms were gathered after 10 cycles of sorption and evacuating the samples. For each sample, 10 sets of 10 cycles were collected (100 cycles total) and analyzed. Findings are presented in the results section.

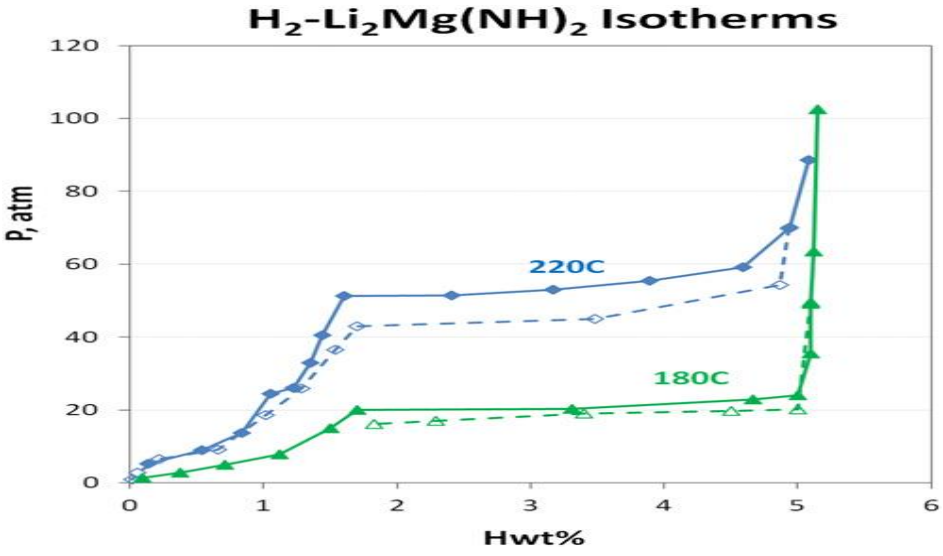

Figure 2.8. Pressure-composition isotherm of KH-catalyzed $2LiNH_2/MgH_2$ H_2 storage system[43]

2.6 Thermogravimetric Analysis (TGA)

Based on the previous studies, researchers determined the activation energy for each of the catalyzed samples through the use of thermogravimetric analysis (TGA) and/or differential scanning calorimetry (DSC)[88]. For the current study, the TGA was used to measure the heat flow along with the change in temperature for the KH-doped, RbH-doped, and the CsH-doped system. **Figure 2.9** shows the Thermogravimetric/ Differential Thermal Analysis instrument that was manufactured by Perkin Elmer. Using **Equation 2.1** below, the Kissinger plot was calculated. It was used to determine the activation energy for each system.[42] In the equation, R represents reaction coefficient 8.314, β is the change in heat, T_{max} equals the temperature at maximum rate, and $F_{KAS}(\alpha)$ is a constant that is a function of transformation.

$$\ln(\beta/T^2_{max}) = (E_a/R)(1/T_{max}) + F_{KAS}(\alpha) \qquad \text{(Eq. 2.1)}$$

In addition, with consideration of the United States Department of Energy's guidelines, the researcher determined the activation energy through the process of Arrhenius plots. The Arrhenius plots were gathered through a series of kinetic analyses at different temperatures in the range of 160 ˚C-180 ˚C. Once collected and assuming that the reaction is a first order, first-order plots was generated for the determination of the rate constant k. Subsequently, Arrhenius plots were constructed and used to determine activation energies for each doped system.

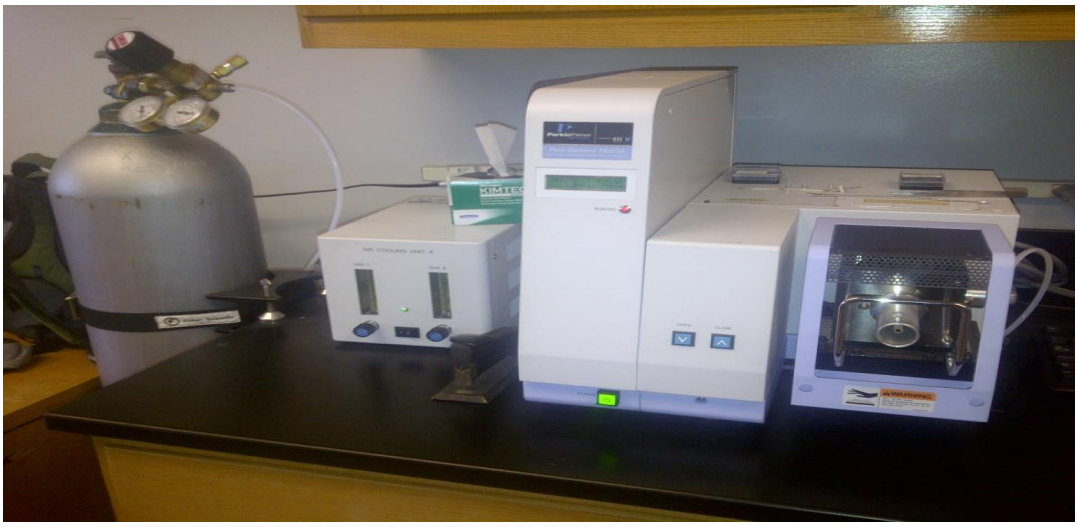

Figure 2.9 Thermogravimetric Analysis (TGA)/Differential Thermal Analysis (DTA)

2.7 Residual Gas Measurement (RGA)

For thermodynamic studies, it is necessary to determine how much ammonia was released from each system after heating at high temperatures. The release of ammonia and other gases can be measured by residual gas analyses and is known as RGA. The instrument that was used for each RGA is the Stanford Research Systems Residual Gas Analyzer (SRS RGA) model RGA Pro-2500 fitted with a quadrupole mass filter, faraday cup detector and a thoria-iridium filament shown in **Figure 2.10**. The RGA was pre calibrated before use. The RGA was coupled to the Advanced Materials Corporation PCI unit for the oven component.

2.7.1 Procedure for RGA

The sample holder was filled with about 0.5 g of the sample and analyzed in argon-filled glove box. The sample holder was plugged with glass wool and covered. The

sample was placed in its compartment and removed from the glove box. The sample holder compartment was clamped on to the PCI unit and connected to the RGA via a 1/8" sampling line. With the sample holder valve closed, a leak test was conducted and the sample and system were purged. The air pressure which controlled the valve opening was set at 40 psi. The RGA was turned on. The roughing pump was turned on followed by the RGA switch. The turbo pump was turned on and monitored until the pressure in the chamber/frequency was around 10^{-4} mbar/1500 Hz.

The RGA must not be operated if the pressure in the chamber is greater than 10^{-4} Torr. The manifold was cleared of residual gases before use. That procedure was executed by closing valve 1. Valve 2 and 3 were opened until the desired pressure in the manifold had been achieved. It must be noted that valve 3 will not open unless valve 2 has already been opened for 5 seconds. The manifold clearing must always be executed prior to use or after the user has finished investigating a current gas sample. The RGA software was started by double clicking on the RGA 3.0 icon on the desktop. The RGA head was connected by clicking on the tool bar's RS232 set up button. A dialogue box showing "buffer is full" was displayed and OK was clicked.

The RGA list was upgraded on a new dialogue box display and the port (COM1) to which the RGA head is connected was selected on the connector column and the connect button clicked. The connection is made when "connected" is displayed in the status column and the tool bar's GO button turns green. The connector list was closed when the connection was completed

The filament was turned on by clicking on the tool bar's filament button. A green status LED on the back panel of the ECU box provides an indication of the emission status of the filament at all times. Also, it provides the fastest way to verify whether or not the filament is emitting electrons. On the tool bar, the mode was clicked and the pressure versus time (P v T) mode was selected. The background measurement was done at room temperature by opening the by-pass valve followed by valve 1 then valve 2 because the measurement was conducted at low pressure and the desorbed gas was allowed to flow directly to the RGA. The toolbar's GO button was clicked. After a small delay, the P v T scan data started to display on the screen. The graph was rescaled by selecting Auto scale from the graph menu. From the background set up feature of the software, "background –scan data" was selected before sample measurements. A sample measurement was conducted in the same manner as the background measurements with the temperature ramped to approximately 400 ^{o}C. After a few seconds, the display of the selected species appeared on the screen with different pressure readings as the temperature rose. This process is similar to the temperature programmed desorption conducted on the PCI machine. The difference is that in TPD the change in mass is being measured whereas in RGA the gases are being determined.

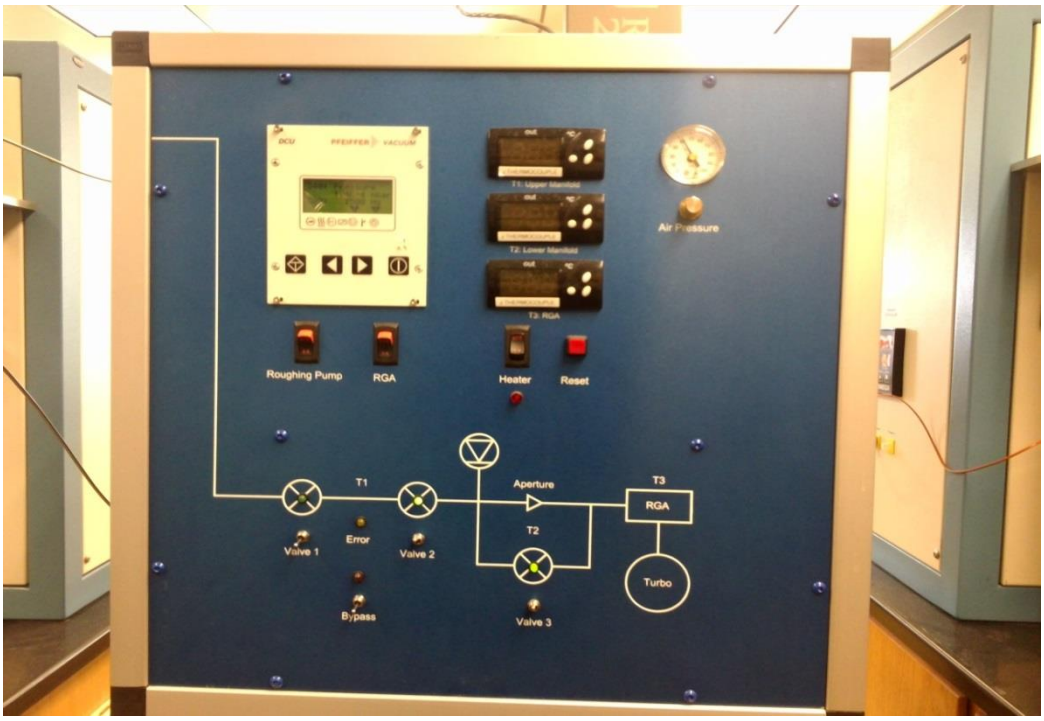

Figure 2.10 The Residual Gas Analyzer coupled to the Advanced Materials PCI unit

2.8 Kinetic Analyses

For hydrogen storage, the United States Department of Energy has a primary concern as to how fast hydrogen gas in a particular system can be absorbed and released at a reasonable rate (discussed in Chapter 1, pg.6). The rate of hydrogen release and absorption has been determined to be a very critical factor for on-board hydrogen storage applications.[55] To achieve the DOE goal for this study, kinetic experiments were collected and analyzed accordingly.[24,34] It should be noted that in the current doctoral dissertation research study, the introduction of absorption studies to the lithium amide-magnesium hydride system (2:1) at constant thermodynamic driving force will be discussed further.[77,78]

All kinetic experiments were conducted on a stainless steel-engineered Sievert's apparatus. The schematic of Sievert's apparatus is presented in **Figure 2.11**. The Sievert's apparatus is designed to measure the rate of the absorption and desorption of hydrogen from sample materials using a constant pressure regulator. For absorption studies, hydrogen is released from the reservoir and is "absorbed" in the sample chamber through a pressure regulator holding the pressure constant. For desorption studies, hydrogen is released from the sample chamber and flows into a reservoir.

To prepare for kinetics, approximately 1.0-2.0 g of the sample was placed into the sample reactor in the glove box. Glass wool was placed in the reactor right after the sample to prevent potential sucking of the sample into the Sievert's apparatus. Next, the sample reactor was sealed and then connected to the apparatus. The tube furnace was turned on so that experiments could be conducted at constant temperature. A thermocouple was placed into the bed of the sample and the sample reactor. The thermocouple was connected to a digital readout in order to monitor a constant temperature. Potential temperatures for kinetic studies were conducted at temperatures below 200 °C, particularly 160 °C.

With kinetics, a constant pressure thermodynamic driving force was required. The constant driving force was denoted as the "N" value which is a ratio of the plateau pressure and the opposing pressure of a sample.[26,56-57] Presented in **Equation 2.2** is the representation of the definition of the N-value pertaining to absorption kinetics and presented in **Equation 2.3** is the representation of the definition of N-value for the

desorption kinetics. P_{op} represents the opposing pressure, whereas P_m represents that plateau pressure that was determined experimentally from the pressure-composition isotherm. For the collection of kinetic data, Daqview software was used to measure the pressure of the hydrogen in the sample, Sievert's apparatus, and in the ballasts.

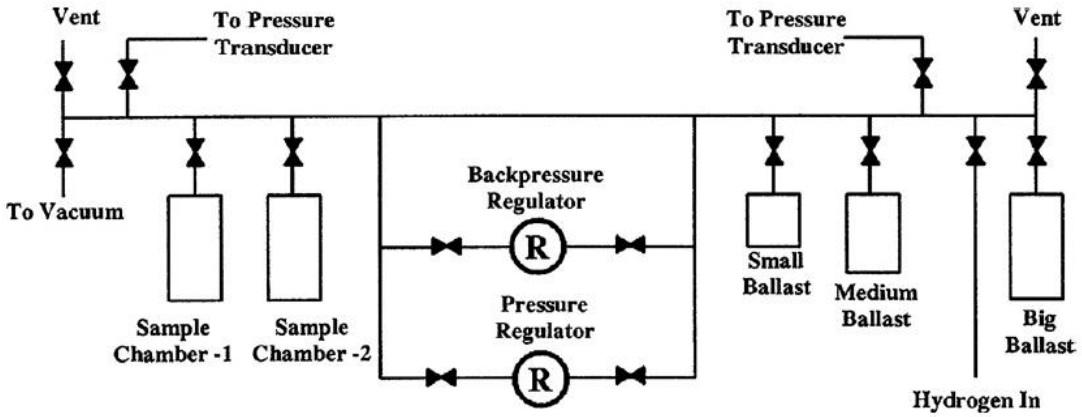

Figure 2.11. The Sievert's apparatus schematic[53]

$N = P_{op}/P_m$ (Eq. 2.2)

$N = P_m/P_{op}$ (Eq.2.3)

CHAPTER 3

THERMODYNAMIC AND STRUCTURAL PROPERTIES OF KH-DOPED, RbH-DOPED, AND CsH-DOPED $2LINH_2/MGH_2$ HYDROGEN STORAGE SYSTEM

Background

In the current study, the effectiveness of several alkali metal hydrides (KH, RbH and CsH) for improving the hydrogen absorption and desorption properties of a $2LiNH_2/MgH_2$ mixture was studied. Results indicated that the relative effectiveness of these additives in decreasing the hydrogen desorption temperature, minimizing the emissions of ammonia and the thermostability of the system is in the order: RbH > KH > CsH. It appears that the alkali elements: K, Rb and Cs partially replace the Li in the product layer. Also, it appears that there is an inductive effect in which the N-H bond is weakened thus leading to lower desorption enthalpies. The lattice expansion is caused by substitution of the larger alkali elements such as K, Rb and Cs for Li.

3.1 XRD analyses

Presented in **Figure 3.1** are the X-ray diffraction patterns of the catalysts that were used. A comparison of the peaks in the three XRD profiles reveals some systematic trends. As was hypothesized, the peaks for corresponding Miller indices generally shift to smaller angles as the size of the alkali metal increases. The calculated lattice parameter

"a", for KH, RbH and CsH are 5.70±0.010, 6.01±0.012 and 6.37±0.015, respectively. Those values are consistent with values that were reported by Elansari et al[50]. Presented in **Figure 3.2** are the XRD profiles of the "As Milled" samples with and without the catalysts. It was observed that the KH, RbH and CsH doped mixtures all followed the same pattern. No catalysts' peaks were identified in the un-doped mixtures. However, KNH_2, $RbNH_2$, and $CsNH_2$ were identified in the doped samples. [63]

Presented in **Figure 3.3** are the dehydrided XRD profiles of the mixtures. Rijissenbeek et al[62] reported that the dehydrided mixtures of the KH doped and the un-catalyzed mixtures result in the formation of a new compound known to be $Li_2Mg(NH)_2$. The XRD patterns in **Figure 3.3** are relatively consistent with those reported by Rijissenbeek et al.[62] They used in situ X-ray diffraction and neutron diffraction to demonstrate that $Li_2Mg(NH)_2$ has an orthorhombic structure at temperatures below 350 °C that undergoes a phase transition to primitive cubic at 350°C and to face centered cubic at 500 °C.[62] The RbH doped mixtures exhibits the same XRD pattern as the un-catalyzed and KH doped mixtures when dehydrided. However, the CsH doped sample results provided a different XRD pattern than the others when dehydrided. The set of peaks at 18.3 and 20.2 degrees in the patterns for the other dehydrided mixtures could not be observed in the dehydrided mixture of the CsH doped sample. Also, that sample possessed a strong singlet peak at 51.6 degrees. The others displayed multiple peaks in that same region. That result can be further explained in **Tables 3.1a-c** in the h, k, l parameters showing that the dopants have cubic structures. The fact that the CsH doped

mixture did not produce the same diffraction pattern as the other mixtures is strong evidence that the Cs containing product has a different crystal structure than the others. Ball milling Cs with a $2LiNH_2/MgH_2$ mixture can result in the formation of a stable amide $Cs_2[Mg(NH_2)_4]$[63], in which Cs partially replaces Li, but evidently the subsequent dehydrogenation does not result in the formation of a Cs substituted imide. [63] **Figure 3.4** shows the XRD profiles of the rehydrided mixtures. Also, an XRD pattern for $Mg(NH_2)_2$ has been included for comparison in **Figure 3.4**. Observed in all of the rehydrided patterns was some evidence of the $Mg(NH_2)_2$. That observation confirms that the mixtures cycle between $Mg(NH_2)_2$+2LiH and $Li_2Mg(NH)_2$, thus indicating reversibility. Based on other studies, it has been reported that the KH doped mixture $2LiNH_2/MgH_2$ shows peaks belonging to the KH catalyst at 27.2 degrees in the dehydrided and rehydrided mixtures[51,64]. A peak at 27.1 degrees did appear in the diffraction patterns for the KH catalyzed mixtures in **Figures 3.3 and 3.4**. That peak corresponds very closely to the (111) peak in the diffraction patterns for the KH dopant in **Figure 3.1**. Thus, it is clear that the KH dopant was present throughout the process.[51,64]

However, this was not the case in the RbH and CsH catalyzed mixtures. Peaks at 25.8 and 23.3 degrees appeared in the diffraction patterns for the RbH and CsH catalyzed mixtures in **Figure 3.4** but not in **Figure 3.3**. The appearance of those peaks in **Figure 3.4** confirms that the catalysts have been regenerated. The fact that no RbH or CsH peaks appeared in the dehydrogenated patterns in **Figure 3.3** indicates that the hydrides may have decomposed into the metals, Rb and Cs. That result was more likely due to the fact

that both of those hydrides decompose at ~170 °C, which is below high temperatures that have been used to operate on these systems.

Since both of the resulting metals (Rb and Cs) have very low melting points (39.5 and 28.4 °C, respectively) they would be liquefied at the relatively high temperatures at 200 °C or above. Thus, they would display no diffraction peaks. The high pressure of 100 bars during rehydriding is enough to regenerate the metal hydrides within the systems. It should be noted that KH doesn't decompose until 400 °C. Thus it remains intact throughout the changing of phases in the experiments.

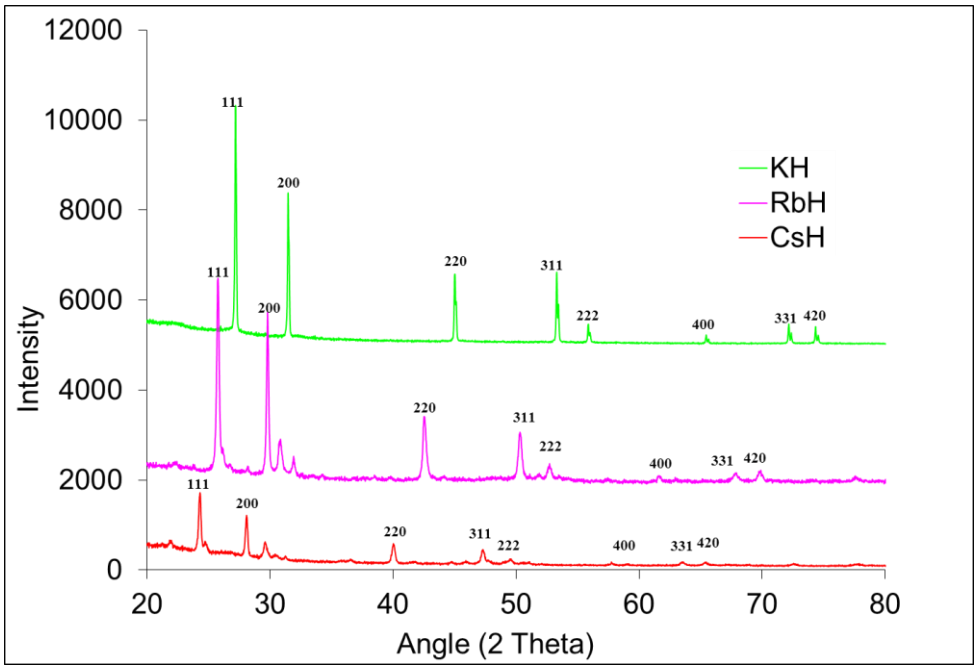

Figure 3.1 X-Ray Diffraction Patterns for the KH, RbH, and CsH dopants

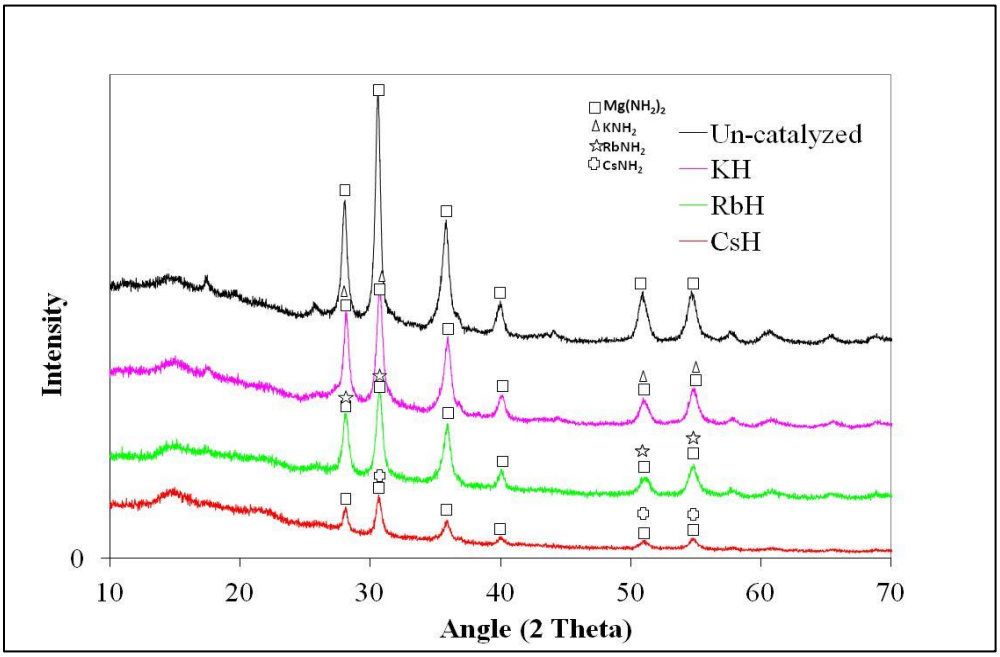

Figure 3.2 X-Ray Diffraction patterns of as milled samples for the alkali metal-doped vs. un-doped sample.

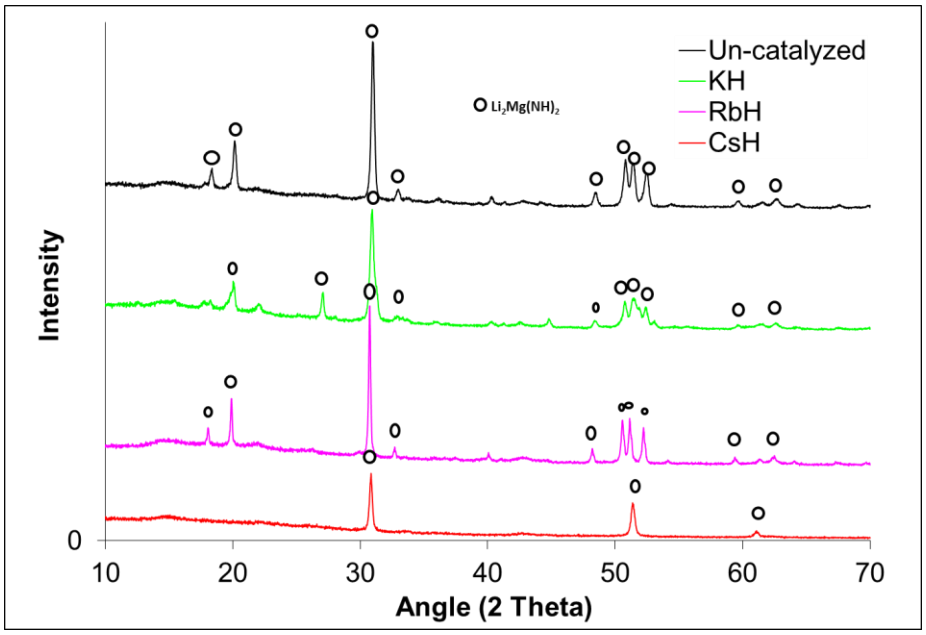

Figure 3.3 X-Ray Diffraction patterns of dehydrogenated samples for the alkali metal-doped vs. un-doped sample.

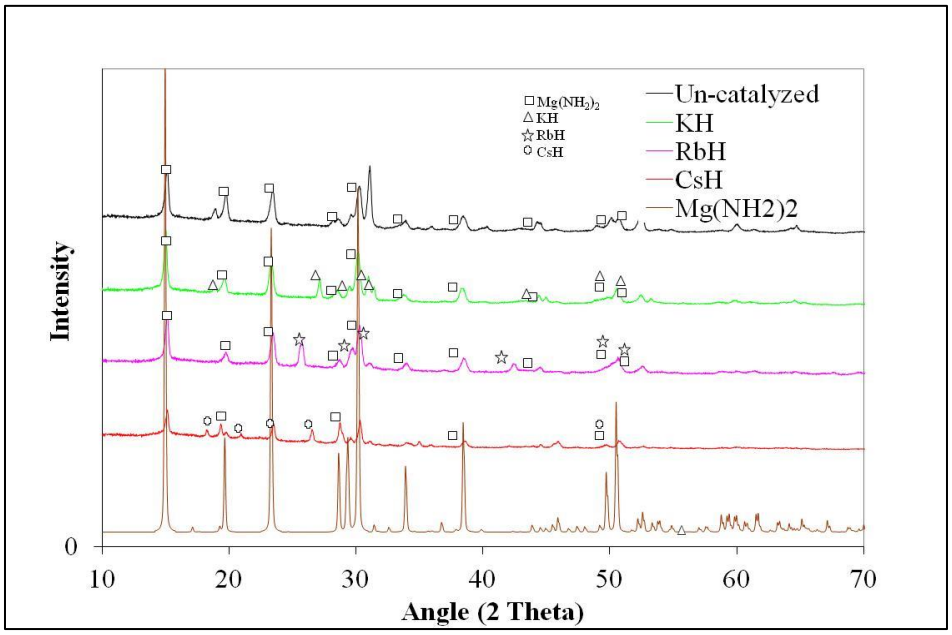

Figure 3.4 Diffraction patterns of rehydrogenated samples for the alkali metal-doped vs. un-doped sample.

KH										
2θ	θ	sinθ	(sinθ)^2	Δ(sinθ)^2	Whole #		N	h,k,l	a	Std. Dev.
27.196	0.2373	0.2351	0.0553	0.055274	1.0108	3	3	111	5.6792689	
31.47	0.2746	0.2712	0.0735	0.018267	0.33405	1	4	200	5.6853641	
45.02	0.3928	0.3828	0.1465	0.073006	1.33507	4	8	220	5.6957266	
53.31	0.4652	0.4486	0.2012	0.054683	1	3	11	311	5.6995717	
55.87	0.4875	0.4684	0.2194	0.018212	0.33305	1	12	222	5.7006269	
65.46	0.5712	0.5406	0.2923	0.072845	1.33212	4	16	400	5.7035777	
72.17	0.6298	0.589	0.3469	0.054622	0.99888	3	19	331	5.7050704	
74.35	0.6488	0.6042	0.3651	0.018175	0.33236	1	20	420	5.7057257	
82.86	0.7231	0.6617	0.4378	0.072731	1.33004	4	24	422	5.70759	
89.13	0.7778	0.7017	0.4924	0.054589	0.99827	3	27	333	5.7083895	
									5.6990912	0.00974

Table 3.1a Lattice parameter calculation for KH

RbH										
2θ	θ	sinθ	(sinθ)^2	Δ(sinθ)^2	Whole #		N	h,k,l	a	Std. Dev.
25.76	0.2248	0.2229	0.0497	0.04969	1.01025	3	3	111	5.990057	
29.80	0.26	0.2571	0.0661	0.01642	0.33384	1	4	200	5.996537	
42.54	0.3712	0.3627	0.1316	0.06547	1.33113	4	8	220	6.011047	
50.32	0.4391	0.4252	0.1808	0.04918	1	3	11	311	6.013673	
52.70	0.4599	0.4439	0.197	0.01626	0.33051	1	12	222	6.016376	
61.59	0.5375	0.512	0.2621	0.06511	1.32389	4	16	400	6.022782	
67.86	0.5922	0.5582	0.3116	0.04945	1.0055	3	19	331	6.019837	
69.85	0.6095	0.5725	0.3277	0.01614	0.32813	1	20	420	6.022228	
									6.011567	0.012096

Table 3.1b Lattice parameter calculation for RbH

CsH										
2θ	θ	sinθ	(sinθ)^2	Δ(sinθ)^2	Whole #		N	h,k,l	a	Std. Dev.
24.301	0.2121	0.2105	0.0443	0.0443	1.01434	3	3	111	6.34379	
28.09	0.2451	0.2427	0.0589	0.0146	0.33423	1	4	200	6.352921	
40.04	0.3494	0.3423	0.1172	0.05827	1.33426	4	8	220	6.369839	
47.29	0.4127	0.4011	0.1608	0.04367	1	3	11	311	6.375079	
49.54	0.4323	0.4189	0.1755	0.01467	0.33593	1	12	222	6.374184	
57.79	0.5043	0.4832	0.2335	0.05794	1.32654	4	16	400	6.381962	
63.50	0.5541	0.5262	0.2769	0.04343	0.99449	3	19	331	6.385862	
65.38	0.5705	0.54	0.2917	0.01477	0.33813	1	20	420	6.38373	
									6.370921	0.015111

Table 3.1c Lattice parameter calculation for CsH

3.2 Fourier Transform Infrared Spectroscopy

Presented in **Figure 3.5** are the FTIR patterns for the un-doped, KH-doped, RbH-doped, and CsH-doped as-milled samples. Also, the $LiNH_2$ and MgH_2 samples were analyzed to identify those compounds in the as-milled samples. The peaks for the $LiNH_2$ samples are located in the 1550 and 3312-3270 range whereas MgH_2 shows little to no observable peaks. This range can also be seen in all of the samples in this dissertation study. According to the standard IR absorption characteristics, there is an N-H stretch in the range of 3250-3400 cm^{-1}. This might indicate that the N-H bonds in each of sample are weakened and formed intermediate species of the as-milled samples.[80]

Presented in **Figure 3.6** are the curves for the dehydrided samples that were analyzed by the FTIR samples. The results indicate that the $LiNH_2$ that was present in each of the systems disappeared and formed the widely known ternary imide, $Li_2Mg(NH)_2$. In **Figure 3.7**, the samples are rehydrided back into the expected species of $Mg(NH_2)_2$ and LiH. In the region between 1530 -1600cm^{-1}, the peaks reappeared for the un-doped and the doped systems as they were observed in the "as-milled" samples. That result indicates that the samples returned back into their original structure.

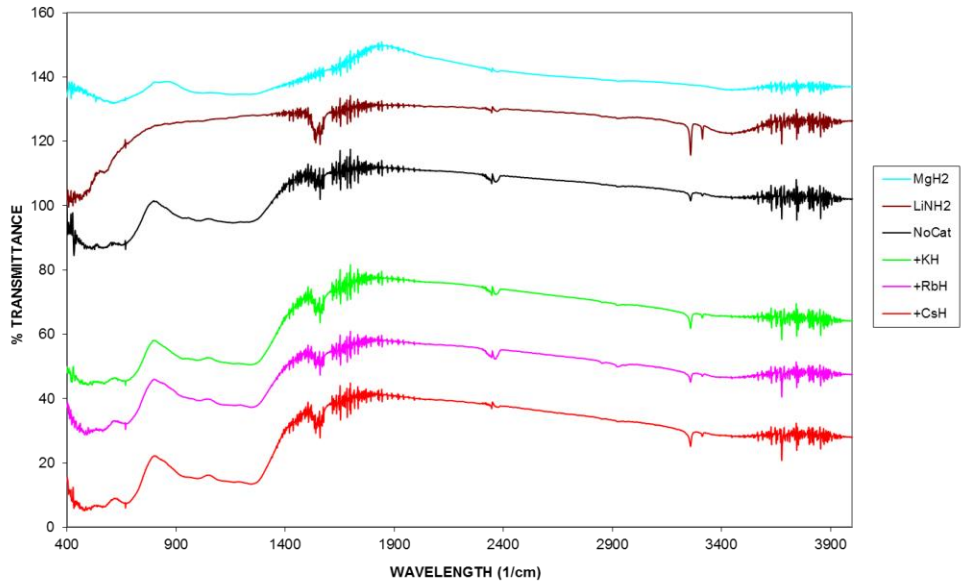

Figure 3.5 FTIR measurements of "as milled" samples of $2LiNH_2/MgH_2$ system.

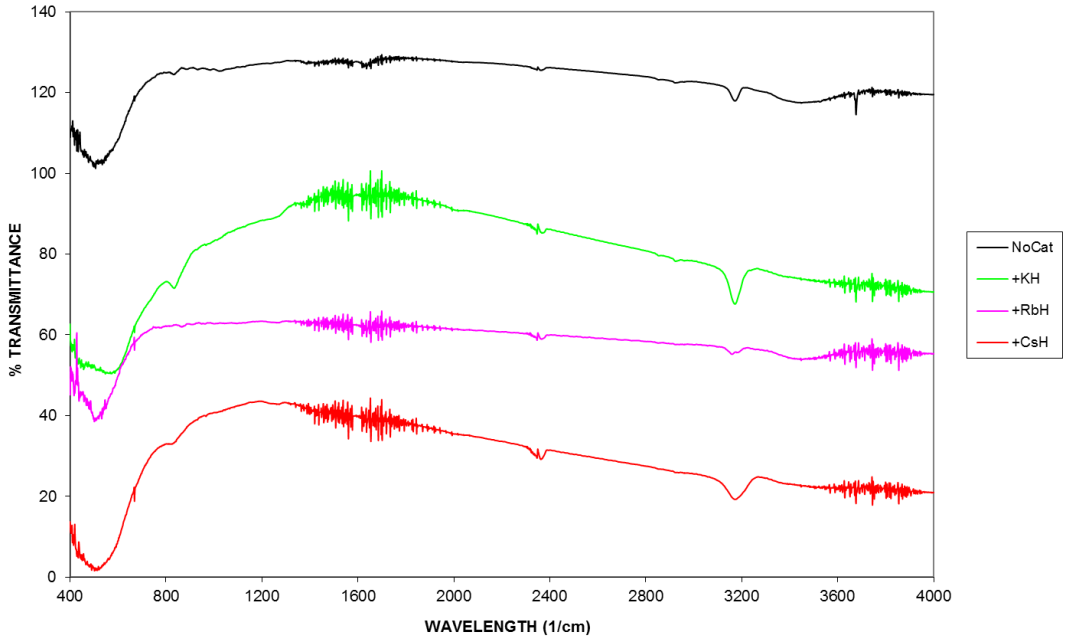

Figure 3.6 FTIR measurements of de-hydrided samples of $2LiNH_2/MgH_2$ system.

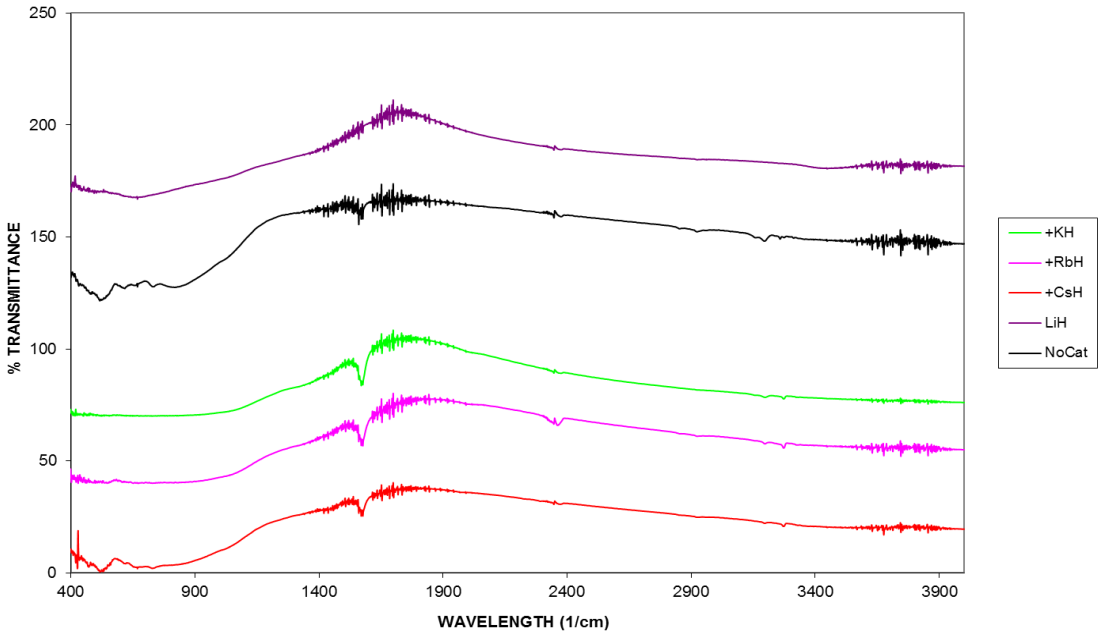

Figure 3.7 FTIR measurements of re-hydrided samples of $2LiNH_2/MgH_2$ system.

3.3 Temperature-Programmed Desorption

Figure 3.8 shows the Temperature Programmed Desorption (TPD) analyses of the various mixtures of $1.9LiNH_2$+$1.1MgH_2$ with and without the catalysts. The samples were heated from 30 to 300 °C at 4 °C/min. All of the mixtures doped with catalysts have onset temperatures below 100 °C. Since most of the hydrogen desorbs along the steep portion of the curves it was decided that a more useful way of comparing the dehydrogenation characteristics of materials would be to use the temperature corresponding to the inflection point of each TPD curve. That temperature has been defined as the desorption temperature (T_d). The order of desorption temperatures are RbH ≤ KH < CsH << uncatalyzed.. **Figure 3.8** below shows the temperature-programmed desorption study. Moreover, the present dissertation research study will not focus on the lower temperatures of the undoped system due to having an onset temperature higher than 200°C unlike the alkali-metal doped systems.

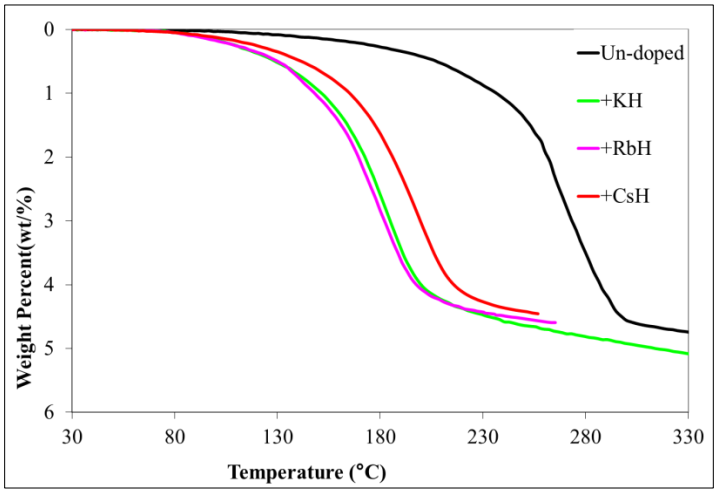

Figure 3.8 Temperature-programmed desorption for all $2LiNH_2/MgH_2$ system with and without catalysts.

3.4 Thermogravimetric Analyses

Presented in **Figures 3.9-3.11** are DTA curves for KH, RbH, and CsH doped mixtures at different heating rates. It is observed that the maxima in the DTA curves move to higher values as the heating rates increase. From the DTA curves, Kissinger plots were constructed from **Equation 2.1**. From that equation, the Kissinger plots were made and the activation energies were determined.

The trends in those curves are similar to those observed for the undoped, KH, RbH doped mixtures. The Kissinger plots for the various mixtures are presented in **Figure 3.12**. The slopes of those curves were used to determine activation energies. The activation energy for CsH doped system was 109.0kJ/mol. The activation energies for KH and RbH doped mixtures were approximately the same, 87 kJ/mol and 89.4 kJ/mol respectively. Again, the explanation of that result is based on the fact that both K and Rb metals have the same Pauling electronegativity value, 0.82. The activation energies follow a similar trend as was seen with enthalpy values: RbH ≈ KH > CsH > Un-catalyzed. Further on in this research study, the investigator presents the comparison results of Arrhenius plots that were calculated by kinetics at various temperatures with the changing of the heat calculated by the TGA.

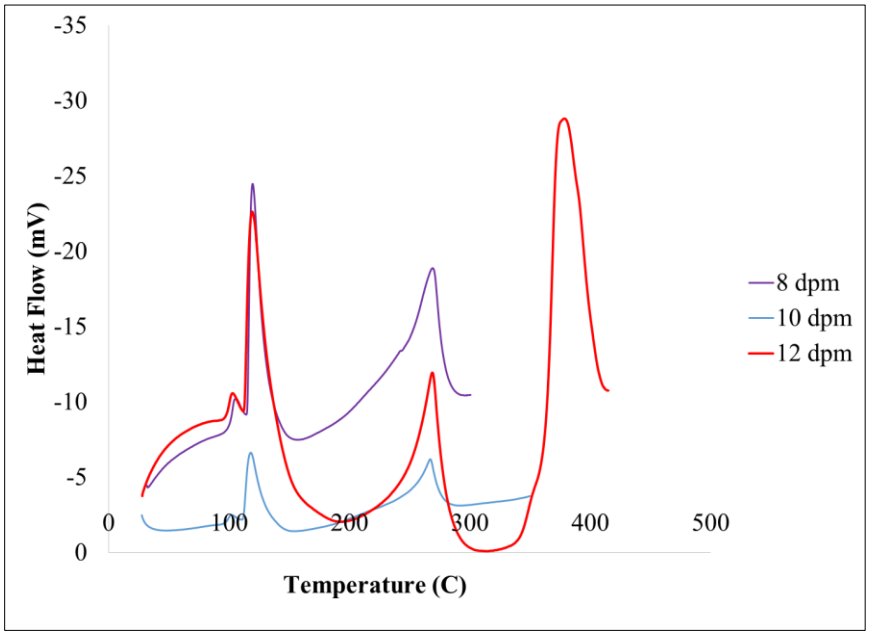

Figure 3.9 Differential Thermal Analysis plot of KH-doped $2LiNH_2/MgH_2$ system

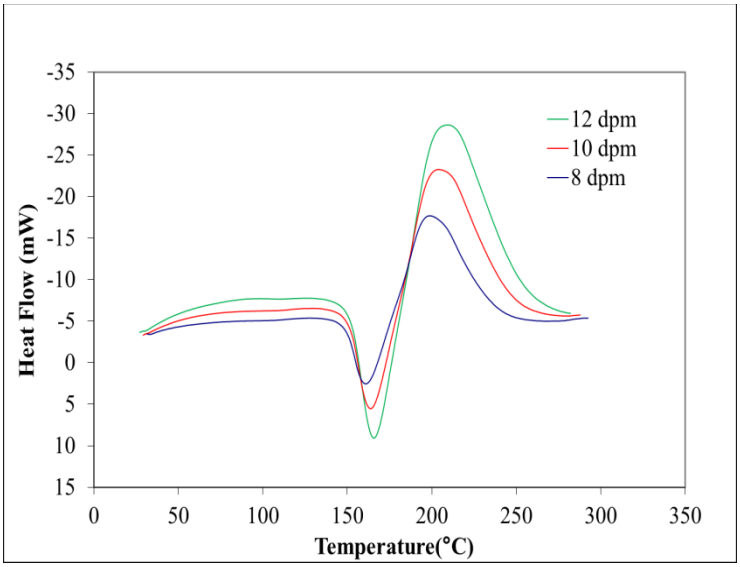

Figure 3.10 Differential Thermal Analysis plot of RbH-doped $2LiNH_2/MgH_2$ system

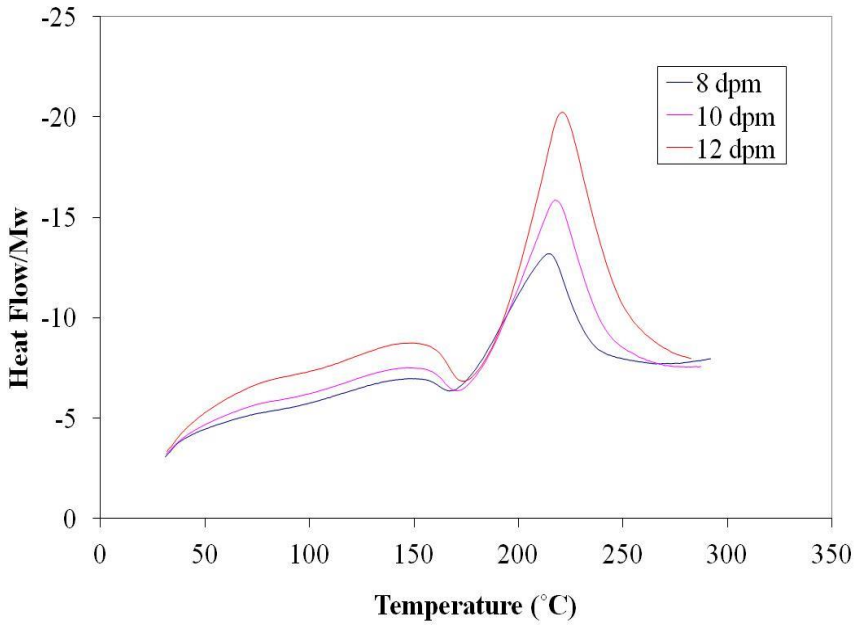

Figure 3.11 Differential Thermal Analysis plot of CsH-doped $2LiNH_2/MgH_2$ system

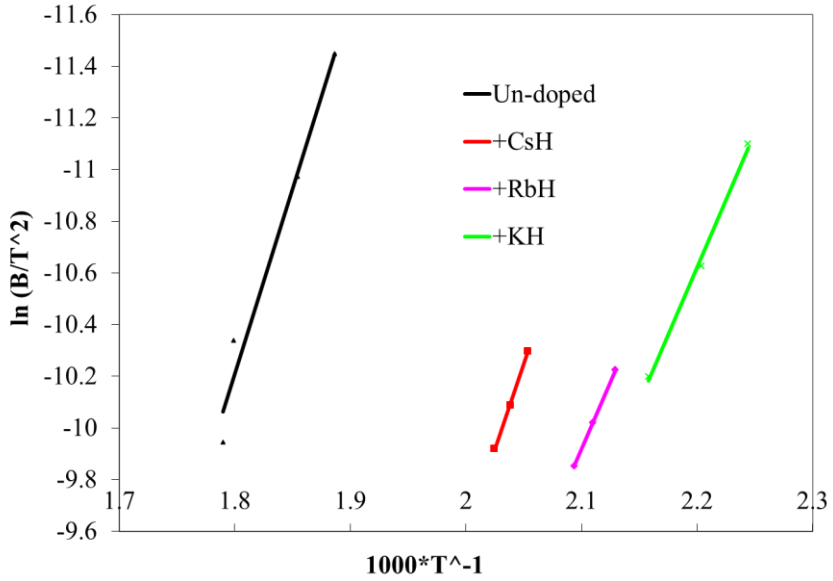

Figure 3.12 Kissinger plots of the un-doped and alkali metal-doped $2LiNH_2/MgH_2$ systems

3.5 Residual Gas Analyses (RGA)

Based on the data collected and analyzed, all doped systems show little to no emission of ammonia as the temperature increases. However, for the un-doped system, as the temperature increased, the ammonia emission did increase significantly as compared to the alkali metal-doped sample. According to the periodic trends, as you go down the group, the size of the alkali metal ionic size increases. Therefore, when the lithium amide-magnesium hydride system was doped, the alkali metal ions (K^+, Rb^+, and Cs^+) suppressed the ammonia release as the temperature increased with the sample during the RGA study. Presented in Figures **3.15-3.16** there appears to be little to no emissions of ammonia from the KH-doped, RbH-doped, and CsH-doped system respectively. It is not clear why these dopants are able to suppress the formation of ammonia. It is clear from **Figure 3.13** that there is a significant amount of ammonia from the un-doped system. Those results indicate that the dopants not only lower temperature and speed up kinetics but suppress the emissions of ammonia due to the heating of samples overall.

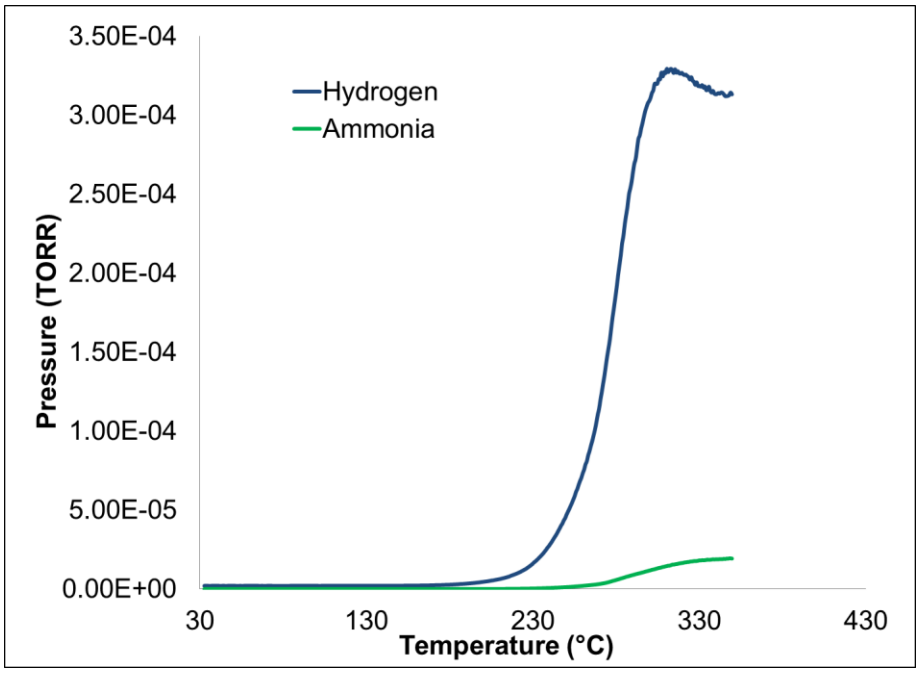

Figure 3.13 RGA data for the undoped $2LiNH_2/MgH_2$ system

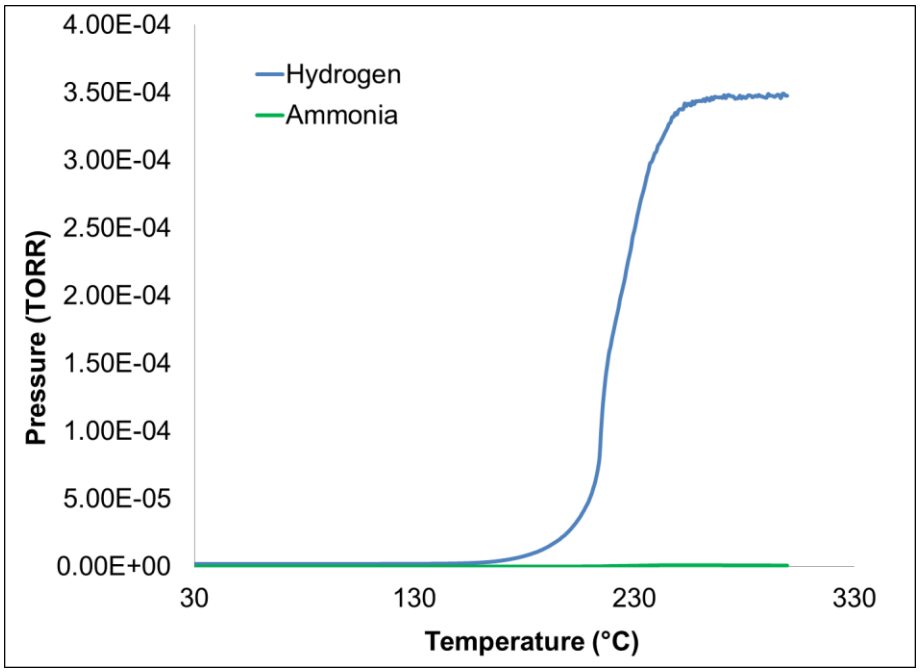

Figure 3.14 RGA data for KH-doped $2LiNH_2/MgH_2$ system

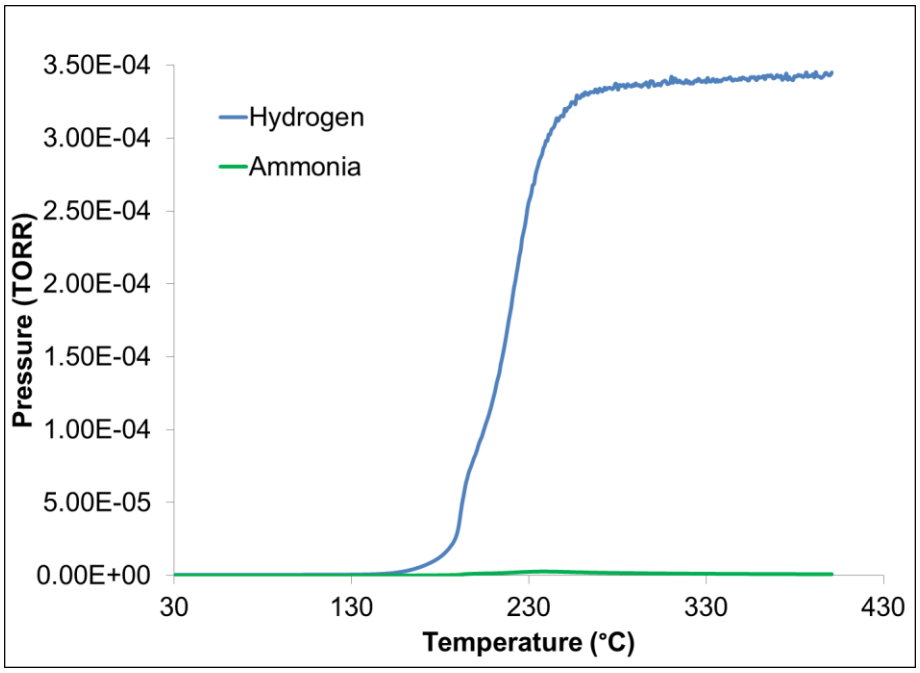

Figure 3.15 RGA Analyses of RbH-doped system.

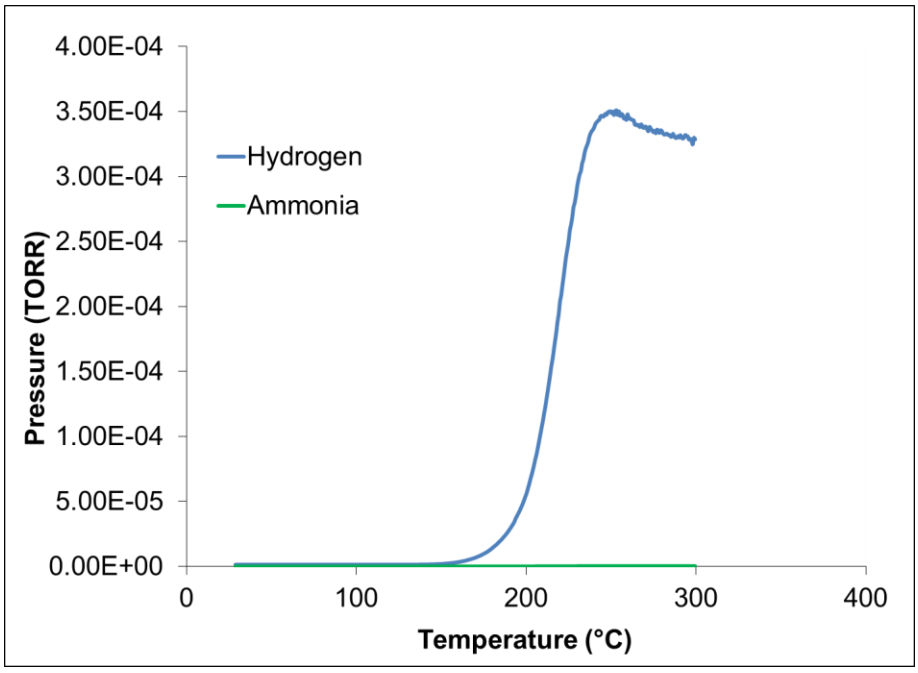

Figure 3.16 RGA Analyses of CsH-doped $2LiNH_2/MgH_2$ system

3.6 Summary

The results of this research have provided evidence about the relative effectiveness of the various alkali hydrides in lowering the desorption temperature, lowering the activation energy and lowering the emissions of ammonia. That relative effectiveness is reflected in the following order: RbH > KH > CsH>>Un-catalyzed. In the RbH and KH doped mixtures, diffusion in the two-phase plateau region occurs through a $Li_2Mg(NH)_2$ product layer in which part of the Li is replaced by Rb or K. The XRD results indicate that the product in the CsH doped mixture may have different structural characteristics than the other mixtures in which Cs may not able to effectively replace the Li in the $Li_2Mg(NH)_2$. The differences in desorption temperatures and enthalpies of the catalyzed and un-catalyzed mixtures may be caused by inductive effects of the alkali metals on the N-H bond in the amide shown in the FTIR analyses.

Activation energies have been demonstrated to be lowered significantly from 119 kJ/mol for the un-doped sample to values of 87.0 kJ/mol, 89.4 kJ/mol and 109.0 kJ/mol for KH-doped, RbH, and CsH-doped samples respectively. RGA analyses demonstrated that the emissions of ammonia have significantly been suppressed as compared to the undoped samples that were analyzed. That result indicates that the large alkali metals maybe the reason for the suppression. Also, it could be the reason for the change of weight percent from approximately 5 wt% to 4 wt%. This discovery shows promise for the PEM fuel cells with further testing of these systems.

Based on the previous research literature, researcher's investigations indicated that they had conducted further studies at 200 °C or above. However, in this research study, the major target was temperatures at 200 °C or below. This approach was designed to be consistent with the United States Department of Energy requirements. The main guidelines of DOE expect that an on-board hydrogen storage system must operate at lower temperatures.

CHAPTER 4

HYDRIDING AND DEHYDRIDING POTASSIUM HYDRIDE-DOPED LITHIUM AMIDE/MAGNESIUM HYDRIDE SYSTEM AT LOW-TEMPERATURES

Background

In the current study, the thermodynamic and kinetic properties of KH doped $2LiNH_2/MgH_2$ were measured. Previous research studies such as the ones done by Luo[43] and Durojaiye[42] focused on the KH doped $2LiNH_2/MgH_2$ system extensively. However, in the current study, there was a more specific focus on the comparison of absorption and desorption analysis of this system in a temperature range of 160 -180 °C in the current study.

4.1 PCT Isotherms and Van't Hoff plots

Isotherm measurements for the $1.9LiNH_2+1.1MgH_2+0.1KH$ were conducted in the range from 150-180°C. The results for absorption and desorption PCT measurements are presented in **Figures 4.1 and Figure 4.2** respectively. Each isotherm displays a well-defined plateau region in which lower temperatures resulted in lower plateau pressures. The isotherms display different maximum weight percent (wt%) in which the weight percent generally increases with increasing temperature.

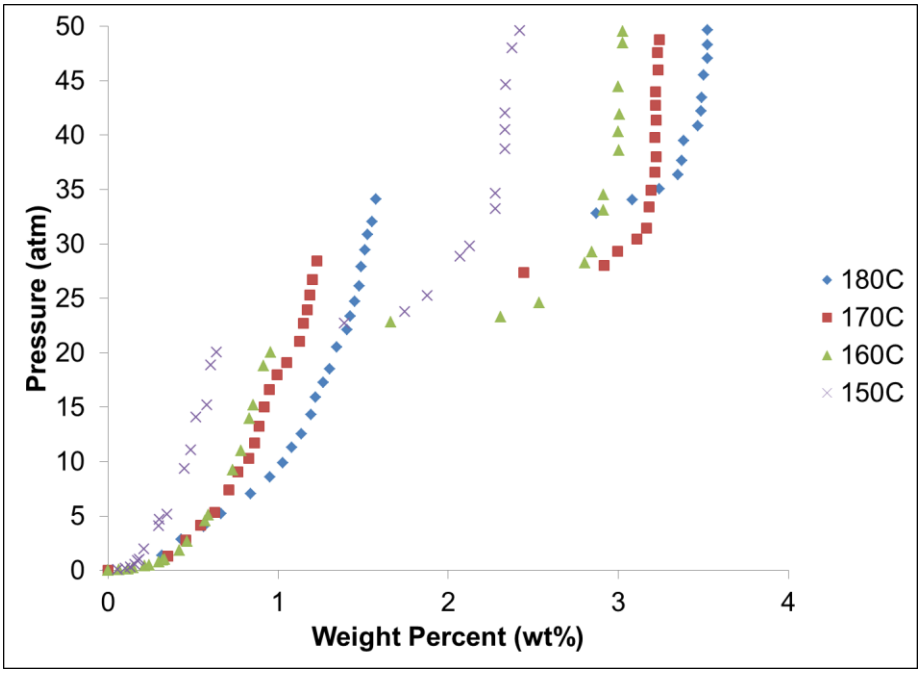

Figure 4.1. Pressure-composition temperature isotherms for absorption study in the range of 150°C-180°C.

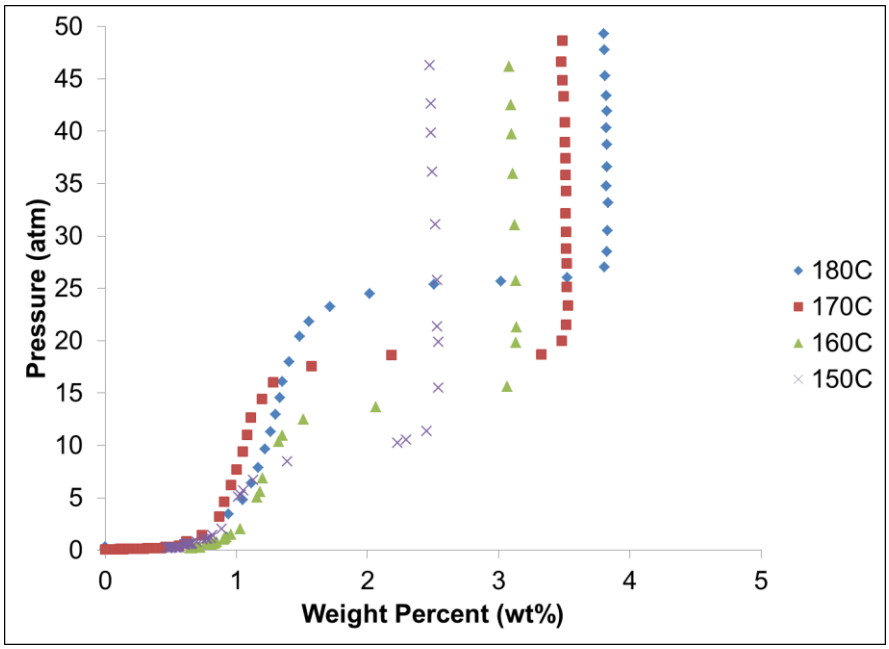

Figure 4.2. Pressure-composition temperature isotherms for desorption in the range of 150°C-180°C.

These isotherms were used to construct the van't Hoff plots shown in **Figure 4.3**. **Equation 4.1** is the van't Hoff equation used to make the plots where P is the plateau pressure, ΔH is the enthalpy of the reaction, R is the gas constant, and T is the absolute temperature. The slopes of these plots were then used to determine enthalpies of absorption and desorption. The values for absorption and desorption enthalpies were found to be 34.3 kJ/mol and 40.9 kJ/mol respectively. In these reactions the absorption process is exothermic whereas desorption is an endothermic process.

$$\ln P = -\Delta H/RT \qquad \text{(Eq. 4.1)}$$

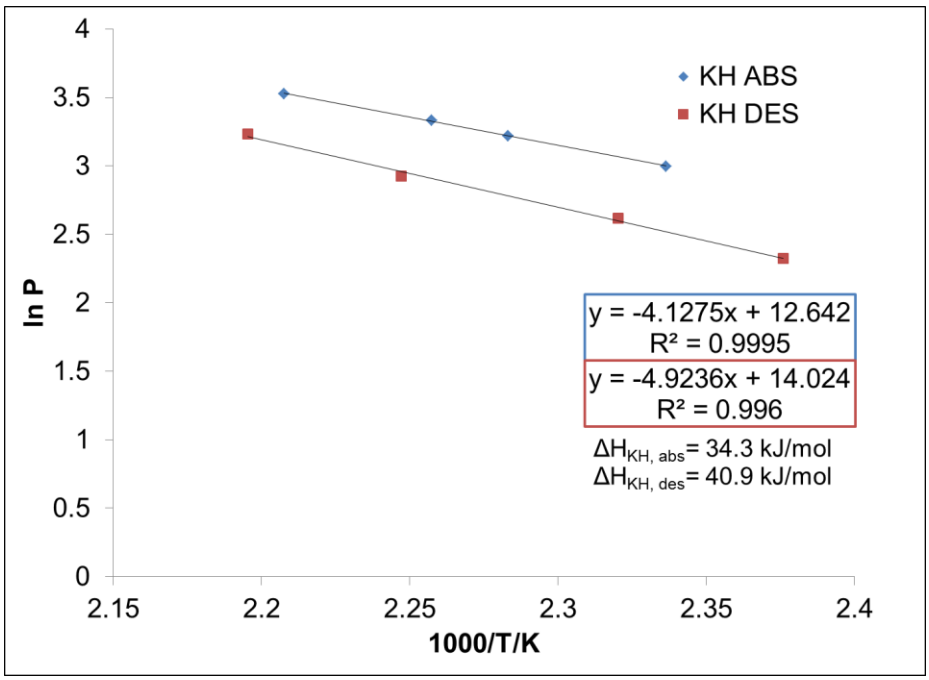

Figure 4.3 Van't Hoff plots for absorption and desorption isotherms of $1.9LiNH_2+1.1MgH_2+0.1KH$ hydrogen storage system.

4.2 Cycling Studies

Cycling studies were conducted on this system to test the durability of the 1.9LiNH2+1.1MgH2+0.1KH system over time. For those experiments, 100 cycles were conducted. Presented in **Figures 4.4 and 4.5** are the plots of PCT isotherms for hydriding and dehydriding cycling studies. The isotherms were measured after every set of 10 absorption/desorption cycles. Those analyses demonstrated how the absorption and desorption plateau changed during pressure/vacuum cycling. In that observation, it was evident that the absorption plateau pressures experienced little variation over time during cycling.

Desorption cycling demonstrated that same phenomena for the plateau pressures for the 10 cycle intervals. This can be seen in **Figure 4.6** with the hysteresis plots. For absorption studies, the plateau pressure was shown to be approximately 47 atm. In contrast, for desorption studies, the plateau pressure was 37 atm.

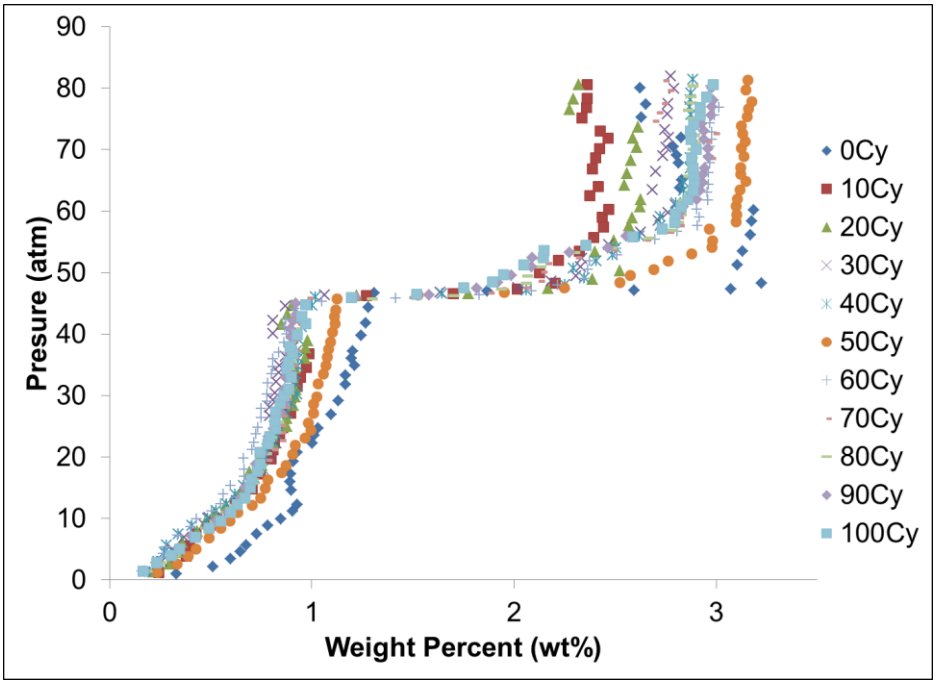

Figure 4.4 Cycling studies for absorption $1.9LiNH_2+1.1MgH_2+0.1KH$ at 200˚C.

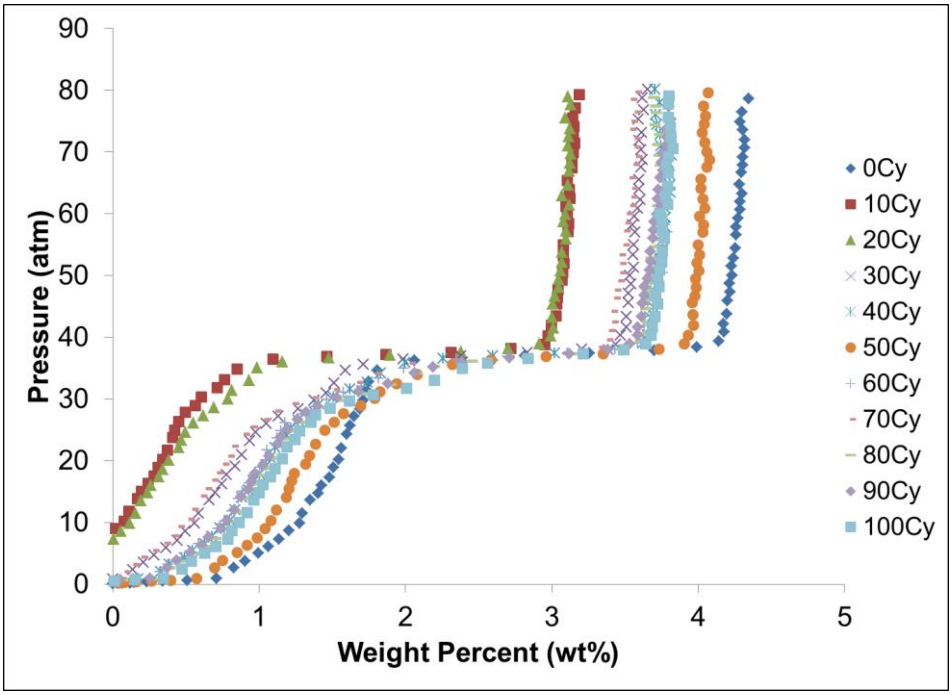

Figure 4.5 Cycling studies for desorption $1.9LiNH_2+1.1MgH_2+0.1KH$ at 200˚C.

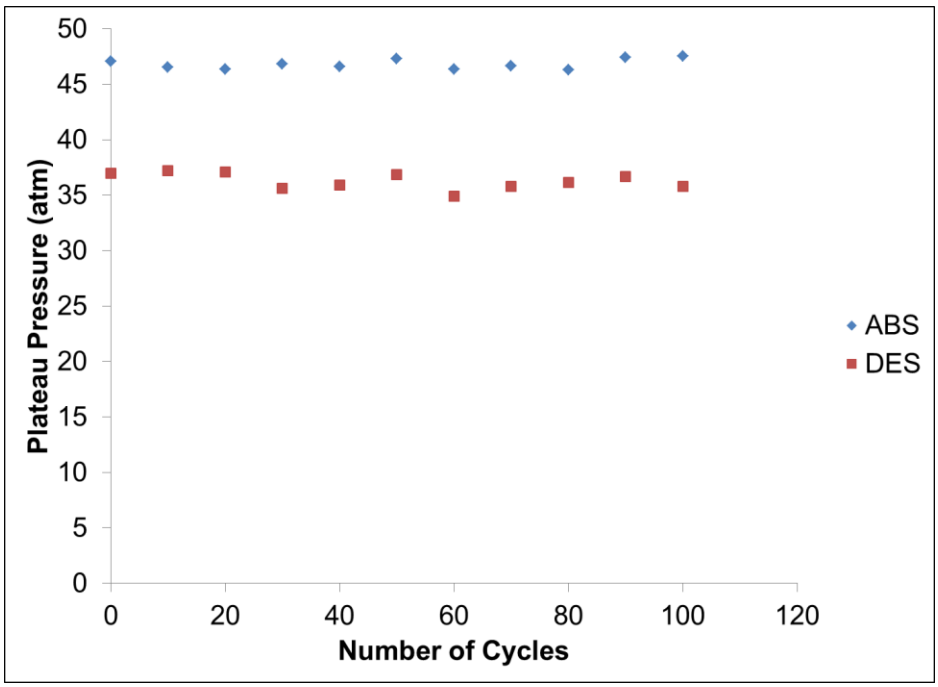

Figure 4.6 Hysteresis plot for absorption and desorption cycling studies of the KH-doped lithium amide-magnesium hydride hydrogen storage system.

4.3 Kinetic and Modeling Studies

Using the plateau pressures from the PCT isotherms, calculations were performed to set the kinetics at a constant thermodynamic driving force. That thermodynamic driving was held constant by a ratio of plateau pressure and the opposing pressure. That ratio is known as the N-value. For desorption studies, the N-value is equal to plateau pressure/opposing pressure. Whereas, the N-value for absorption studies is equals to the opposing pressure/plateau pressure. Table 4.1 shows the mid-plateau pressure and opposing pressure values used for experiments.

For the current study, an N-value of 3 was set for both absorption studies and desorption studies for the KH-doped hydrogen storage system. Both absorption and desorption studies were conducted in a range of 160-180 C. Plots of Reacted Fraction

versus time are presented in **Figures 4.7 and 4.8** in temperature range from 160-180 °C. For absorption studies, the reaction appeared to be 90% completed in approximately 183 minutes for 180°C, 366 minutes for 170°C, and 641 minutes for 160°C. For desorption absorption studies, the time it took for 90% of the reaction to be completed are 455 minutes for 180°C, 683 minutes for 170°C, and 1021.5 minutes for 160°C. This shows that the absorption rates are approximately twice as fast as the desorption rates.

Temperature	**P_m(abs)**	**P_{op}(abs)**	**P_m(des)**	**P_{op}(des)**
160 °C	25 atm	75 atm	13.7 atm	4.6 atm
170 °C	28 atm	84 atm	18.6 atm	6.2 atm
180 °C	32.5 atm	97.5 atm	25.4 atm	8.5 atm

Table 4.1 The plateau pressures and opposing pressure for absorption and desorption kinetic studies at N=3

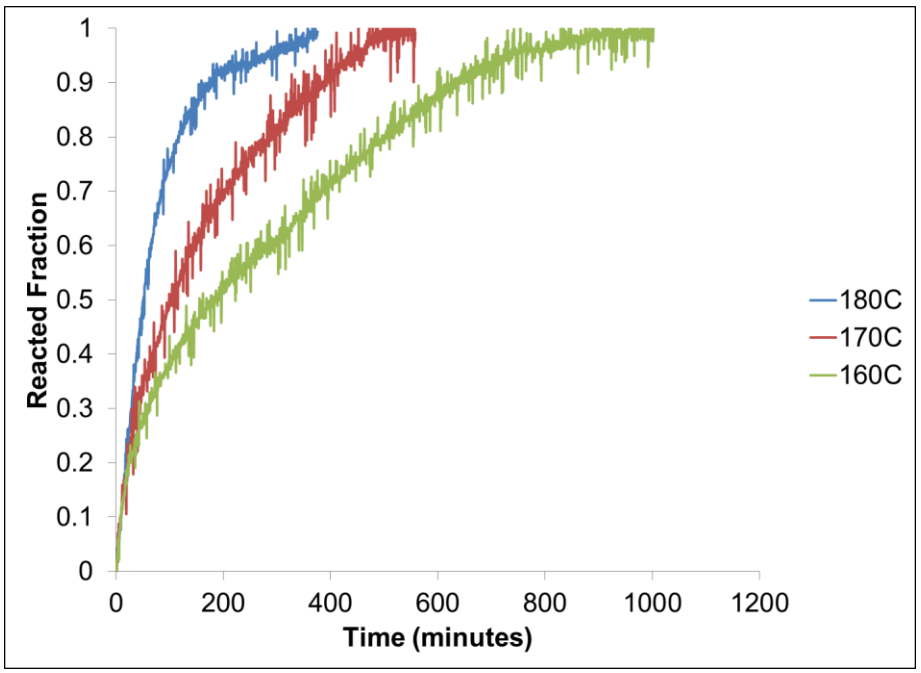

Figure 4.7 Absorption studies for KH-doped $2LiNH_2/MgH_2$ system.

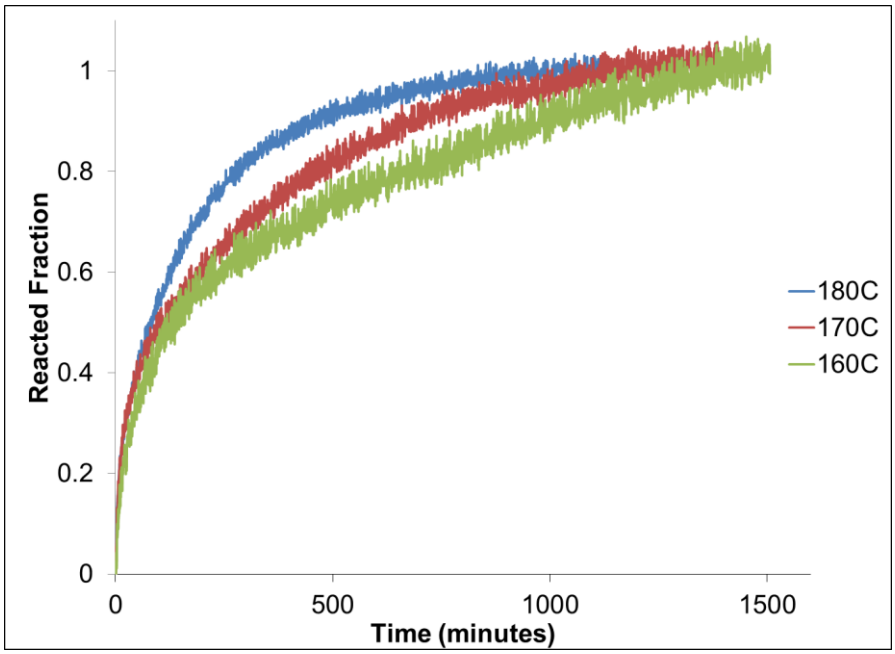

Figure 4.8 Desorption studies for KH-doped $2LiNH_2/MgH_2$ system.

According to physical chemistry criteria, the rate-determining step is the slowest step that occurs in any reaction.[58] For the kinetic analyses of absorption and desorption studies for the KH-doped system, three kinetic models are used to analyze the rate determining step that occurs in a solid-state chemical reaction. Those models consist of diffusion, phase boundary, and nucleation, and growth. Based on existing research literature, there are modeling techniques that can determine how the models fit with the experimental data. The techniques are the following: the shrinking core model technique[42-50], the Hancock and Sharp modeling technique[41], and the Johnson-Mehl-Avarami model techniques. [41,53]

4.3.1 Shrinking Core Model

The shrinking core model has been used and applied to other kinetic reactions of solid state materials. [26,56-57,59] In theory, the chemical particles in a sample are thought to have a core where the gas (in this case, hydrogen) is saturated in the pores. When the particles are heated (or excited in anyway) the gases in the pores will be released out of the system. That process will create a new layer called the product layer while the core "shrinks".[56-57,59]

The model is used to understand the process of the rate-determining step in the reversible reaction of $2LiNH_2/MgH_2$. Presented in **Figure 4.9** is a representation of the theoretical understanding of what occurs in the $2LiNH_2/MgH_2$ using the shrinking core model. For absorption studies, as the hydrogen is added back into the system, the magnesium amide and lithium hydride layer is formed while the $MgLi_s(NH)_2$ (the core)

shrinks. For desorption studies, the hydrogen diffuses out from the system as the $MgLi_2(NH)_2$ layer grows back. There are three processes that were used to determine which model best demonstrates the experimental kinetic data: diffusion, phase boundary (moving boundary), and nucleation and growth. Information presented in **Equations 4.2 and 4.3** represent the diffusion model and phase boundary model. In the current research study, experimental data was obtained and modeled to determine if the same model would fit or if different types of reactions would occur.[41]

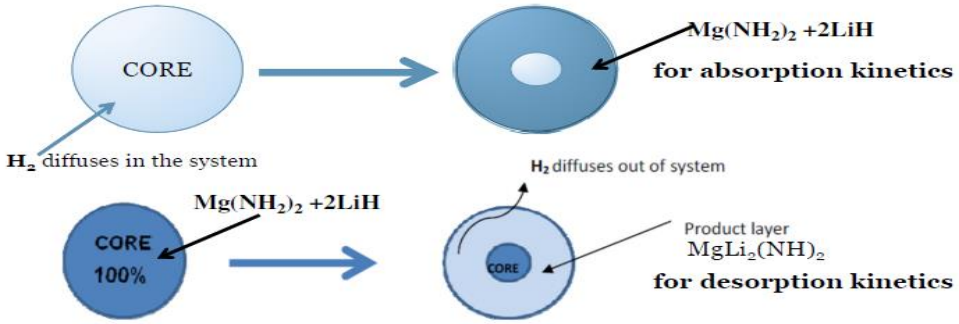

Figure 4.9. Shrinking core model applied to the reversible reaction of
$Mg(NH_2)_2 + 2LiH \leftrightarrow MgLi_2(NH)_2 + 2H_2$

$$\frac{t}{\tau} = 1 - (1 - X_B)^{1/3} \qquad \text{(Eq.4.2)}$$

where $\tau = \dfrac{\rho_B R}{b k_s C_{Ag}}$

$$\frac{t}{\tau} = 1 - 3(1 - X_B)^{2/3} + 2(1 - X_B) \qquad \text{(Eq.4.3)}$$

where $\tau = \rho_B R^2 / 6 b D_e C_{Ag}$,

The value of τ will be determined by statistical analysis. The terms in the equations are the following: X_B is the fraction of the metal shrinking core model; R is the

initial radius of the hydride particles; '*b*' is a stoichiometric coefficient of the metal; *C* is the gas Ag phase concentration of reactant; *D* is the effective diffusivity of hydrogen atoms in the hydride. r is the density B of the metal hydride; and *k* is a rate constant.

Based on the shrinking core model, the results show that the experimental data for absorption at 180°C (**Figure 4.10**) fits the reaction controlled model better during the first 70% of the reaction. The last 30% of the reaction is shown to be controlled by a diffusion mechanism. A possible explanation for the observed behavior is that when hydrogen is absorbed a hydrided product is formed on the surface. As the hydrogen continues to be absorbed, the product layer becomes thicker and the core of dehydrided material shrinks. During this process, hydrogen must diffuse from the outer surface of the particle to the phase boundary between two layers. Thus, there are two processes going on simultaneously: diffusion through the outer product layer and reaction at the phase boundary. The slower of these two processes is the rate controlling step. Initially, the outer product layer is very thin and diffusion through it occurs very quickly. Therefore, reaction at the phase is the slow step. Diffusion becomes the slow step of the reaction when the product layer become relatively thick. A similar phenomenon occurs for the modeling of 170 °C (**Figure 4.11**) and 160 °C (**Figure 4.12**) respectively. When the reaction curves for 180, 170, and 160 does not fit either of the curves, it shows that the thermodynamic driving force changes over time as the reaction is not on the plateau anymore.

For desorption studies however, the experimental curves follows the diffusion mechanism for approximately 70% of the reaction. After that, the curve diverge due to the change of N-value as the reaction moves off the plateau.

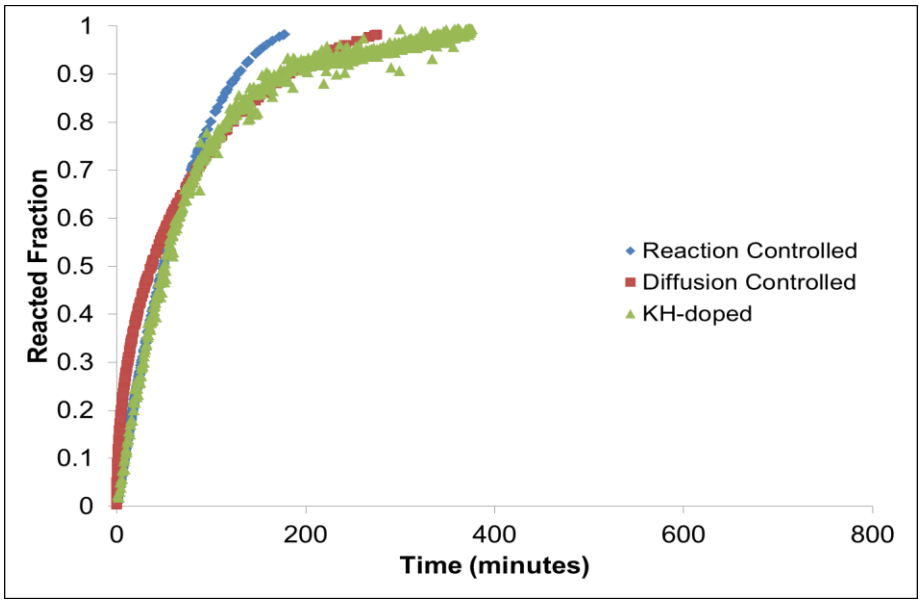

Figure 4.10 Shrinking core model for absorption studies for KH-doped $2LiNH_2/MgH_2$ system at 180 °C.

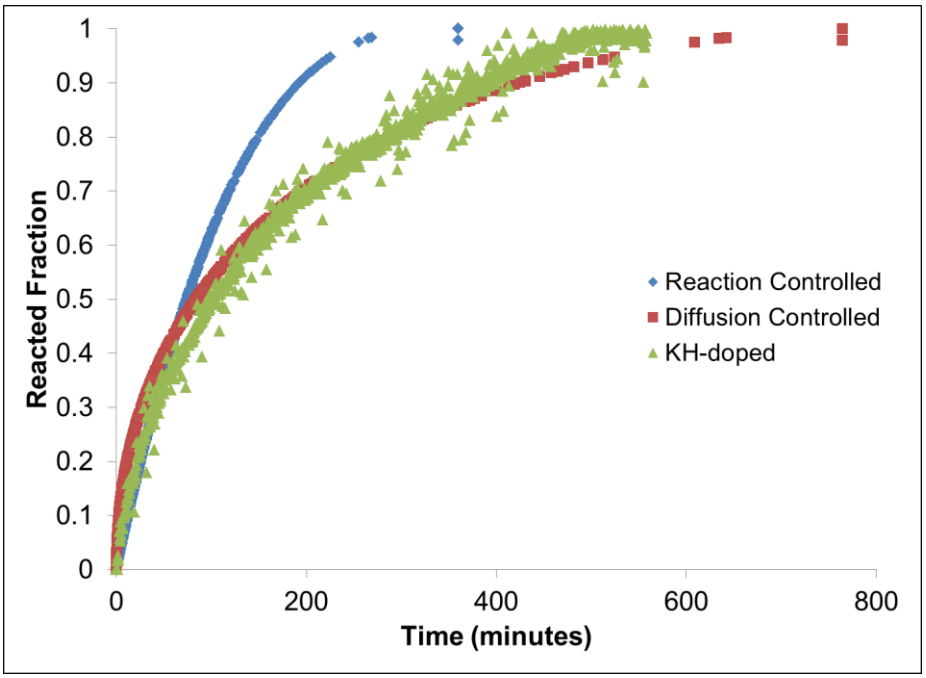

Figure 4.11 Shrinking core model for absorption studies for KH-doped $2LiNH_2/MgH_2$ system at 170 ˚C

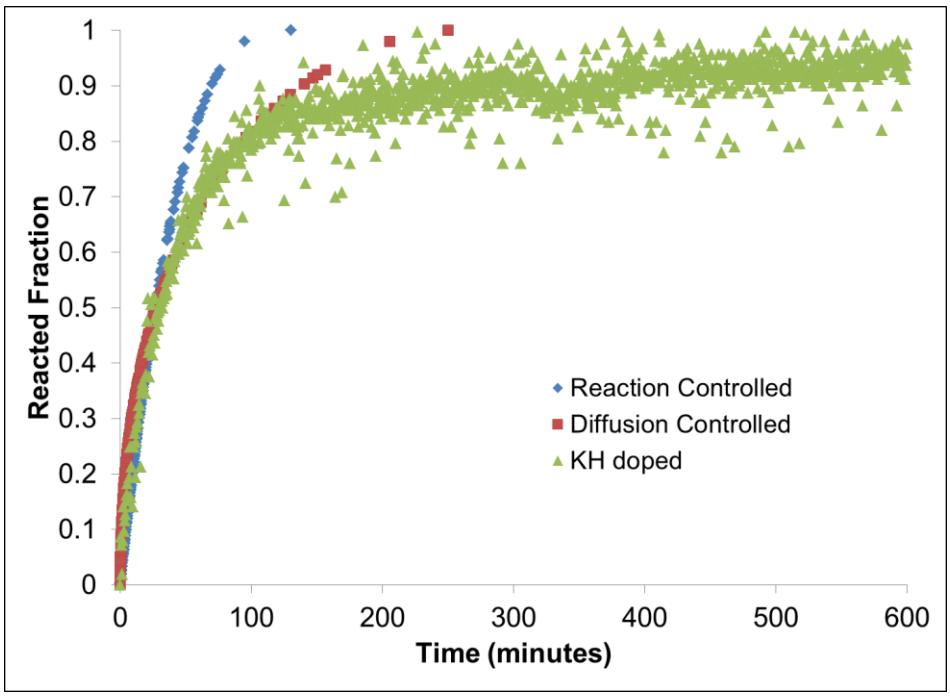

Figure 4.12 Shrinking core model for absorption studies for KH-doped $2LiNH_2/MgH_2$ system at 160 ˚C

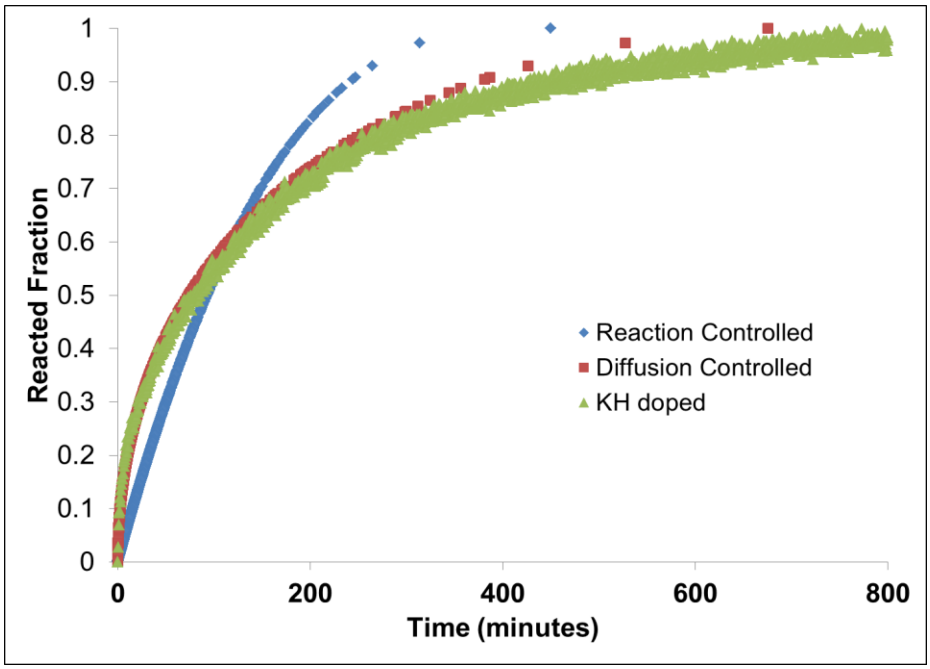

Figure 4.13 Shrinking core model of $1.9LiNH_2+1.1MgH_2+0.1KH$ desorption study at T=180 °C.

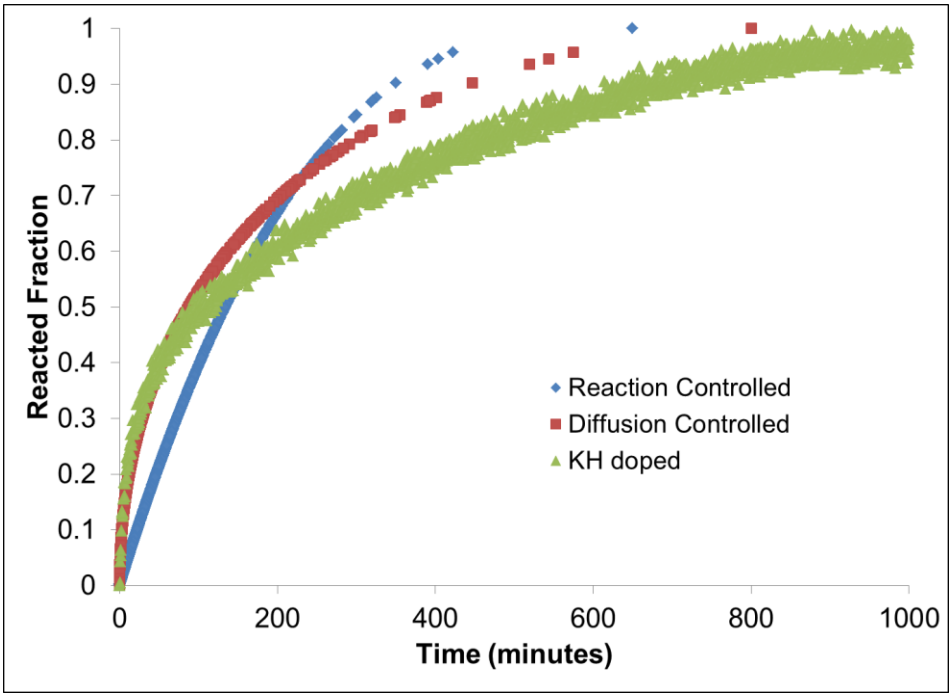

Figure 4.14 Shrinking core model of $1.9LiNH_2+1.1MgH_2+0.1KH$ desorption study at T=170 °C.

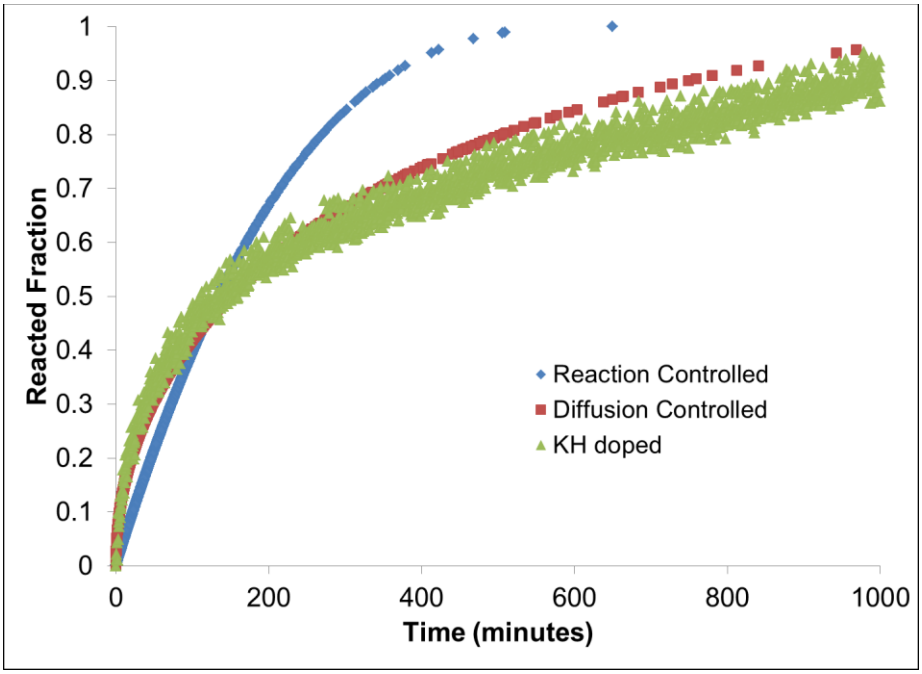

Figure 4.15 Shrinking core model of $1.9LiNH_2+1.1MgH_2+0.1KH$ desorption study at T=160 °C.

4.3.2. Johnson-Mehl-Avrami (JMA) Equations for Modeling

For the current experimental studies, Johnson-Mehl-Avrami equations were used to analyze the phase transformations that occurred in the $1.9LiNH_2+1.1MgH_2+0.1KH$ hydrogen storage system. Based on various research studies, the JMA equations have been consistently used to explain theoretical mechanisms of solid-state materials (particularly hydrogen storage). Based on the Arrhenius equations, it is understood that most average solid-state materials undergo first-order rate reactions.[56] Based on the 1939 - 1942 research papers, three scientists collectively formulated equations that are still used to help described the reactions for the kinetics of many solid-state materials. Yang et al used JMA plots for explaining the kinetic results of dehydrogenation and rehydrogenation under constant pressure driving forces for sodium alanate.[53] The three equations that have been used in the existing research literature and were used in the current study are the following:

$$(1-f)^{1/3}= 1- (\sqrt{kt})/R \qquad \text{(Eq.4.4)}$$

$$(1-f)^{1/3}= 1- (k/R)t \qquad \text{(Eq.4.5)}$$

$$f=1-\exp(-kt^n) \qquad \text{(Eq.4.6)}$$

Eqs 4.4-4.6 The Johnson-Mehl-Avarami kinetic modeling equations for calculating rate-determining step.

Equation 4.4 represents diffusion controlled model, **Equation 4.5** represent reaction-controlled model, **and Equation 4.6** represents nucleation and growth model. F is the reacted fraction, k is a constant, t is the time, and R is the gas constant value 8.314.

Theoretically, it can be determine which mechanism occurs in the experiment and how much the experimental data correlates with the linearity of the equation. According to Yang et al, it has demonstrated that there are two different mechanisms for the sodium alanate system. For desorption, it has been demonstrated that the reaction is controlled by diffusion whereas the absorption process is reaction controlled.

Durojaiye et al, they reported the KH-doped system follows the diffusion model for its rate-determining step in desorption studies.[77] In addition, the present results from the shrinking core model have presented evidence that diffusion is the rate-determining step as well. In order to provide further confirmation in the current this study, JMA plots for both absorption and desorption were prepared and then analyzed. These plots can be seen in **Figures 4.16-4.18** for absorption and desorption studies respectively. For absorption studies, it can be observed that the plots for temperature range 160-180°C present a change in slope at the end of the plots for both reaction controlled and diffusion shown in **Figures 4.16 and 4.17**. This confirms the change from the reaction-controlled model to diffusion-controlled in the shrinking core model observed in **Figures 4.10-4.12** for temperatures at 180 °C, 170 °C, and 160 °C respectively.

For desorption studies, the JMA model results indicate that there was a strong linear correlation for the diffusion controlled model. This confirms the results that were discussed in the shrinking core model for the desorption studies at each given temperature.

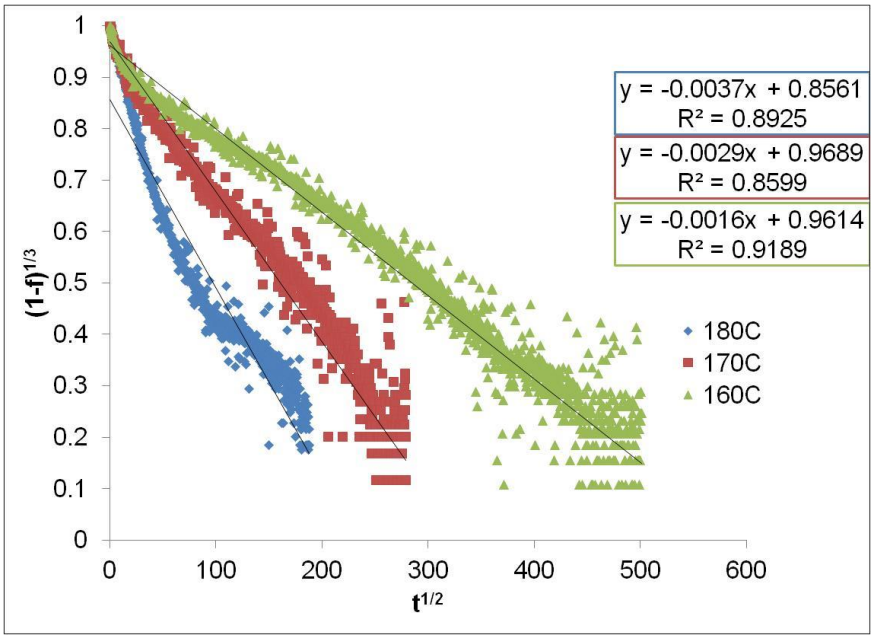

Figure 4.16 JMA model of diffusion for $1.9LiNH_2+1.1MgH_2+0.1KH$ absorption study at various temperatures.

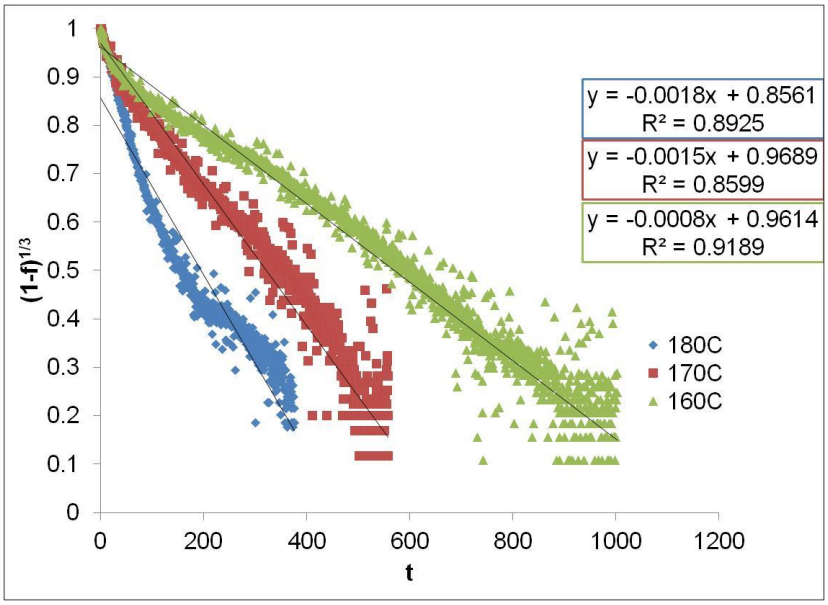

Figure 4.17 JMA model for phase boundary for$1.9LiNH_2+1.1MgH_2+0.1KH$ absorption study at various temperatures

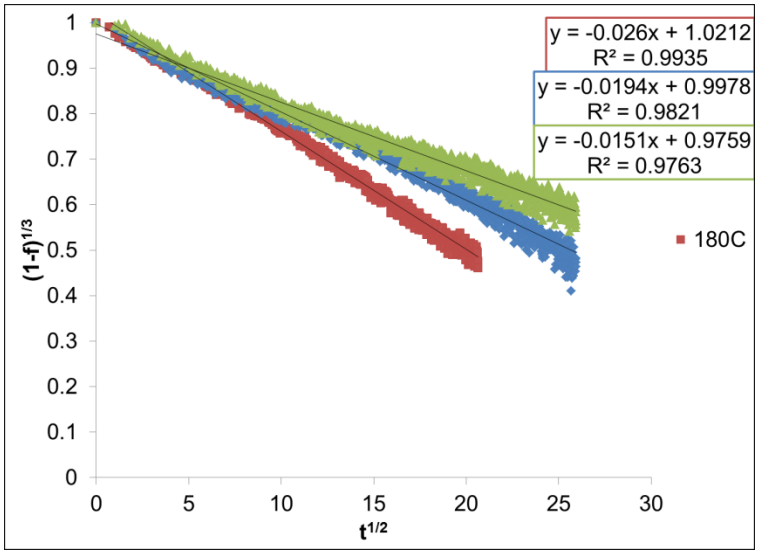

Figure 4.18 JMA model of diffusion for $1.9LiNH_2+1.1MgH_2+0.1KH$ desorption study at various temperatures.

4.3.3. Hancock and Sharp Model

In 1972, two scientists, Hancock and Sharp derived an equation based on the JMA equations. This equation can be seen in **Equation 4.7** below where t is the time at which the reactions occurred whereas f is the reacted fraction. Their objective was to analyze specifically the decomposition of calcium carbonite ($CaCO_3$) and the mechanism of its decomposition. According to metallurgy and solid-state materials, calcium carbonate is known to be a test material for testing out novel kinetic models. For the Hancock and Sharp method, certain values of the slope from the equation are analogous to the three different models that were discussed in a previous publication: diffusion, reaction-controlled, and nucleation and growth.[60]

$$\text{Ln } t = \text{Ln ln}(1-f) \qquad \text{(Eq.4.7)}^{60}$$

In the studies that will be discussed, this model was used to further describe desorption kinetic results of the KH-doped system. This kinetic model will also be used

and discussed in the latter chapters 5 and 6 for RbH-doped and CsH-doped lithium amide/magnesium hydride hydrogen storage systems respectively. However, this modeling technique was only used to describe the desorption studies regarding the system of our primary focus.[60]

The Hancock and Sharp model was also used to confirm the desorption studies for the KH-doped system. That model indicates that the slope will determine if the rate-controlling step is either diffusion controlled or reaction controlled at the phase boundary. According to the Hancock and Sharp model, if the slope is in the range of 0.50-0.60, the rate-controlling step is diffusion. Whereas, if the range is 0.60 and above, it will be phase boundary-controlled. Based on the kinetic results of the KH-doped system in **Figure 4.19**, the plots indicated that the slopes were 0.6058, 0.5354, 0.5215, for 160 °C, 170 °C, 180 °C respectively. The slope values indicate that at each temperature, the KH-doped sample is diffusion-controlled for desorption studies.

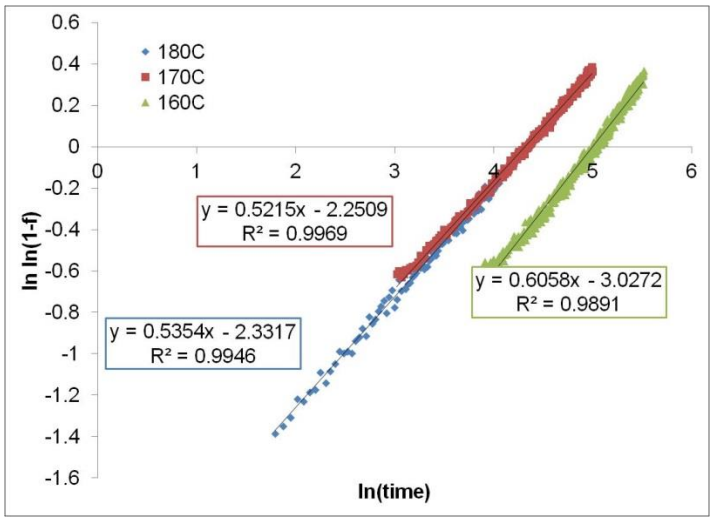

Figure 4.19 Hancock and Sharp model of $1.9LiNH_2+1.1MgH_2+0.1KH$ desorption study at various temperatures.

4.4 Activation Energy Determination

To show that KH had acted as a catalyst in regards to the $2LiNH_2/MgH_2$ system, observations of the activation energy had to be conducted. According to findings in the previous research literature and other chapters in the current study, the activation energy of the un-doped system was 119 kJ/mol. The activation energy for the KH-doped material was reported to be 87.0 kJ/mol from the Kissinger plot in **Figure 4.23**. For the current study, the activation energy of the sample was analyzed by using both Kissinger plots and Arrhenius plots. The activation energies for absorption studies were determined by Arrhenius plots and not Kissinger plot. A comparison of Kissinger plots and Arrhenius plots for desorption studies will be determined.

For absorption studies, a first-order equation (**Equation 4.8**) was used to construct the first-order plots shown in **Figures 4.20 and 4.21** where f represent the reacted fraction, k is the slope (rate constant), and t is the time for the reaction. The first-order plot slopes were used to determine the Arrhenius plots and thus the activation energy of the system. Based on the Arrhenius plot in **Figure 4.22**, the activation energy for absorption study of KH-doped system was determined to be 83.9 kJ/mol. Based on the Arrhenius plot for desorption (**Figure 4.22**), the activation energy results was 89.3 kJ/mol compared to 87.0kJ/mol resulted from the Kissinger plot in **Figure 4.23**.

$$\ln(1-f) = -kt \qquad \text{(Eq. 4.8)}$$

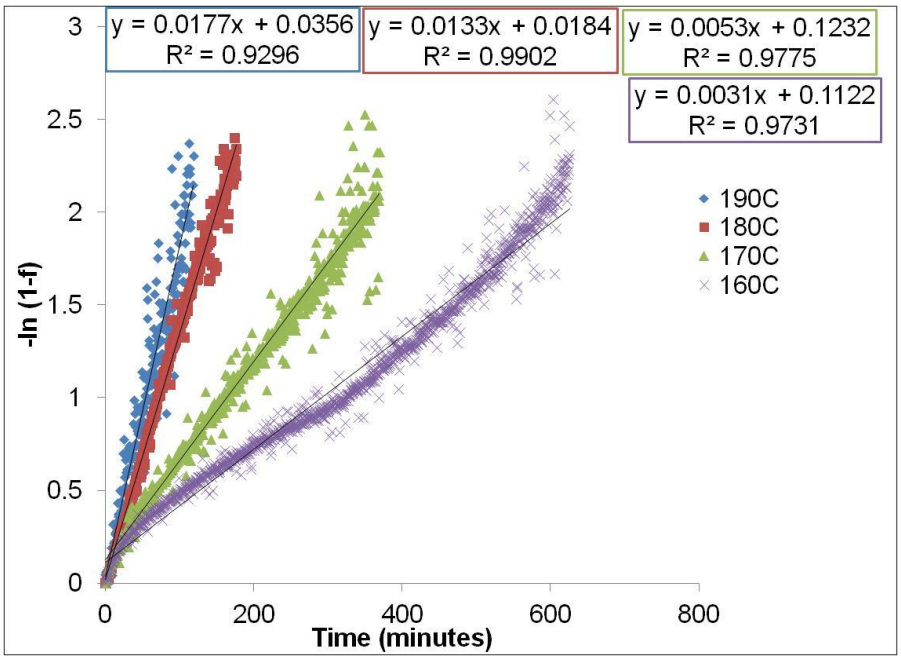

Figure 4.20 First order plots for absorption studies of KH-doped $2LiNH_2/MgH_2$ hydrogen storage system

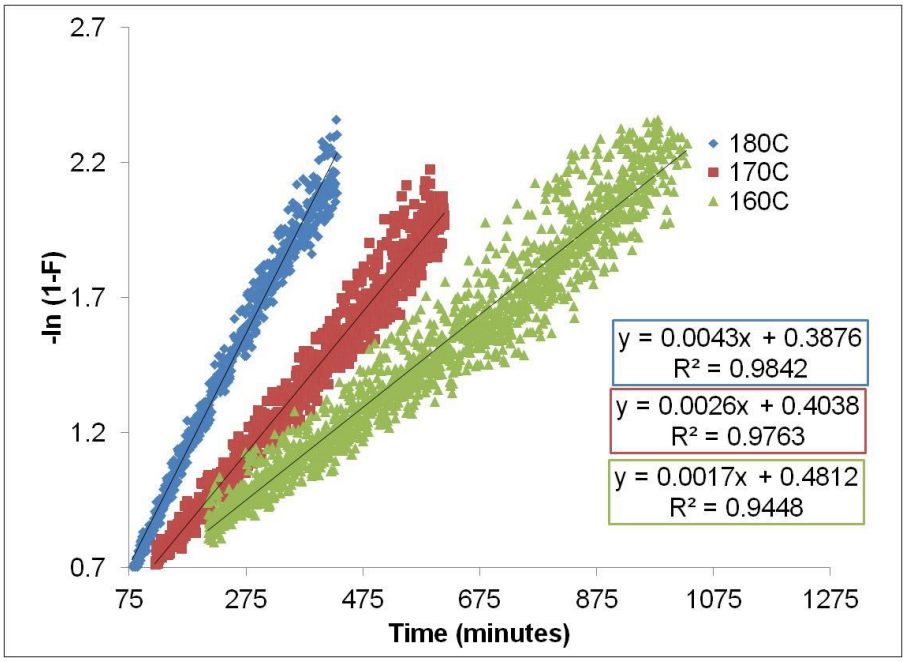

Figure 4.21 First order plots for desorption studies of KH-doped $2LiNH_2/MgH_2$ hydrogen storage system

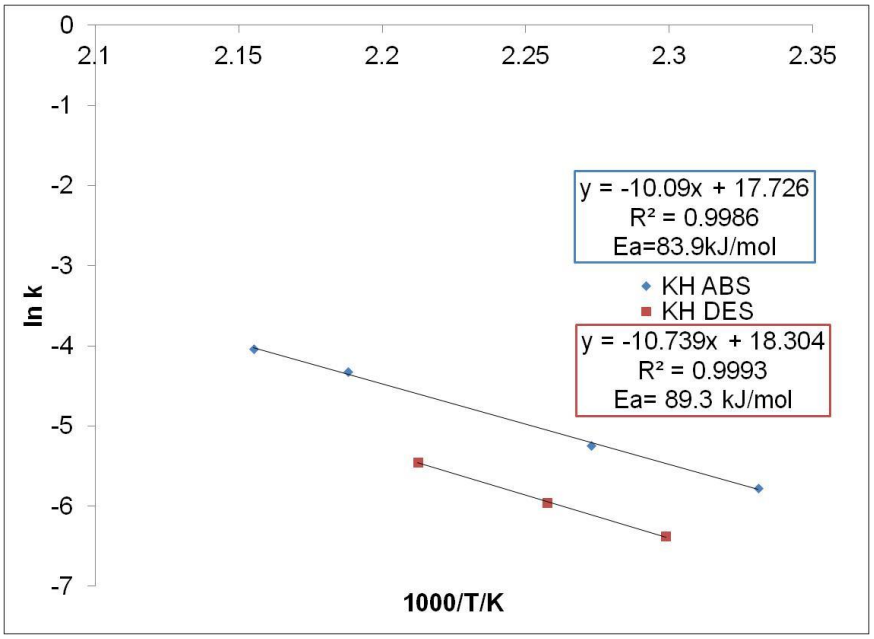

Figure 4.22 Arrhenius plots for absorption and desorption studies of KH-doped $2LiNH_2/MgH_2$ hydrogen storage system

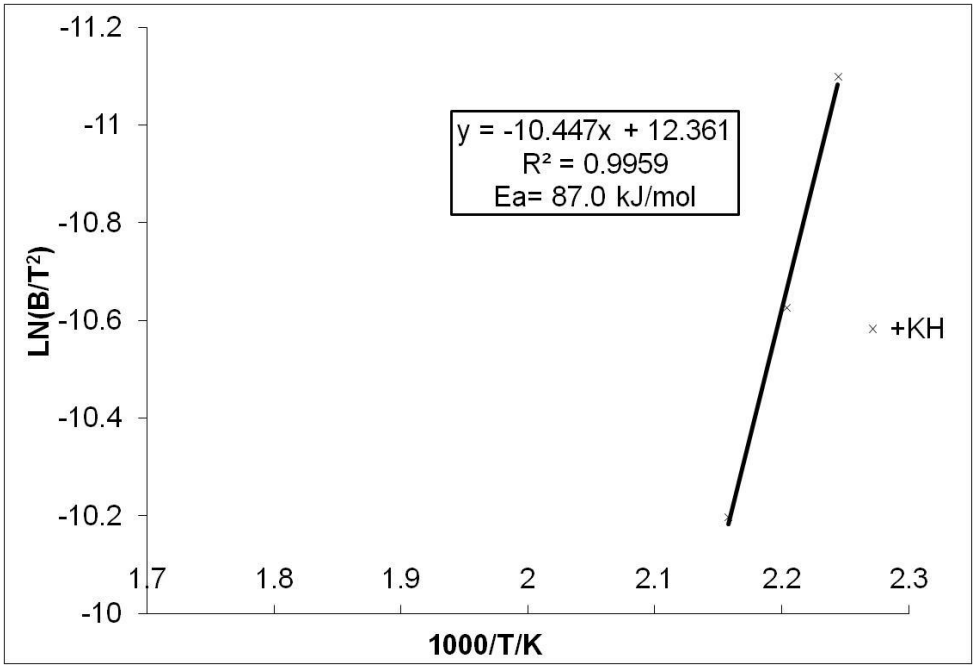

Figure 4.23 Kissinger plot for desorption kinetic studies of KH-doped system

4.5 Summary

Findings of the current study indicated that KH is an effective catalytic additive for increasing the rates of both hydrogen absorption and desorption from the $2LiNH_2/MgH_2$ system. The enthalpy values for absorption were significantly less than the desorption values thus indicating that the hydrides were more stable than the dehydrided reactants. For cycling studies, there was little to no variation in the amount of hysteresis in this system. However, the weight capacity of the KH-doped system increased during the first 50 absorption/desorption cycles. Moreover, after the 50 cycles, a 30% decrease began to appear until the completion of up to the 100 cycles. Modeling studies revealed that the absorption studies are controlled by reaction at the phase boundary during the first part of the reaction and diffusion in the latter stages. However, for desorption, diffusion is the rate limiting step for the entire process until the N-value changes in the reaction. This shows that diffusion occurs much faster during the absorption studies than in the desorption studies. In determining activation energies, Arrhenius plot and Kissinger plots for KH-doped system were constructed. For absorption studies, the Arrhenius plots showed that the activation energy was 83.9 kJ/mol. For desorption studies, Arrhenius plots showed 89.3 kJ/mol to be the activation energy value whereas the Kissinger plot resulted in a value of 87.0 kJ/mol for the activation energy. This shows that the Kissinger method and Arrhenius method are similar in determining the activation energy for the desorption processes.

CHAPTER 5

HYDRIDING AND DEHYDRIDING RUBIDIUM HYDRIDE-DOPED LITHIUM AMIDE-MAGNESIUM HYDRIDE SYSTEM

Background

In the current research study, thermodynamic and kinetic properties of RbH-doped $2LiNH_2/MgH_2$ were measured. In addition, measurement results were inspected to determine consistency regarding hydrogen absorption and desorption in the temperature range of 150-180 °C. All of those efforts were geared toward meeting or exceeding the United State Department of Energy required standards.

5.1 PCT Isotherms

Isotherm measurements for the $1.9LiNH_2+1.1MgH_2+0.1RbH$ were conducted in the range of 150-180 °C. The results for absorption PCT measurements are presented in **Figure 5.1**. As was hypothesized, each isotherm displays a well-defined plateau region in which lower temperatures resulted in lower plateau pressures. Additional observations indicated that the weight percent generally increased with increasing temperatures. Similar plots were obtained for desorption PCT isotherms and are presented in **Figure 5.2**. Those isotherms were used to construct the van't Hoff plots that are presented in **Figure 5.3**. Then the slopes of those plots were used to determine enthalpies of absorption and desorption. The resulting values for absorption and desorption enthalpies were 39.7kJ/mol and 43.0kJ/mol respectively. The desorption enthalpy value is similar to

the desorption enthalpy value that was reported by Durojaiye et al.[41] Their measurements were done in the 200-230°C range. Currently, the existing research literature does not contain reports regarding any other absorption enthalpies reported for the RbH-doped system.

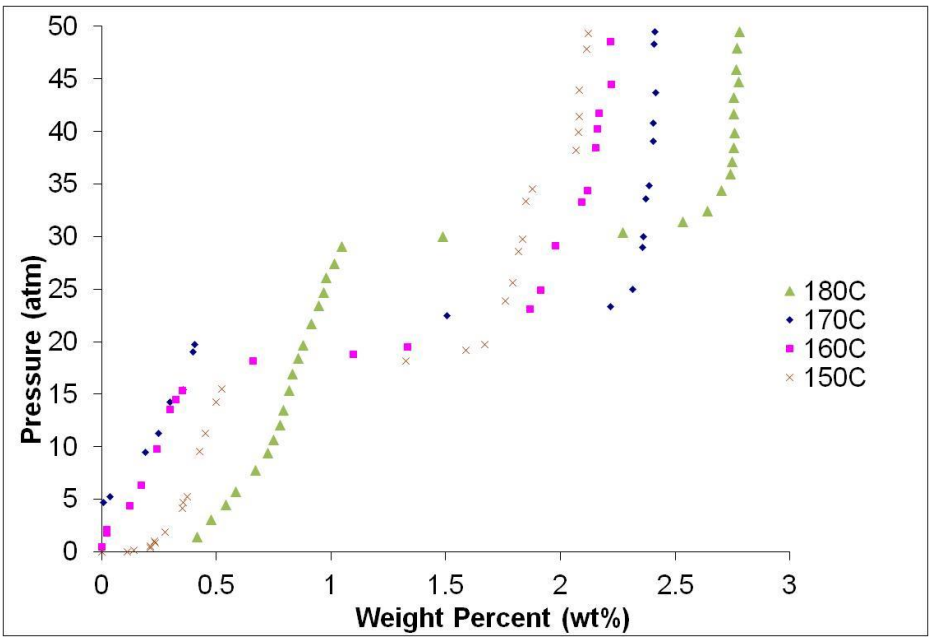

Figure 5.1 The Absorption PCT isotherms for RbH-doped $2LiNH_2/MgH_2$ system.

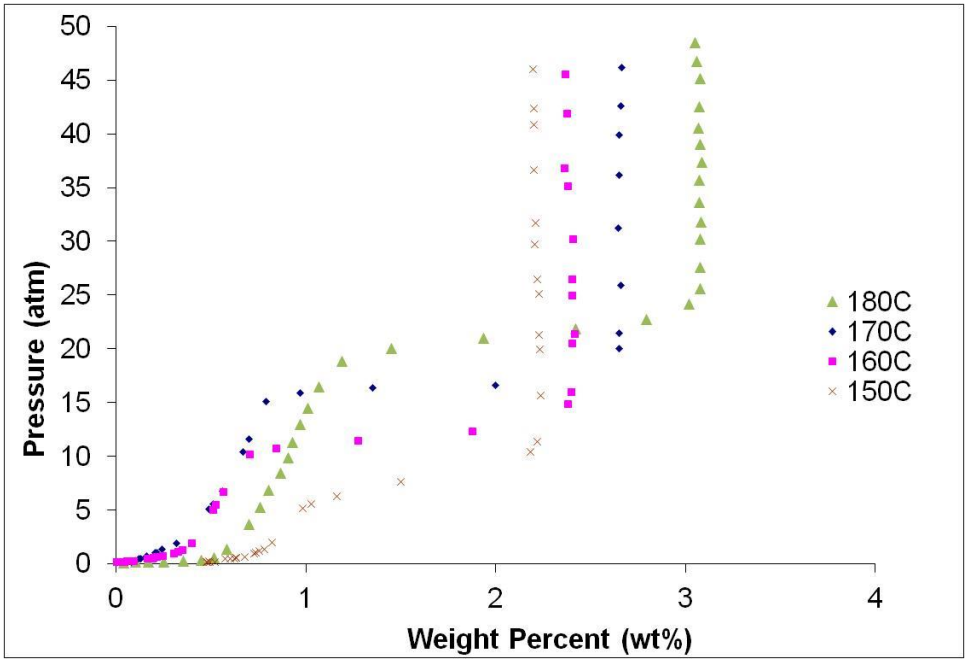

Figure 5.2 The Desorption PCT isotherms of RbH-doped $2LiNH_2/MgH_2$ system

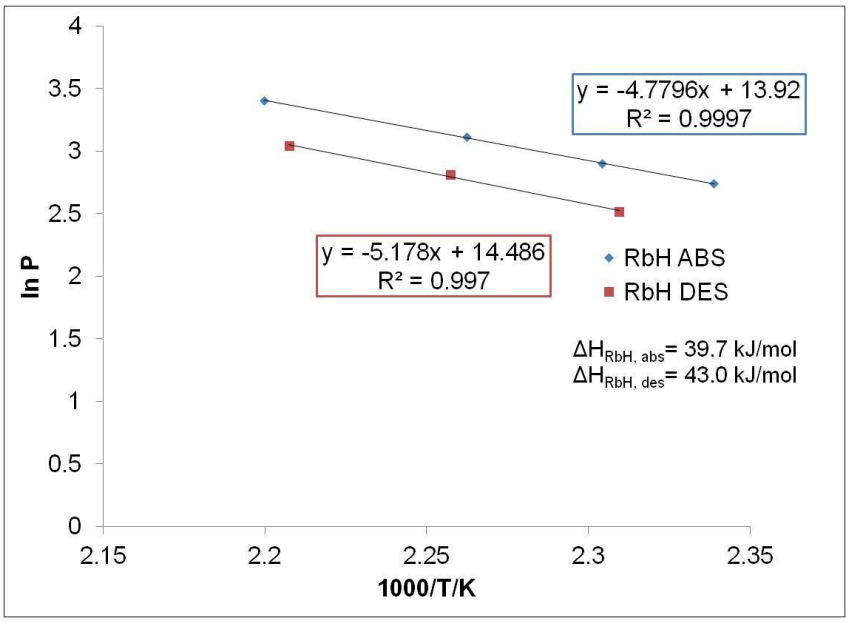

Figure 5.3 The Van't Hoff plots of both absorption and desorption PCT isotherms for RbH-doped system

5.2 Cycling Studies

Cycling studies were conducted on this system in order to measure the durability over time after 100 cycles. Presented in **Figures 5.4 and 5.5** are the results of the cycling studies that were conducted using PCT isotherms at a constant temperature of 200 °C. Presented in **Figure 5.6** is a pair of absorption and desorption isotherms that were obtained at 200°C after 20 absorption/desorption cycles. Those plots demonstrate that there is a significant amount of hysteresis in the system. Presented in **Figure 5.7** are plots of the cycle number versus plateau pressure. The isotherms were measured after every set of 10 absorption/desorption cycles. Results of those analyses demonstrate how the absorption and desorption plateau pressure changed during pressure/vacuum cycling. The resulting evidence indicates that the absorption plateau pressures gradually increase. At

the same time, desorption pressures decrease during cycling. The difference between the absorption and desorption plateau prior to cycling was 8 atm. The results in **Table 5.1** show the increase and decrease of absorption and desorption plateau pressures respectively. The difference increased to 50 atm after 70 cycles. Also, the hydrogen holding capacity decreased by approximately 30% when moving from 0 to 70 cycling.

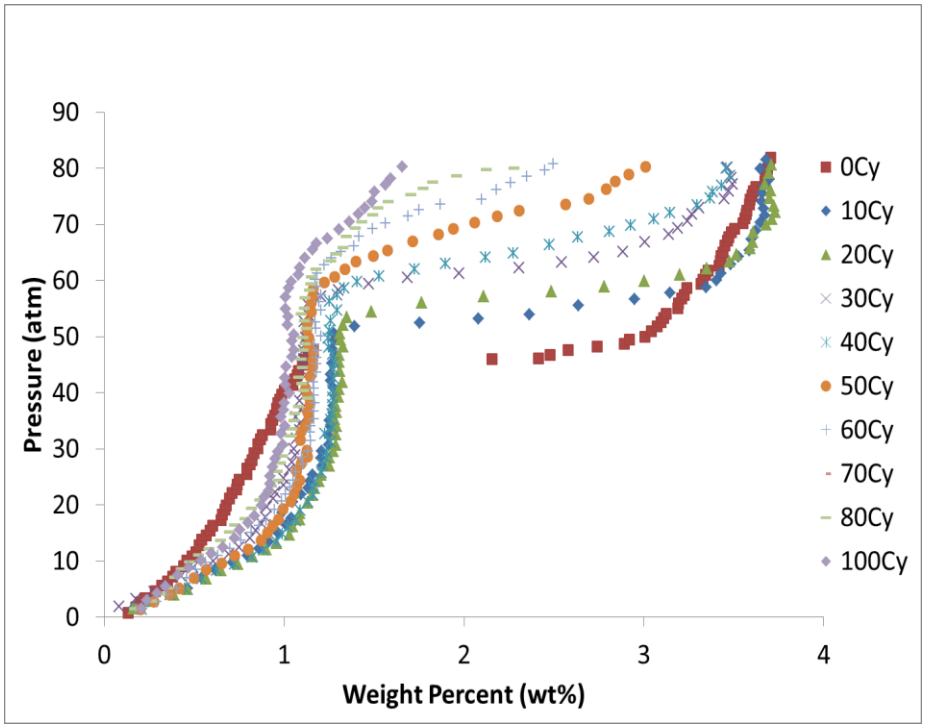

Figure 5.4 The Cycling studies of PCI absorption for the RbH-doped system

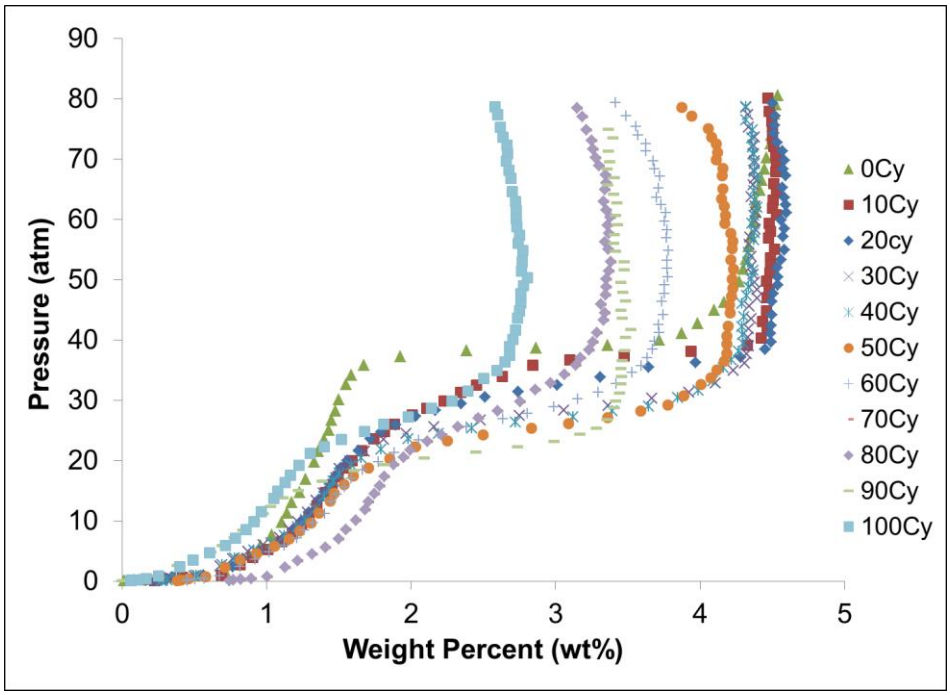

Figure 5.5 The Cycling studies for PCI desorption for the RbH-doped system.

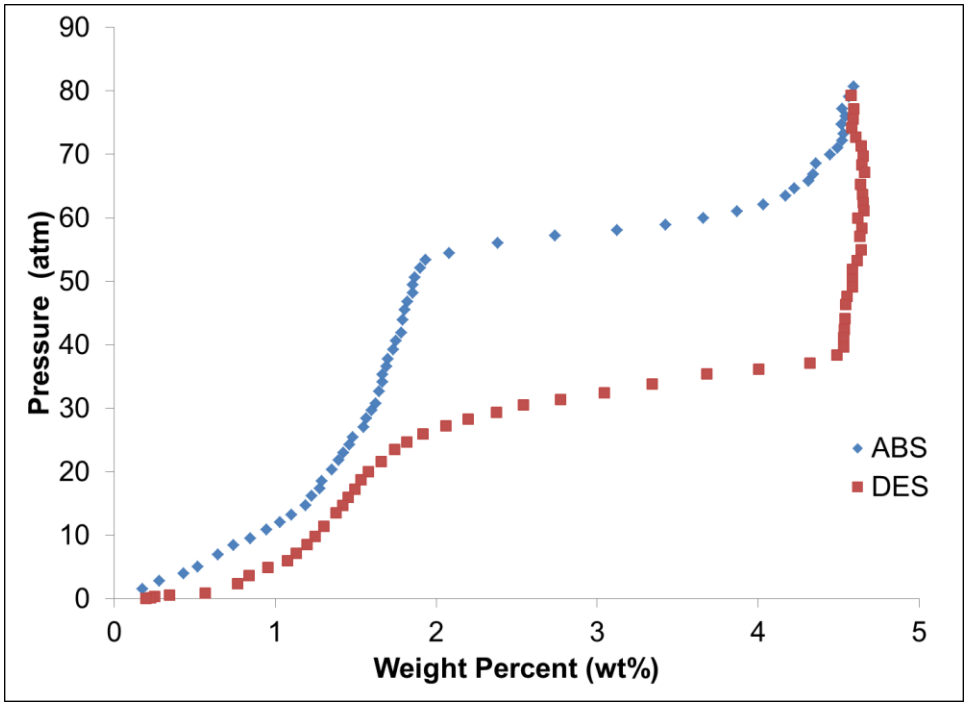

Figure 5.6 The Absorption and desorption isotherm after 20 cycles at a constant temperature at 200 ˚C.

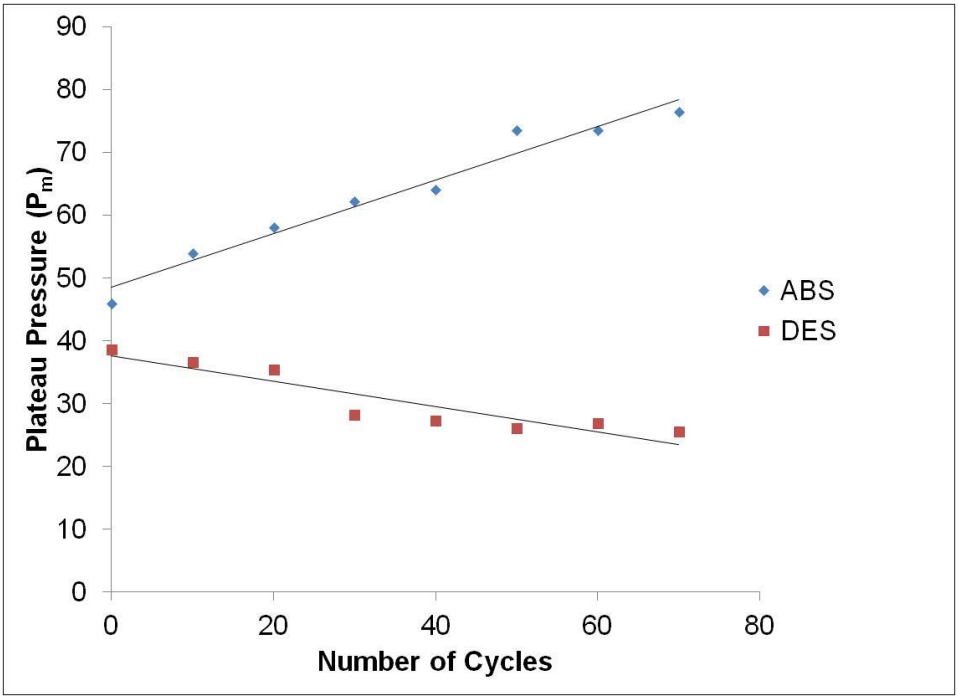

Figure 5.7 The Hysteresis plot of absorption and desorption plateau pressures during the cycling study

Number of Cycles	**Plateau Pressure ($P_{m\,(abs)}$) R^2= 0.9633**	**Plateau Pressure ($P_{m\,(des)}$)** R^2= 0.6824
0	45.99	38.68
10	53.97	36.6
20	58.04	35.44
30	62.22	28.19
40	64.06	27.27
50	73.5	26.07
60	73.59	26.85
70	76.43	25.53
80	No P_m formed	29.697
90	No P_m formed	22.277
100	No P_m formed	25.97

Table 5.1 Cycling studies that were conducted on the RbH-doped system.

5.3 Kinetics and Modeling Studies

In order to be utilized for many practical applications, a potential hydrogen storage system should undergo hydriding and de-hydriding reactions rapidly and reversibly. Therefore, kinetics measurements were done and comparisons were made of the absorption and desorption rates of the RbH-doped $2LiNH_2/MgH_2$ system at a temperature range of 160°C-180 °C under equivalent conditions. That inspection process was accomplished by using an N-value of 3 for the hydriding and dehydriding processes. Presented in **Table 5.2** are the mid-plateau pressures and the opposing pressures at N=3. Presented in **Figure 5.8** are the absorption kinetic plots for the RbH-doped $2LiNH_2/MgH_2$ system at temperatures of 160 °C, 170 °C, and 180 °C. The absorption reactions appeared to be 90% when completed in approximately 107.5 minutes for 180 ˚C, 225 minutes for 170 °C, and 405 minutes for 160 °C.

Temperature	**P_m(abs)**	**P_{op}(abs)**	**P_m(des)**	**P_{op}(des)**
160 °C	18.2 atm	54.6 atm	12.3 atm	4.1 atm
170 °C	22.5 atm	67.5 atm	16.7 atm	5.6 atm
180 °C	30.1 atm	90.2 atm	21.1 atm	7.03 atm

Table 5.2 The plateau pressures and opposing pressure for absorption and desorption kinetic studies at N=3

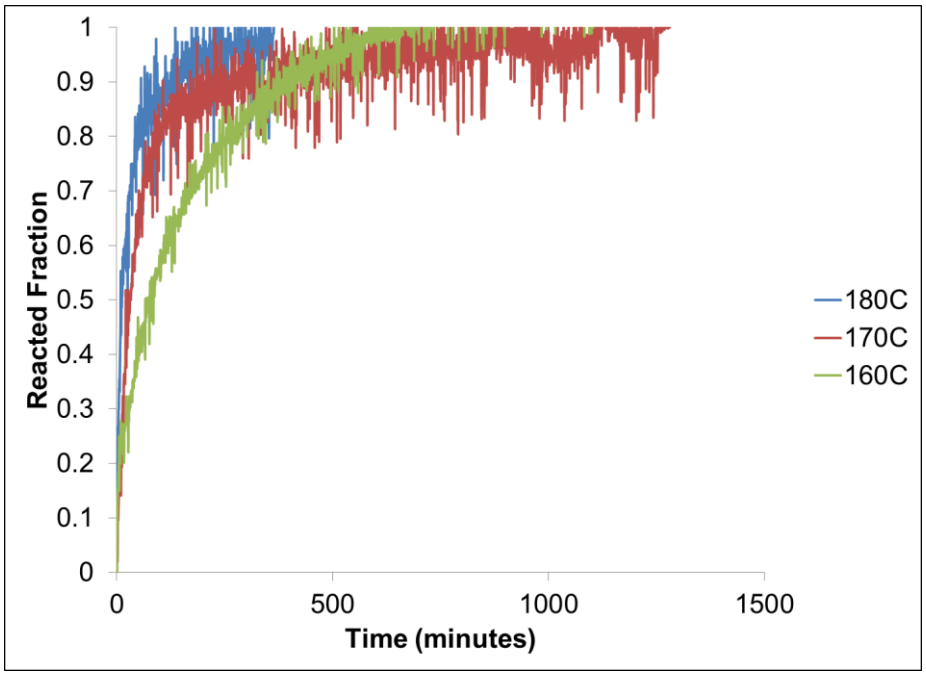

Figure 5.8 The absorption studies of RbH-doped $2LiNH_2/MgH_2$ hydrogen storage system

Presented in **Figure 5.9** are desorption kinetics results in the temperature range of 160°C-180 °C. The results of the desorption kinetic studies show that ninety percent (90%) of the reactions were completed in approximately 213 minutes , 439 minutes, and 804 minutes at 180 °C, 170 °C, and 160 °C respectively. As was previously hypothesized, the lower the temperature, the slower the reaction. Comparing to the absorption studies, desorption rates are shown to be approximately twice as slow as absorption.

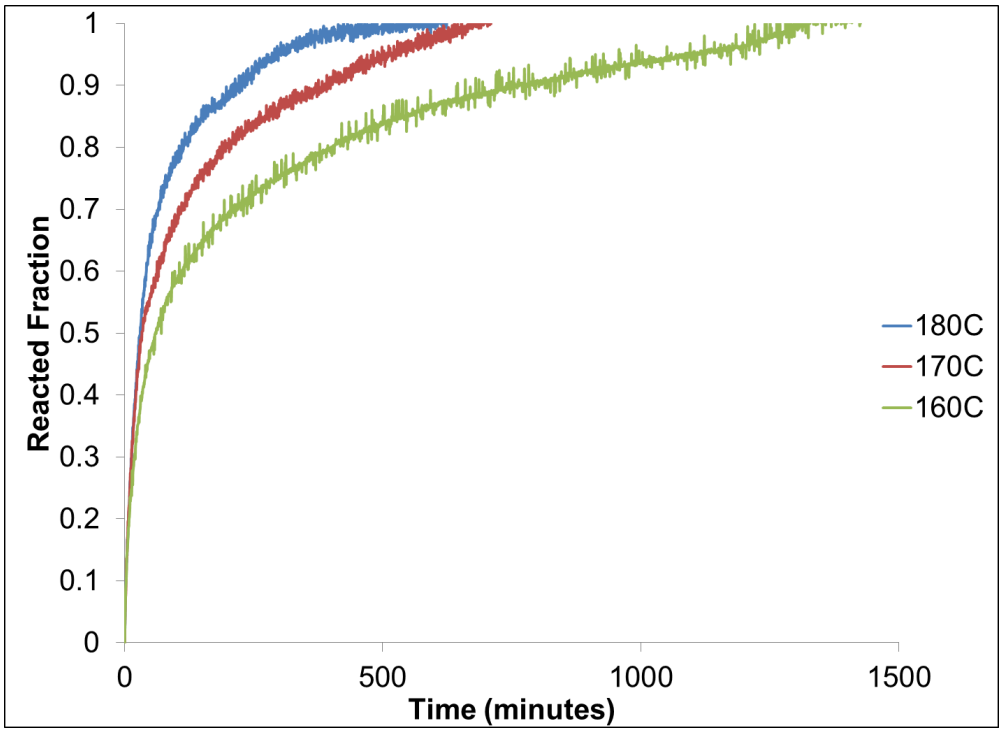

Figure 5.9 The desorption studies of RbH-doped $2LiNH_2/MgH_2$ hydrogen storage system.

To provide additional evidence regarding the mechanism of those reactions, various models were used. Models used for this purpose were: the shrinking core model and the Hancock and Sharp model. **Equations 4.1 and 4.2** in Chapter 4 of this research study were used for the shrinking core modeling. Presented in **Equation 4.1**, is the computation method used to determine if chemical reaction at the phase boundary controls the rate of the reaction. Presented in **Equation 4.2** is the computation method used to determine if diffusion controls the rate of the reaction.

In the case of absorption, it is observed in **Figures 5.10-5.12** that data generated from the model that reaction-controlled fits during the first part of reaction and then crosses over to diffusion in the latter stages of the reaction. This is similar behavior to the

KH-doped system that was discussed in Chapter 4. Therefore, the similar phenomenon has occurred concerning the shell of the system. This can be seen in the temperature range 160 °C-180 °C for the RbH-doped system.

For desorption studies that are presented in **Figures 5.13-5.15**, the diffusion model fit the experimental data only for the first 70% of the reaction. During the last 30% of the reaction, results indicated that neither model was a good fit with the experimental data. It appears that during the first 70% of the reaction, desorption occurred along the plateau region whereas the pressure remained relatively constant. Therefore, the N-value was constant and the thermodynamic driving force was constant. When the reaction reached the left edge of the plateau region the pressure decreased sharply and the thermodynamic driving force decreased. At that point, the kinetics slowed more rapidly than either model had previously hypothesized.[78,81]

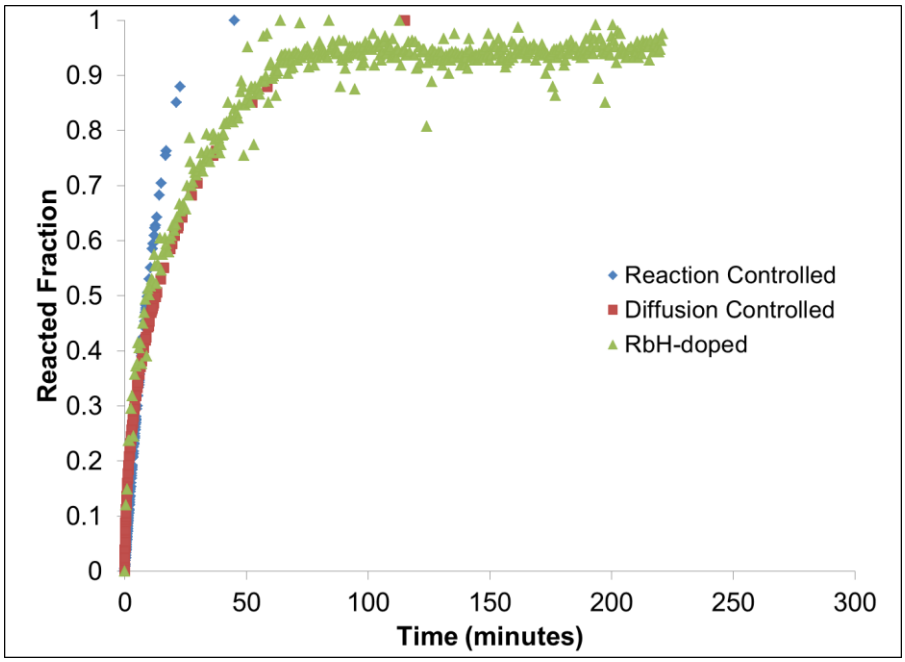

Figure 5.10 The kinetic model for absorption studies of RbH-doped $2LiNH_2/MgH_2$ system at 180˚C.

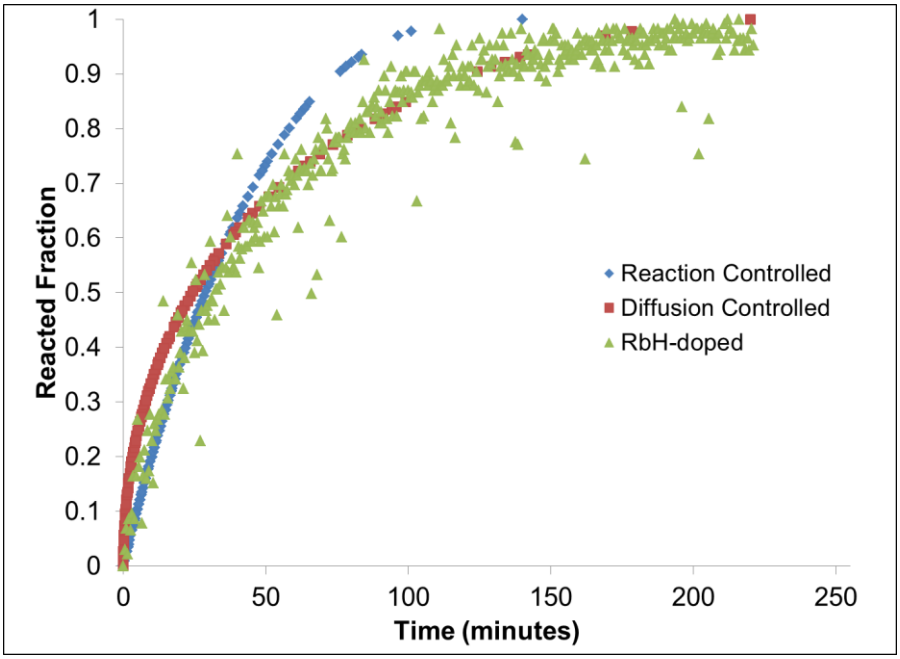

Figure 5.11 The kinetic model for absorption studies of RbH-doped $2LiNH_2/MgH_2$ system at 170˚C.

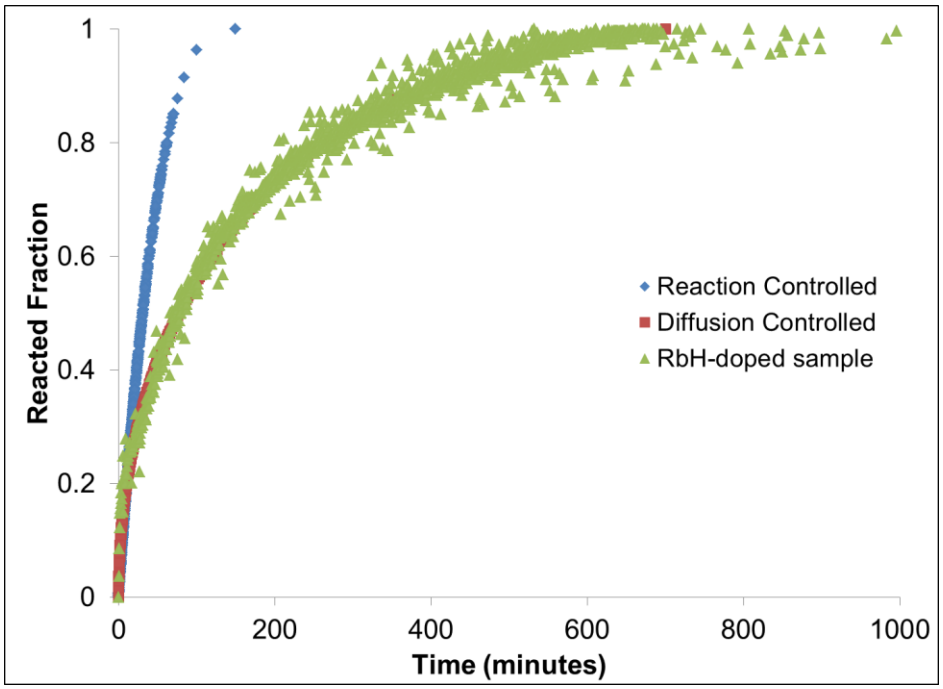

Figure 5.12 The kinetic model for absorption studies of RbH-doped $2LiNH_2/MgH_2$ system at 160°C.

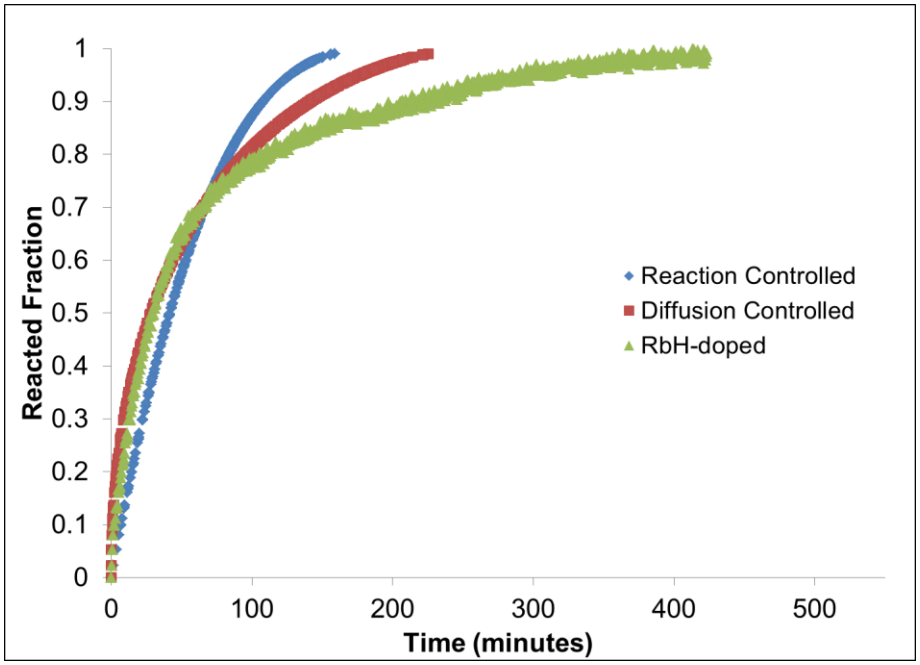

Figure 5.13 The kinetic studies for desorption studies of RbH-doped $2LiNH_2/MgH_2$ system at 180°C

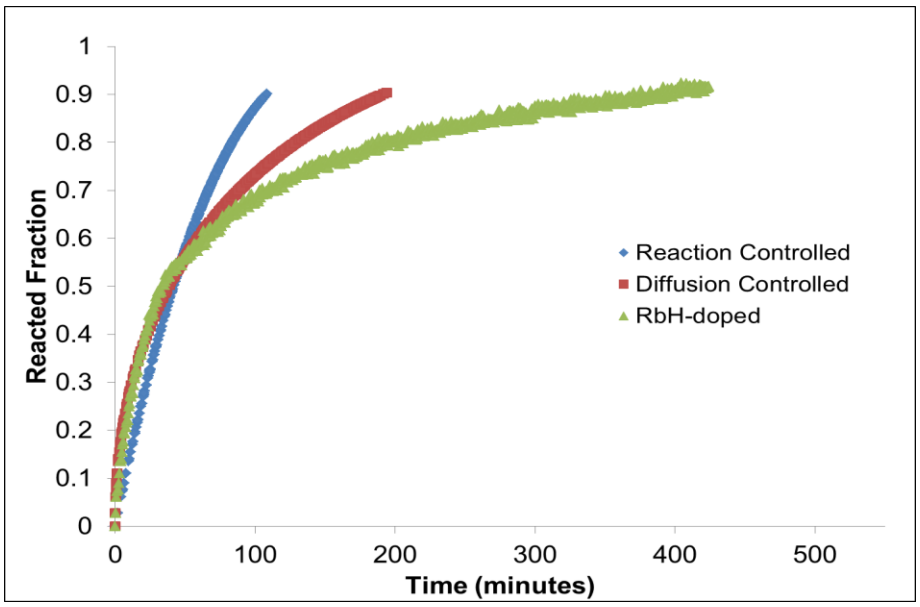

Figure 5.14 The kinetic studies for desorption studies of RbH-doped $2LiNH_2/MgH_2$ system at 170°C.

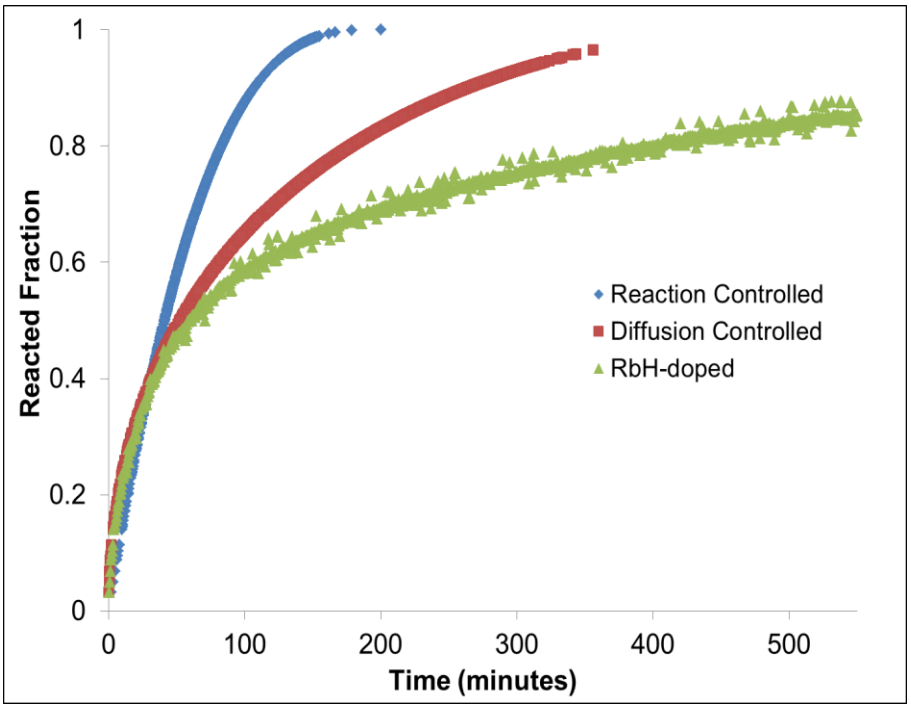

Figure 5.15 The kinetic studies for desorption studies of RbH-doped $2LiNH_2/MgH_2$ system at 160°C

To confirm the rate-limiting step from the shrinking core model, JMA plots were constructed. To construct the JMA plot, the kinetic data was modeled from Equation 4.3. For JMA plots, desorption studies (**Figure 5.17**) show that the diffusion-controlled the kinetic processes. For absorption, it shows linearity for both reaction controlled and diffusion model at the top to y=0.6 of each plot. This confirms that the two mechanisms do partake in the reaction like the shrinking core model. However, for desorption studies, it has confirmed that diffusion had the strongest correlation like the shrinking core model.

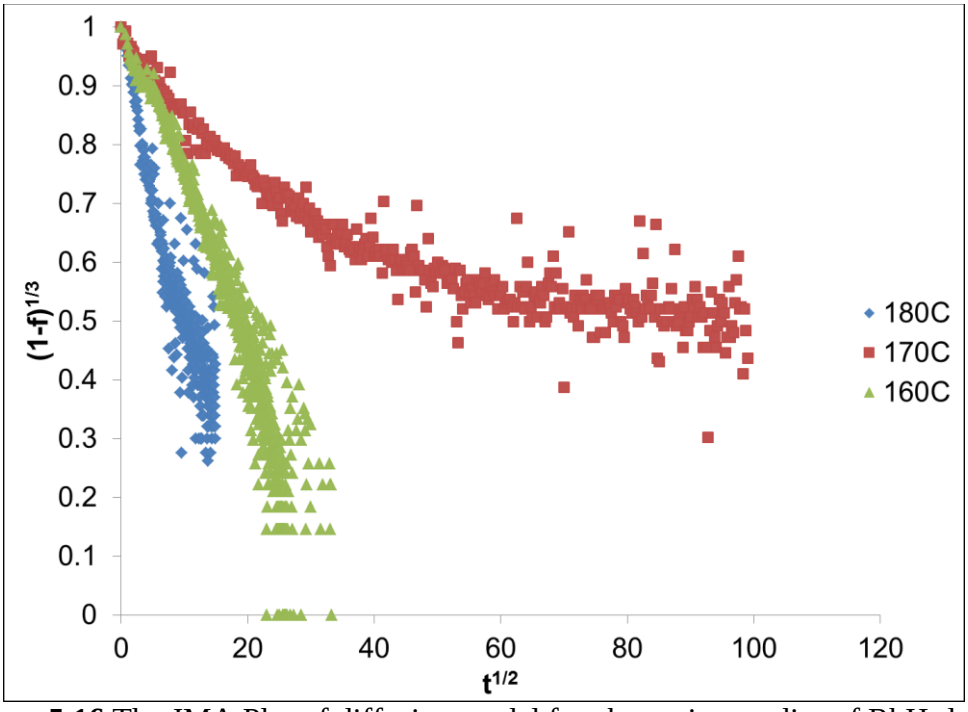

Figure 5.16 The JMA Plot of diffusion model for absorption studies of RbH-doped system

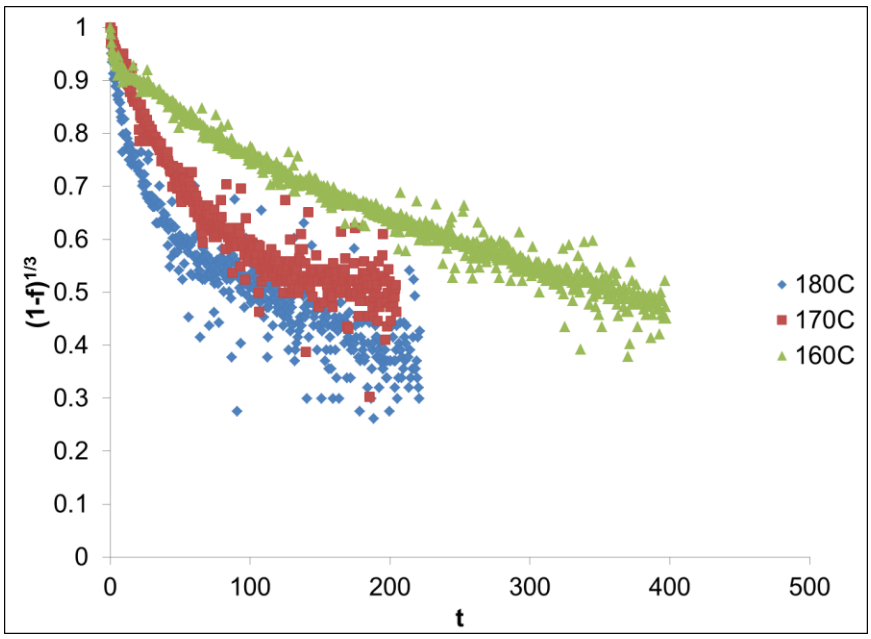

Figure 5.17 The JMA Plot of reaction-controlled model for absorption studies of RbH-doped system

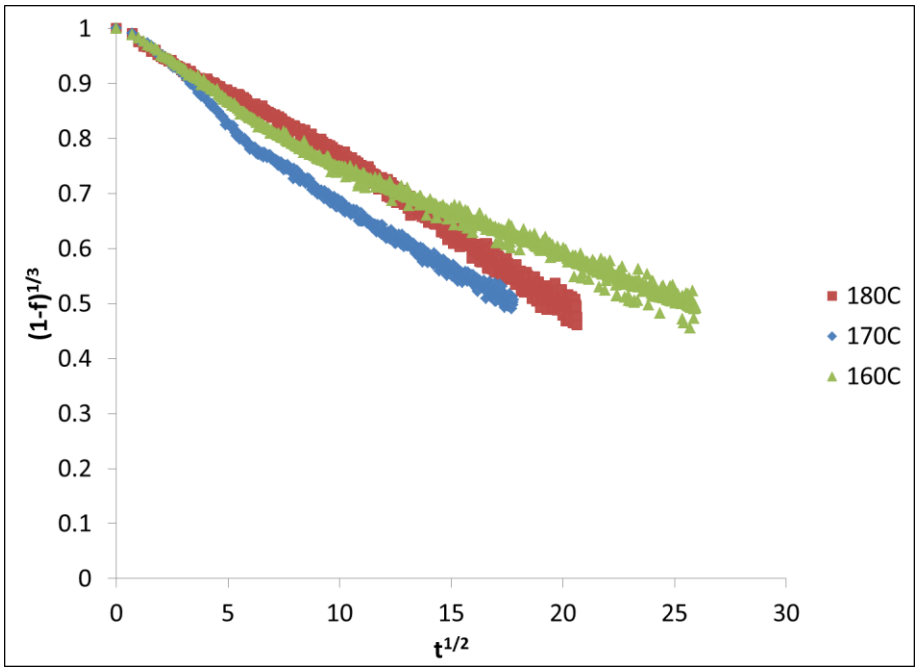

Figure 5.18 The JMA Plot of diffusion model for desorption studies of RbH-doped system.

The Hancock and Sharp model was used to analyze only the desorption studies. Based on the slopes of the plots produced for each temperature and presented in **Figure 5.19,** it was observed that the RbH-doped system is controlled by the diffusion model for the rate-limiting step. Overall, during each of the kinetic modelling studies, it was determined that the diffusion model results are more strongly correlated with the experimental curve than with the phase boundary curves. Therefore, the concluding evidence demonstrates that the hydrogen gas diffuses in and out of the lattice structure of the lithium amide-magnesium hydride hydrogen storage system. [77-78]

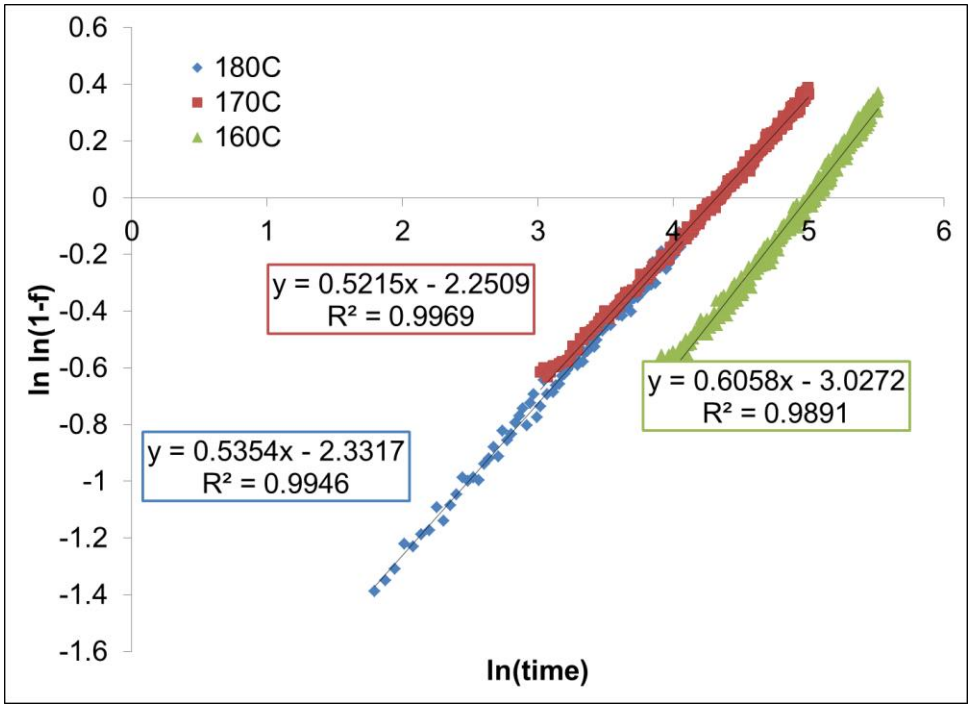

Figure 5.19 The Hancock and Sharp Model for the 1.9LiNH2+1.1MgH2+0.1RbH hydrogen storage system

5.4 Activation Energy Determination

As stated in the previous chapter, Arrhenius plots and Kissinger plots were used to determine the activation energy for doped systems. To determine the activation energy for absorption studies, an Arrhenius plot was used. For desorption studies, Arrhenius plots and Kissinger plots were constructed and the activation energies were compared. For absorption studies, first order plots were constructed (**Figure 5.20**) to determine the slopes which are the k values for each temperatures. Using the k values, the activation energy for RbH-doped system was found to be 81.7 kJ/mol based on the Arrhenius plot in **Figure 5.22**.

For desorption studies, Kissinger and Arrhenius plots have been constructed and compared. First order were constructed (**Figure 5.21**) followed by the Arrhenius plot. Based on the Arrhenius plot, the activation energy was found to be 86.8 kJ/mol (**Figure 5.22**) which is exactly the same value found in the Kissinger plot (**Figure 5.23**).

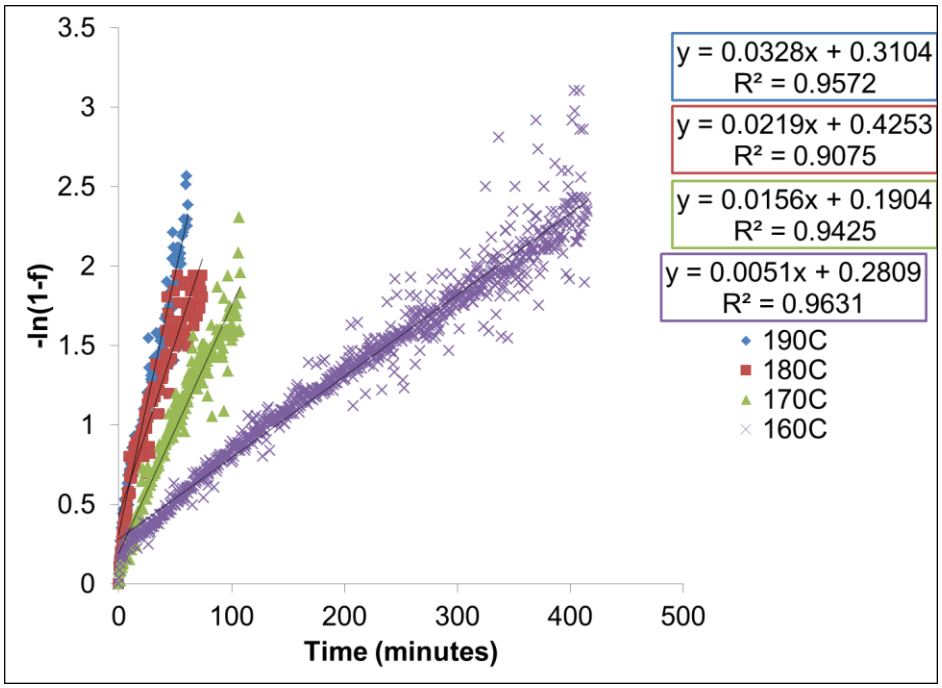

Figure 5.20 First order plots for the absorption studies of RbH-doped system

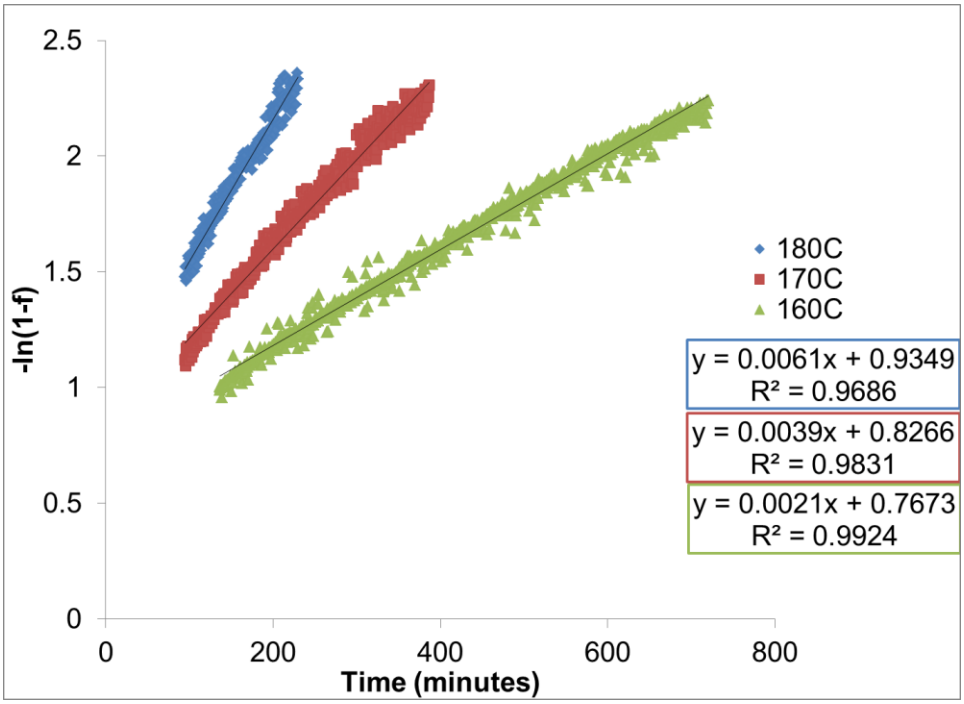

Figure 5.21 First order plots for desorption studies of RbH-doped system.

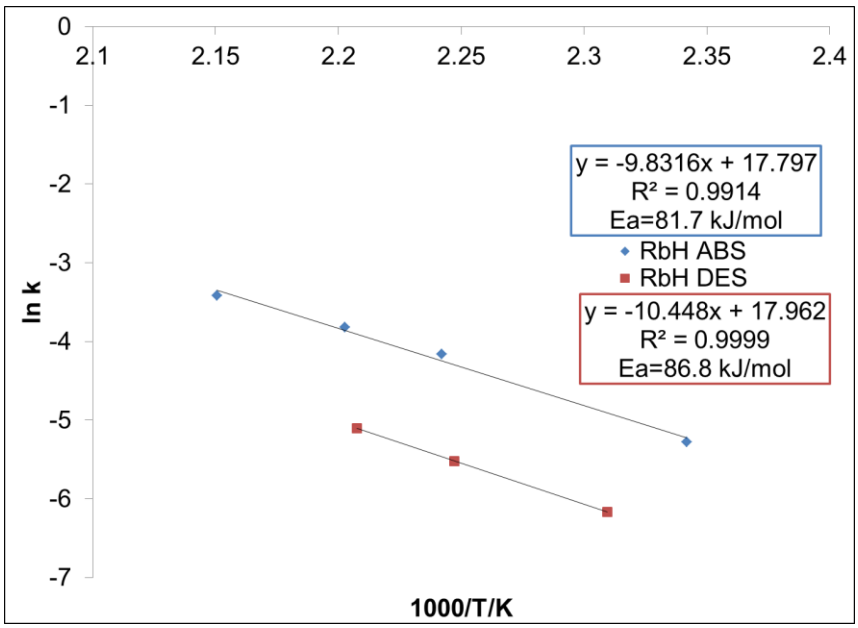

Figure 5.22 Arrhenius plots for absorption and desorption studies of RbH-doped system.

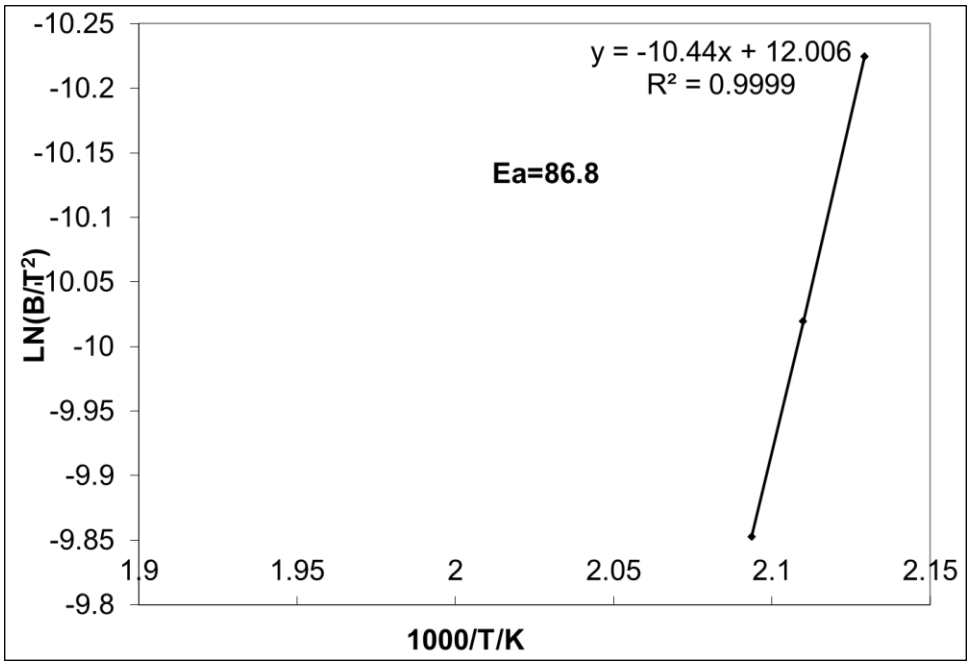

Figure 5.23 Kissinger plot for desorption studies of RbH-doped system

5.5 Summary

This research study has shown that RbH is an effective catalytic additive for increasing the rates of hydrogen absorption and desorption from the $2LiNH_2/MgH_2$ system. Absorption rates are approximately twice as fast as the desorption rates. All modeling studies (shrinking core, Johnson-Mehl-Avarami, Hancock and Sharp) indicate that the rates of desorption studies are controlled by a diffusion process. For absorption, shrinking core model and JMA plots shows that both reaction-controlled and diffusion took place during the reactions. Also, there is a substantial amount of hysteresis in this system and the magnitude of result increases during the first 70 absorption/desorption cycles. Moreover, results indicate that there is approximately a 30% decrease in the storage capacity of that system during the first 70 cycles. The activation energies for absorption of RbH-doped system have been found to be 81.7 kJ/mol which is a value less than 86.8 kJ/mol for desorption. This is exact compared to the value of 86.8 kJ/mol reported from the Kissinger plots.

CHAPTER 6

HYDRIDING AND DEHYDRIDING CESIUM HYDRIDE-DOPED LITHIUM AMIDE-MAGNESIUM HYDRIDE SYSTEM

Background

In the current study, there is a further investigation of the cesium hydride-doped system, which is the last alkali metal catalyst that will be discussed in this dissertation research. We will focus attention on the kinetic properties using a constant pressure thermodynamic driving force. In addition, absorption and desorption modeling studies will be discussed as well as cycling studies and activation energy of the system. The temperature range for the studies of the current system is 160-180 °C.

6.1 PCT Isotherms

Isotherm measurements for the $1.9LiNH_2+1.1MgH_2+0.1CsH$ were conducted in the range from 150 -180 °C. The results for absorption PCT measurements are presented in **Figure 6.1**. As was seen in the other alkali hydride doped systems, each isotherm displayed a well-defined plateau region in which lower temperatures resulted in lower plateau pressures. The isotherms display different maximum weight percent (wt%). It was observed that the weight percent generally increased with increasing temperature. Similar plots were obtained for desorption isotherms shown in **Figure 6.2**. The mid-

plateau pressures from the isotherms were used to construct the van't Hoff plots presented in **Figure 6.3**. The slopes of those plots were then used to determine enthalpies of absorption and desorption. The values for absorption and desorption enthalpies were found to be 40.98 kJ/mol and 46.1 kJ/mol respectively. Currently, no other absorption enthalpies have been reported for the CsH-doped system.

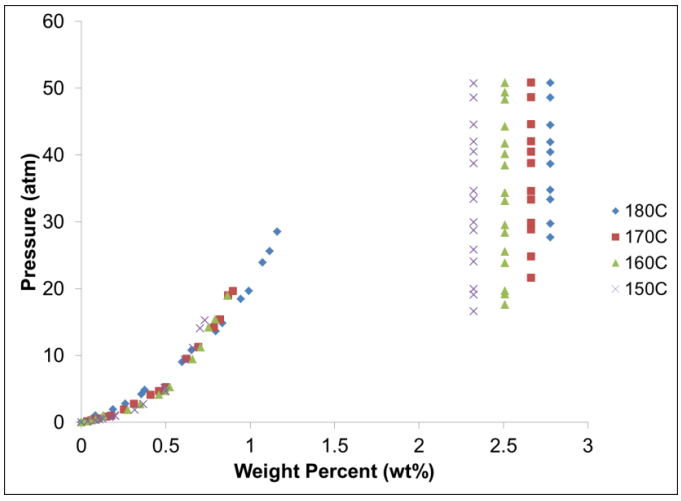

Figure 6.1 Pressure-composition-temperature absorption isotherms for $1.9LiNH_2+1.1MgH_2+0.1CsH$

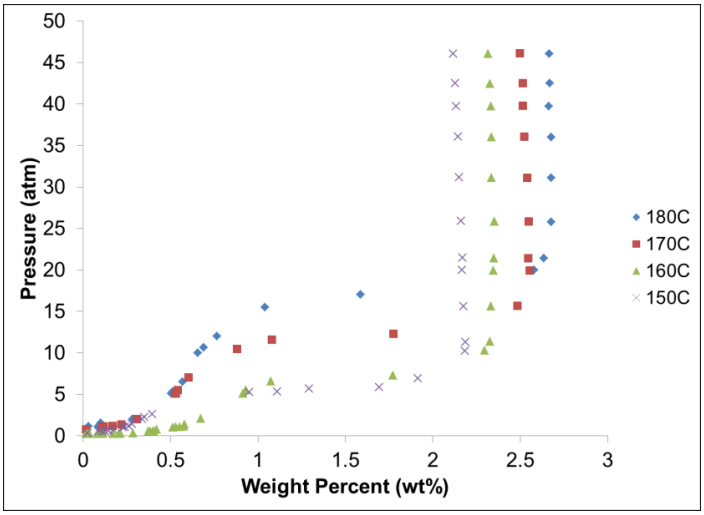

Figure 6.2 Pressure-composition-temperature desorption isotherms for $1.9LiNH_2+1.1MgH_2+0.1CsH$.

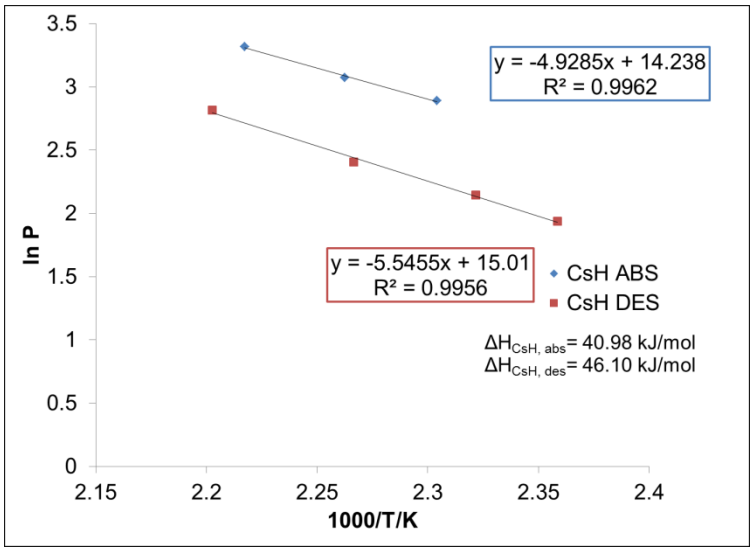

Figure 6.3 Van't Hoff plots for H_2 absorption and desorption isotherms from the CsH-doped system.

6.2 Cycling Studies

As has been stated from previous reviews of other systems, cycling studies are used to determine the durability of the hydrogen storage system. In the current study, the $1.9LiNH_2+1.1MgH_2+0.1CsH$ system was cycled at a constant temperature of 200 °C. Based on the results presented in **Figures 6.4-6.6**, there is little change in the amount of hysteresis in this system. **Figure 6.6** presents a hysteresis plot of the system after it was cycled over 100 times. The isotherms were measured after every set of 10 absorption/desorption cycles. Those analyses demonstrated how the absorption and desorption plateau changed during pressure/vacuum cycling. Those results indicate that the absorption plateau pressures remains constant through 100 cycles while the desorption pressures have the same result. However, the hydrogen holding capacity changed over time with each cycle as is presented in **Figure 6.4** and **Figure 6.5.**

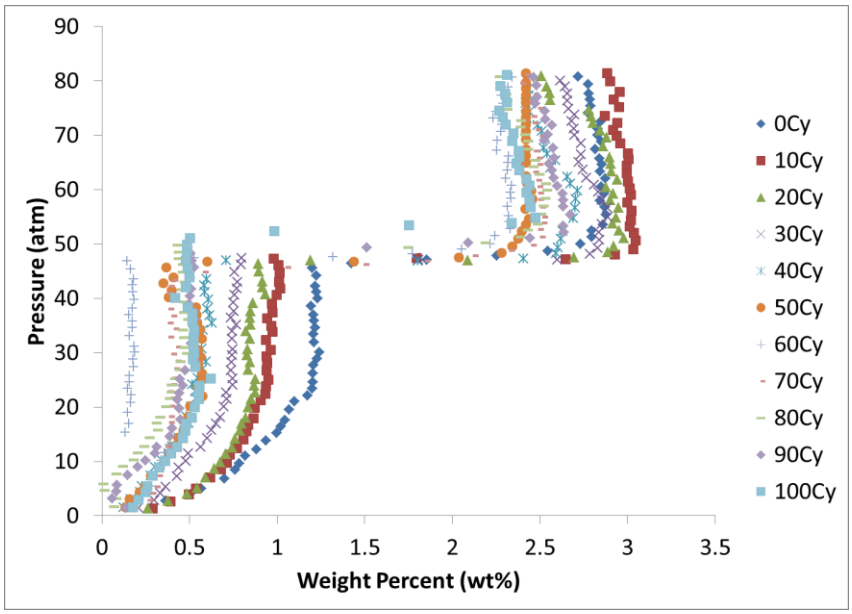

Figure 6.4 Absorption cycling studies for 1.9LiNH$_2$+1.1MgH$_2$+0.1CsH hydrogen storage system at 200˚C.

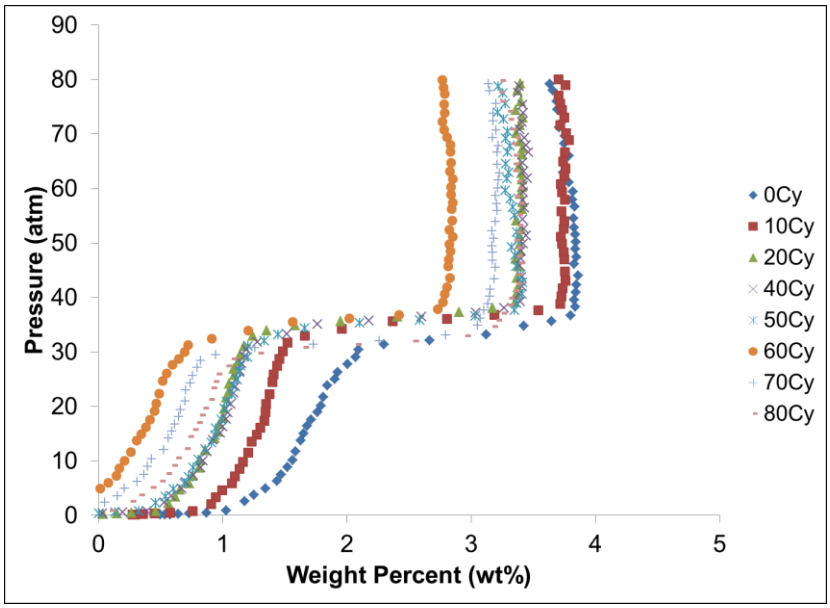

Figure 6.5 Desorption cycling studies for 1.9LiNH$_2$+1.1MgH$_2$+0.1CsH hydrogen storage system at 200 ˚C.

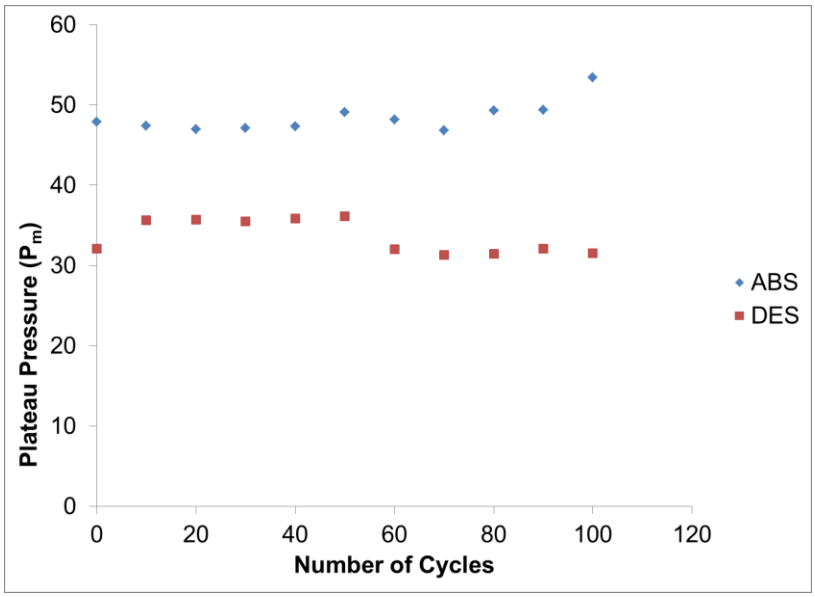

Figure 6.6 Hysteresis plot for CsH-doped lithium amide-magnesium hydride hydrogen storage system at 200 ˚C.

6.3 Kinetic and Modeling Studies

Measurements of kinetics were conducted and comparisons were made of the absorption and desorption rates of the CsH-doped $2LiNH_2/MgH_2$ system at 160-180 °C under equivalent conditions. That process was accomplished by using an N-value of 3 for the hydriding and de-hydriding processes. In conducting absorption studies presented in this chapter, the N-value is equal to opposing pressure/mid-plateau pressure whereas the N-value for desorption is equal to mid-plateau pressure/opposing pressure. Those equations can be further examined in the experimental section for additional clarification in **Equations 2.1 and 2.2**. **Figures 6.7 and 6.8** present the absorption and desorption kinetic studies in the temperature range of 160-180 °C respectively. The absorption reactions appear to be 90% complete in approximately 301 minutes at 180 ˚C, 626 minutes at 170 ˚C, and 1256 minutes at 160 ˚C. The desorption reactions appear to be

90% completed in 455 minutes at 180˚C, 1164 minutes at 170˚C, and 2400 minutes at 160 ˚C. These results show that for the CsH-doped system absorption rates are faster than desorption rates.

To elucidate the mechanism of those reactions, various models were used. The models that were used are: the shrinking core model, the Johnson-Mehl-Avarami model, and the Hancock and Sharp model used with **Equations 4.1 and 4.2** in Chapter 4.

The curve labeled "CsH-doped" is the experimental curve; the curves labeled "diffusion controlled" and "reaction-controlled" are labeled accordingly to the model represented. The results in **Figures 6.9-6.12** indicate that the reaction controlled occurred in the first part of the reactions whereas diffusion controlled model occurred approximately in the latter stages of the absorption reaction.

However, this does not occur in the results of the modeling studies for the desorption reactions. **Figures 6.12-6.14** presents the shrinking core model for the temperatures 180 ˚C, 170 ˚C, and 160 ˚C respectively. For the 180 ˚C desorption study, diffusion controls the reaction up to 70 percent. Also, that finding can be observed from the results of the PCIs. On the plateau, the hydrogen diffused across the plateau from right to left for 70 percent of the reaction. The other 30 percent of the desorption reaction provides evidence that the N-value is not constant. Therefore, since the N-value is not constant it changes as the rest of the hydrogen releases. This phenomenon also occurs for 170 ˚C and 160 ˚C desorption studies. Based on desorption models, diffusion control the reaction for 60 percent for 170 ˚C and 160 ˚C respectively.

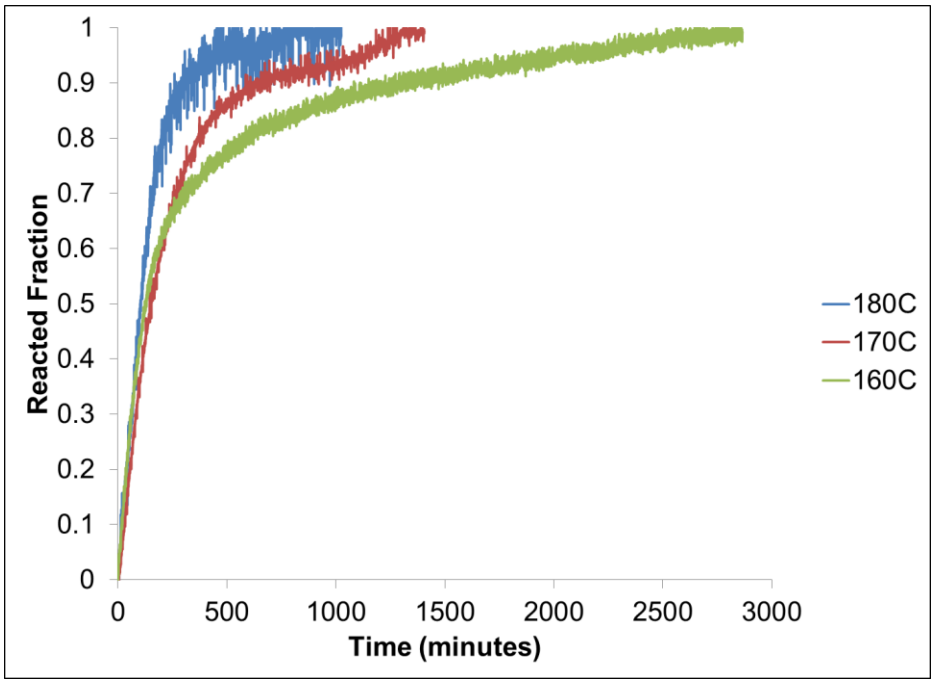

Figure 6.7 Absorption kinetic studies for $1.9LiNH_2+1.1MgH_2+0.1CsH$ hydrogen storage system at N-value of 3.

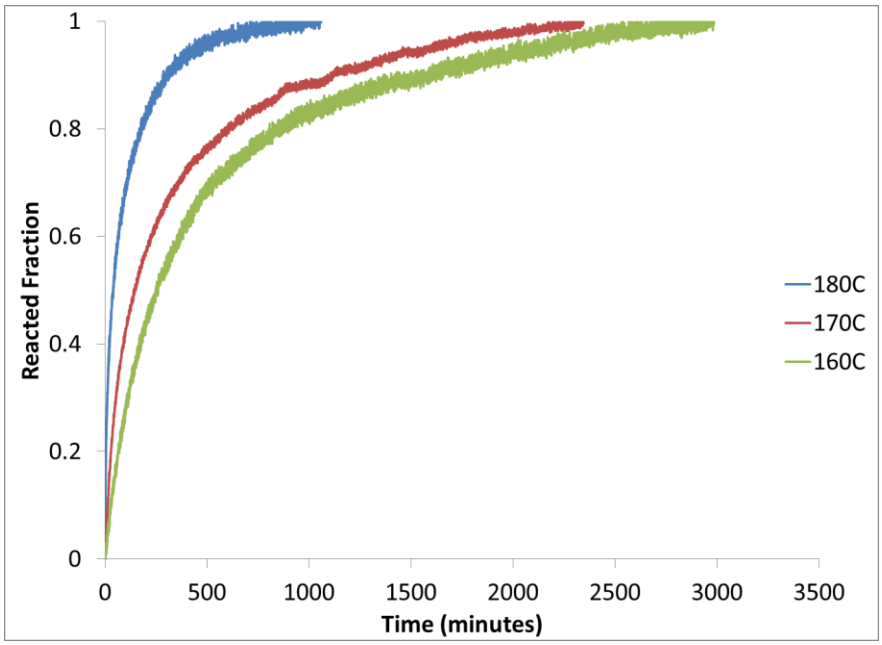

Figure 6.8 Desorption kinetic studies for $1.9LiNH_2+1.1MgH_2+0.1CsH$ hydrogen storage system at N-value of 3.

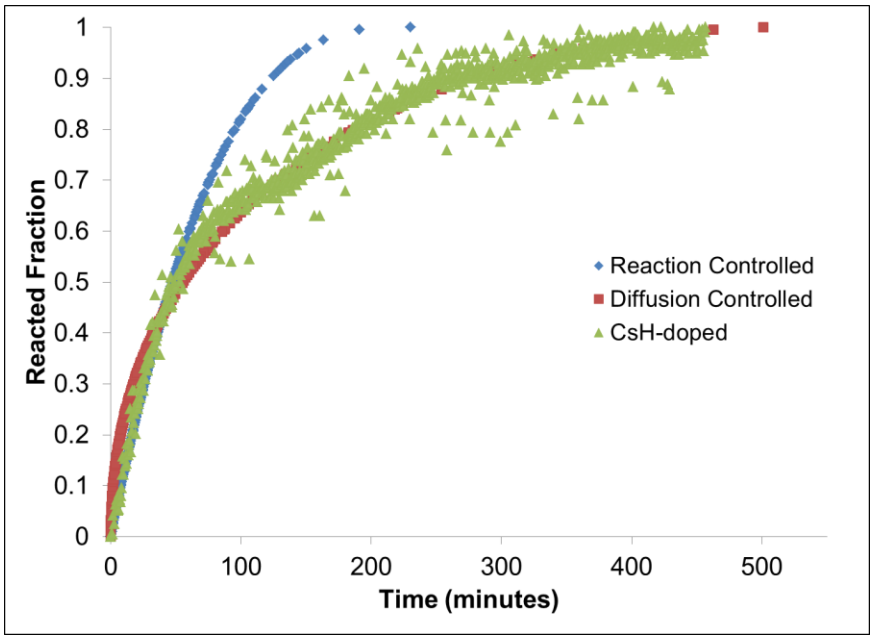

Figure 6.9 Shrinking core model for absorption studies of $1.9LiNH_2+1.1MgH_2+0.1CsH$ at T=180 ˚C

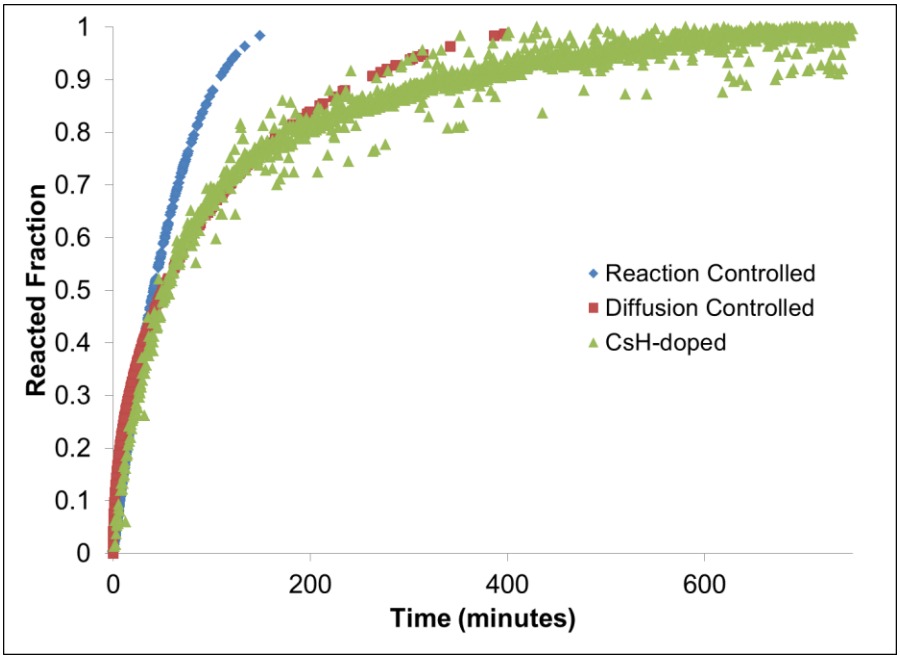

Figure 6.10 Shrinking core model for absorption studies of $1.9LiNH_2+1.1MgH_2+0.1CsH$ at T=170 ˚C

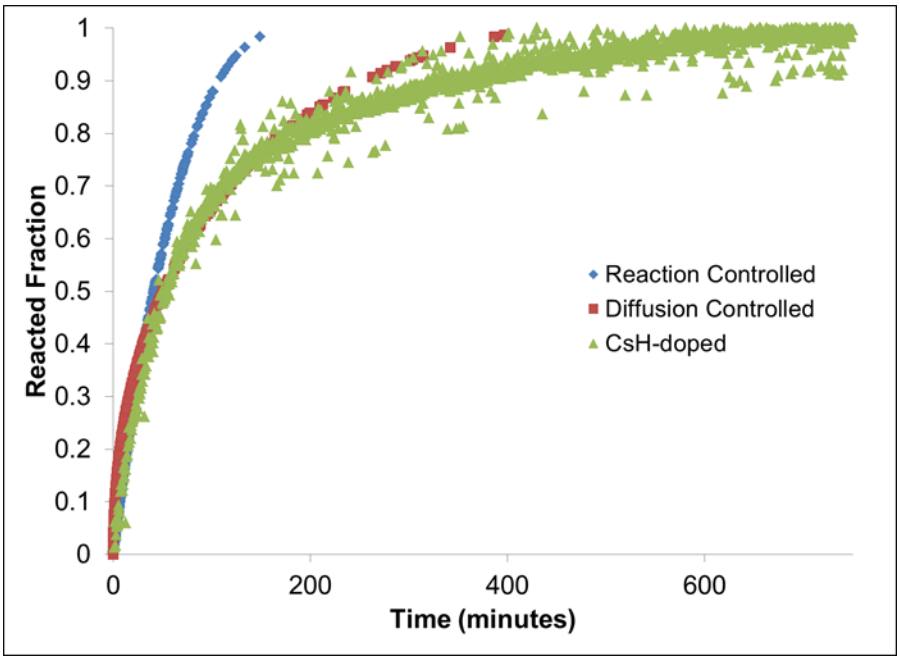

Figure 6.11 Shrinking core model for absorption studies of $1.9LiNH_2+1.1MgH_2+0.1CsH$ at T=160 ˚C

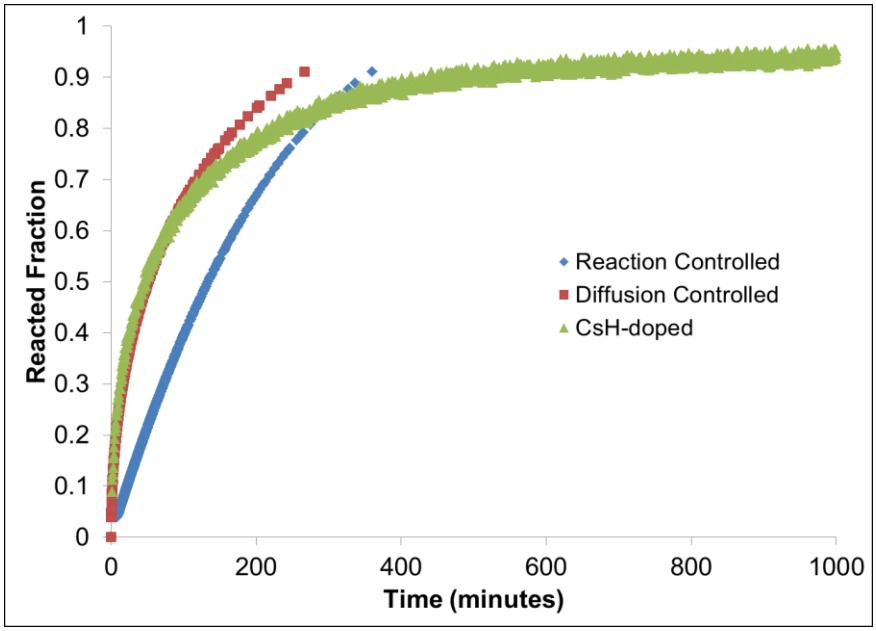

Figure 6.12 Shrinking Core Model for CsH-doped $2LiNH_2/MgH_2$ system at 180°C for desorption study.

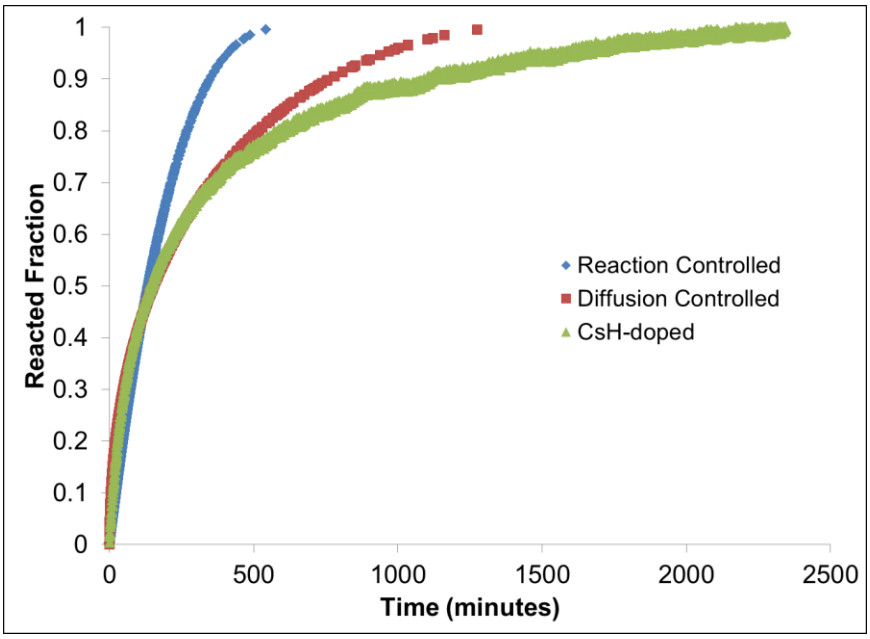

Figure 6.13 Shrinking Core Model for CsH-doped $2LiNH_2/MgH_2$ system at 170 °C for desorption study.

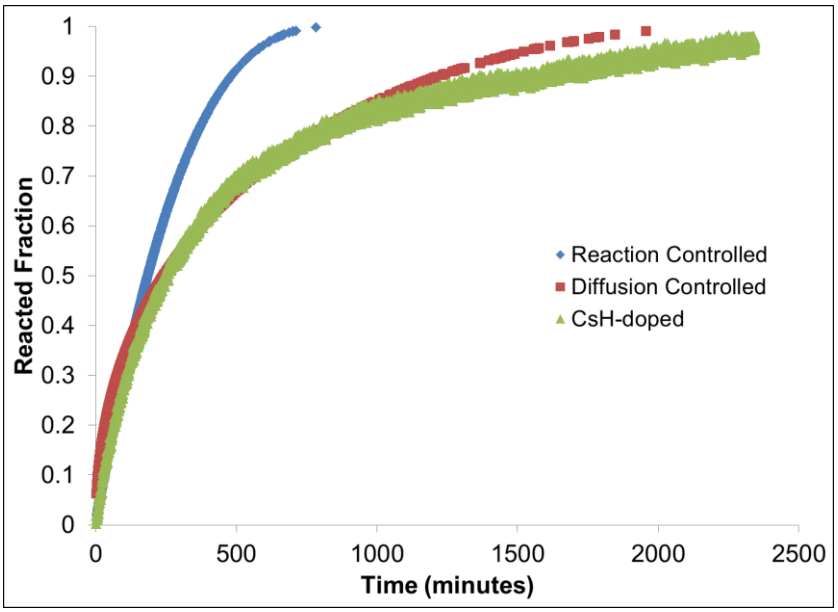

Figure 6.14 Shrinking Core Model for CsH-doped $2LiNH_2/MgH_2$ system at 160 °C for desorption study.

As reported in Chapter 5, the JMA plots for absorption showed that reaction at the phase boundary and diffusion are both the rate-limiting step for the reaction at temperatures 180, 170, and 160˚C. **Figures 6.15** (diffusion-controlled) **and 6.16** (reaction-controlled) indicate to have linearity from the 0.9 to the 0.7 range for both models. This is to confirm that the CsH-doped absorption study react at the phase boundary and diffusion. For desorption studies, the results have shown that diffusion is the mechanism for the rate-limiting step. This can be seen in **Figures 6.17** below as the plots shown a strong correlation for linearity for the diffusion model explained in Chapter 2. Figure 6.17 show that there is linearity throughout the diffusion model confirming that diffusion is the rate-controlling step for desorption studies.

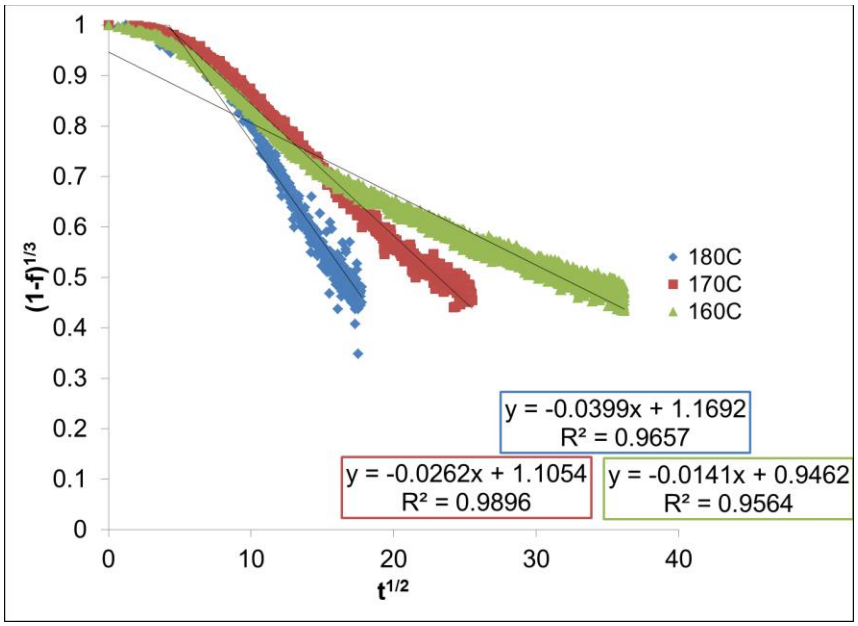

Figure 6.15 The JMA plots for absorption studies for CsH-doped system for diffusion controlled mechanism.

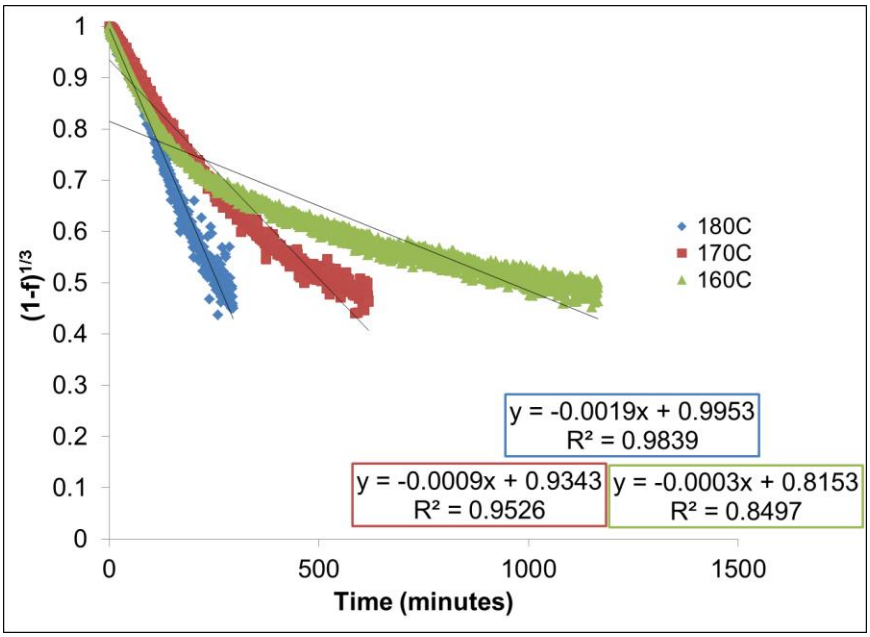

Figure 6.16 The JMA plots for absorption studies for CsH-doped system for reaction controlled mechanism

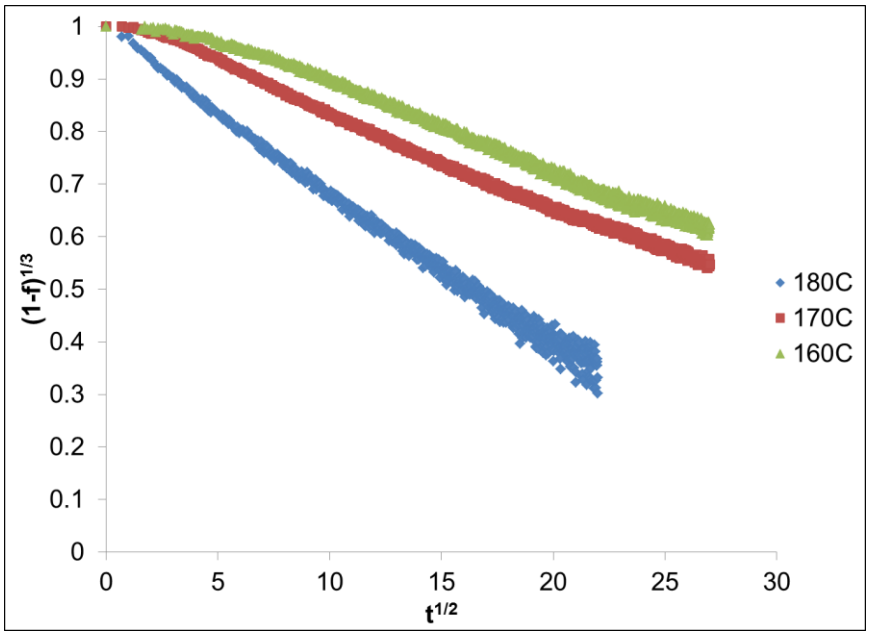

Figure 6.17 The JMA plots for diffusion of desorption studies for CsH-doped system

Also, the Hancock and Sharp model was used to analyze the rate-controlling step for the kinetics of desorption studies. According to the theory of the Hancock and Sharp models, the slope from the plot of the model indicates the rate-controlling step for the reaction conducted. The slope range for the model is given in Table 1 of the paper. Based on the paper and the slopes shown in **Figure 6.18** below, this finding demonstrated that diffusion controls the rate-determining step for the reaction in the temperature range from 160 - 180 °C.

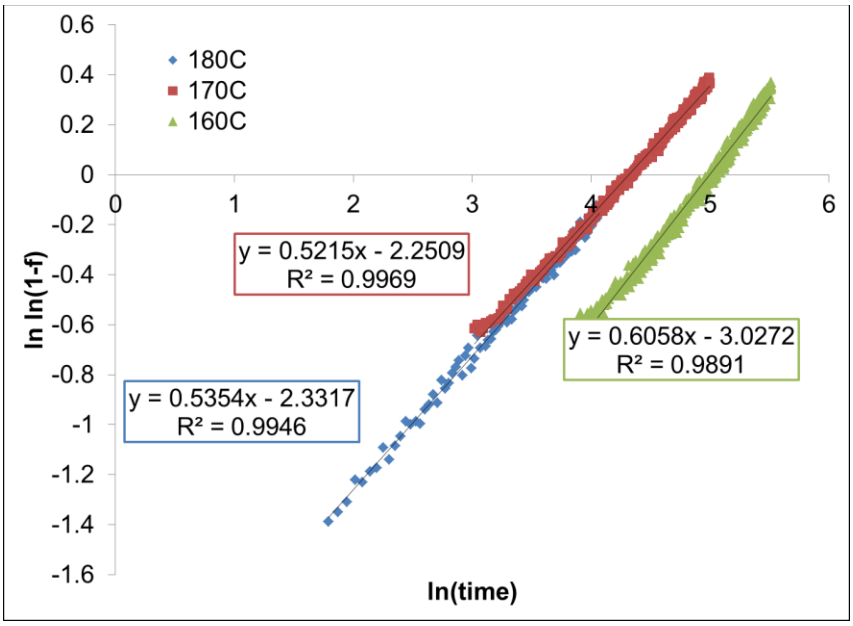

Figure 6.18 Hancock and Sharp model for desorption studies of $1.9LiNH_2+1.1MgH_2+0.1CsH$ hydrogen storage system.

6.4 Activation Energy Determination

To define and show that CsH has acted as a catalyst towards the $2LiNH_2/MgH_2$ system, observations of the activation energy must be recorded. Assuming that the reactions are first-order, first order plots were constructed from **Equation 4.4**. The first order plots can be seen in **Figures 6.19 and 6.20** for absorption and desorption study respectively. For absorption study, the Arrhenius plots were constructed and gave a value of 105.9 kJ/mol for activation energy in **Figure 6.21**. The author also analyzed the activation energy of the sample by using both Kissinger plot and Arrhenius plot for desorption studies. Based on the Arrhenius plot, the activation energy resulted to be 110.5 kJ/mol (**Figure 6.21**) which is significantly close to 109.0 kJ/mol reported in **Figure 6.22**.

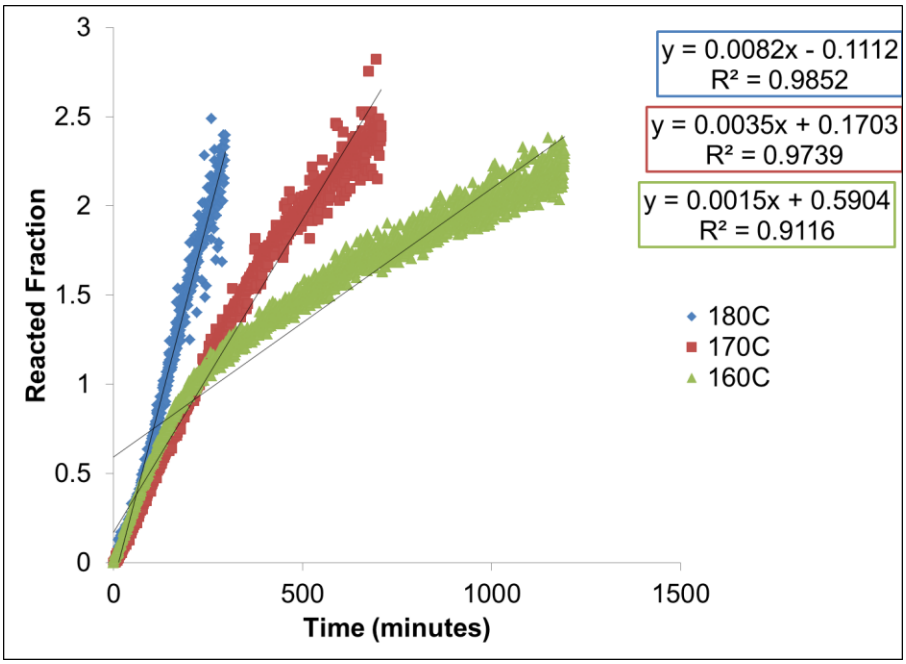

Figure 6.19 First order plots for the absorption studies of $1.9LiNH_2+1.1MgH_2+0.1CsH$

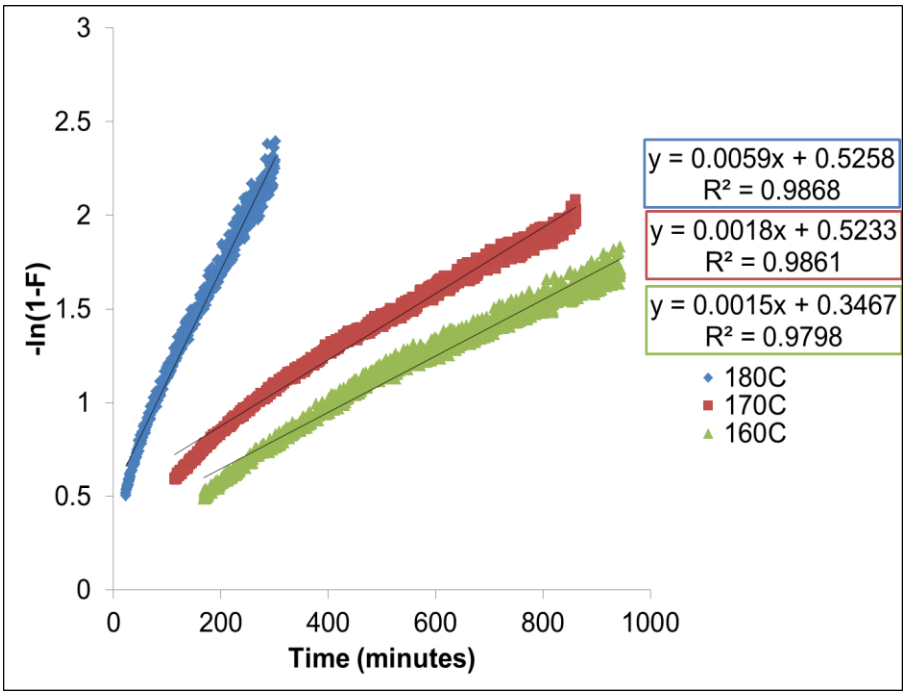

Figure 6.20 First Order plot for the desorption studies of $1.9LiNH_2+1.1MgH_2+0.1CsH$

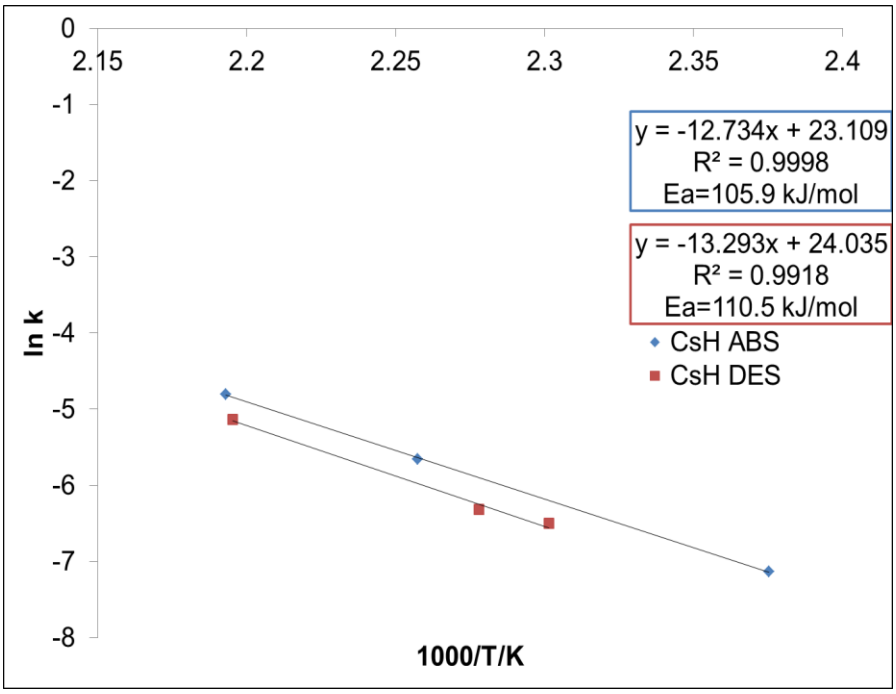

Figure 6.21 Arrhenius plots for absorption and desorption studies of $1.9LiNH_2+1.1MgH_2+0.1CsH$

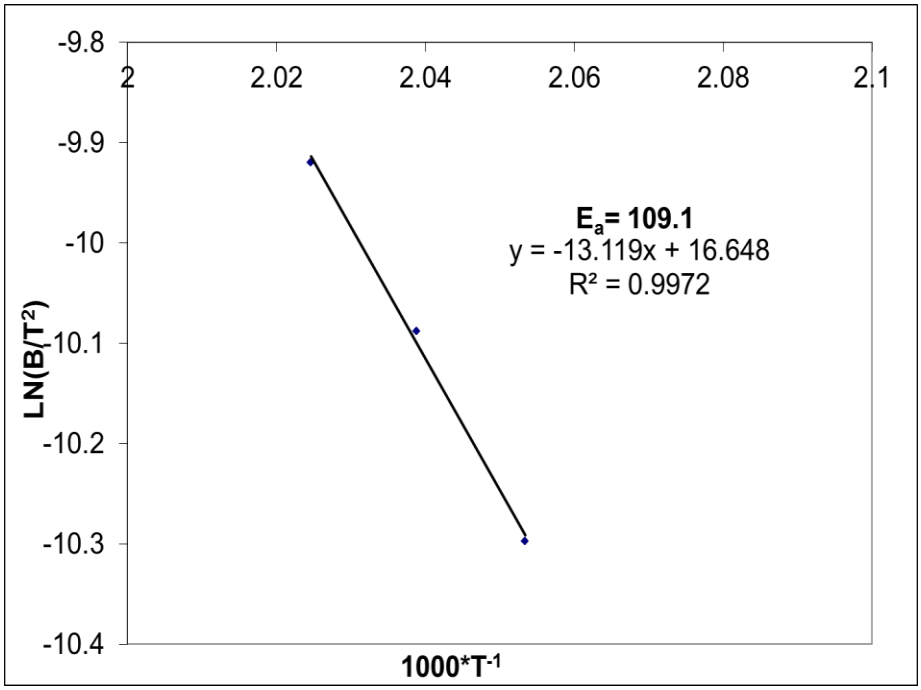

Figure 6.22 Kissinger plot of $1.9LiNH_2+1.1MgH_2+0.1CsH$

Summary

This study demonstrated that the CsH is a good dopant for increasing the rate and operating at a low temperature particularly in the range at 160 ˚C-180 ˚C. Cycling studies provided evidence that the plateau pressures remained consistent throughout the 100 cycles. However, the weight percent did change over time with each hydriding and dehydriding phase. For absorption kinetic studies, it was found that there were two rate-controlling steps. The reaction at the phase boundary occurred in the beginning of the reaction and diffusion occurred in the later part of the reaction for all three temperatures. For desorption studies however, Modeling studies at different temperature ranges demonstrated that diffusion controls the rate-limiting step. JMA plots and Hancock and Sharp models confirmed these observations. A comparison of the activation energies for desorption, results indicated that the Arrhenius plot resulted in activation energy was 110.5 kJ/mol as compared to the Kissinger value which was 109.1 kJ/mol. For absorption studies however, the activation energy results to be 105.9 kJ/mol based on the Arrhenius plots constructed which is smaller than the desorption value.

CHAPTER 7

COMPARATIVE ANALYSIS OF ALKALI-METAL DOPED SYSTEM AT CONSTANT TEMPERATURE

In the current chapter, a comparative analysis between the alkali metal-doped lithium amide-magnesium hydride hydrogen storage systems will be made. All comparisons will be at 180˚C and for kinetic analysis at an N-value of 3. The kinetic models have been discussed in Chapters 4, 5, and 6 respectively using the shrinking core, Johnson-Mehl-Avarami, and Hancock and Sharp models. In addition, all of the results and parameters that have been discussed in the previous chapters will be summarized in a table at constant temperature of 180 ˚C and 200 ˚C for cycling studies.

7.1 PCT Isotherms

Figure 7.1 and 7.2 shows the pressure-composition absorption and desorption isotherms for the KH-doped, RbH-doped, and CsH-doped systems at 180 °C. Desorption isotherms have been reported for these systems. It showed that the trends for the dopants were the following: KH <RbH <CsH. However, absorption studies are reported for the first time. The plots in Figures 7.1 and 7.2 show that the plateau pressures at 180°C for the doped systems are in the following order: KH > RbH > CsH. Absorption and desorption PCIs were also determined in the 160-180°C range for each system. Based on

the van't Hoff equation (**Equation 4.1**), a plot of Ln P vs. 1/T was constructed to determine the enthalpy values which were calculated and discussed in the previous chapters. The values are shown in Table 7.1. These results show that enthalpy values are in the following order: CsH > RbH > KH. As discussed earlier, the absorption enthalpy values are smaller than desorption enthalpy values. However, the desorption values are similar to those reported in previous publications.[77]

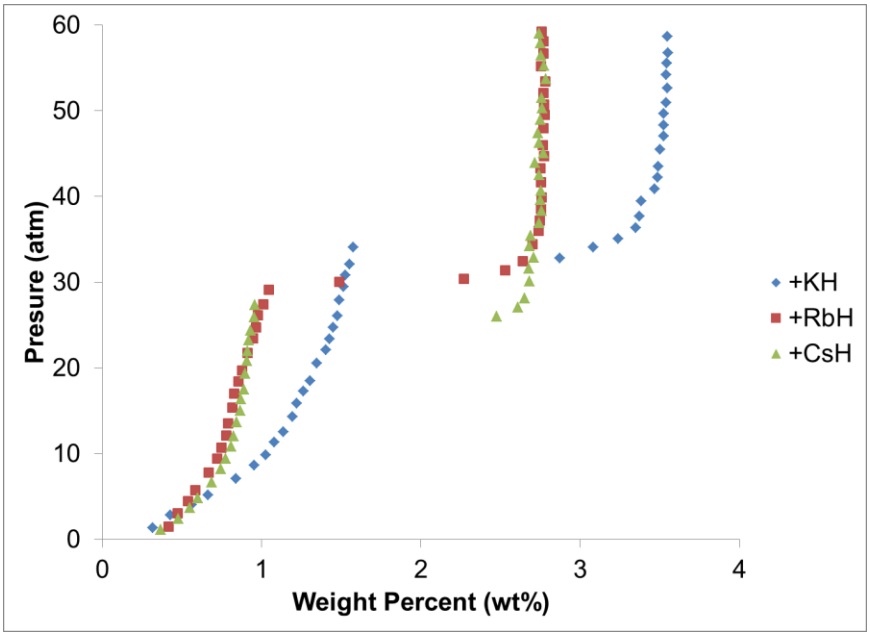

Figure 7.1 Absorption isotherms at 180 °C for the alkali-metal doped system.

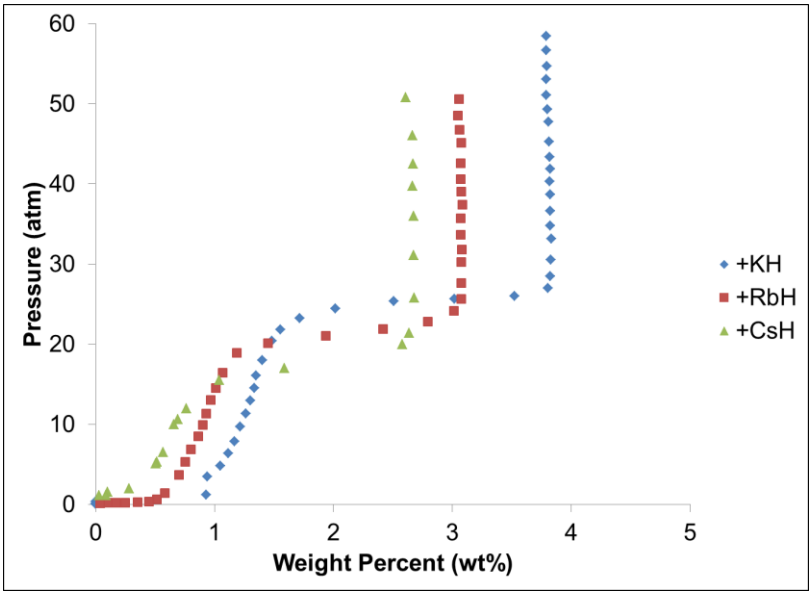

Figure 7.2 Desorption isotherms at 180 °C for the alkali-metal doped system.

7.2 Cycling Studies

Based on the trends presented in the KH-doped and CsH-doped samples, the plateau pressures for absorption and remained constant. In addition, the results clearly demonstrate that the RbH-doped sample follows a different trend compared to the others. That trend provides evidence of a constant increase with absorption and a constant decrease with desorption which caused an increase of hysteresis over time as shown in the RbH-doped sample graphs in **Figures 7.3 and 7.4**. Currently, there is no precise explanation as to why the phenomenon occurs until 70 cycles. Further research is necessary to gain insight on that phenomenon. As was previously stated in the prior chapters, the conditions for cycling the catalyzed systems were conducted at a constant temperature of 200 °C.

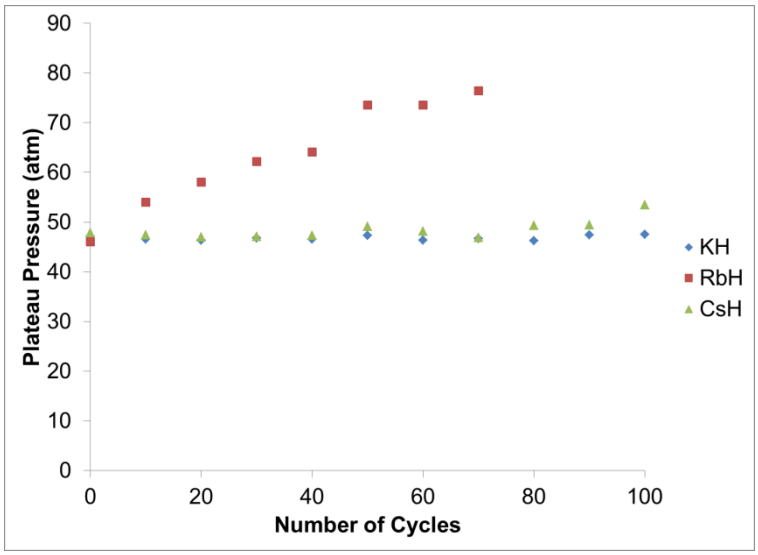

Figure 7.3 Absorption plateau pressures during absorption/desorption cycling studies at 200 °C. A comparative analysis of alkali-metal doped system.

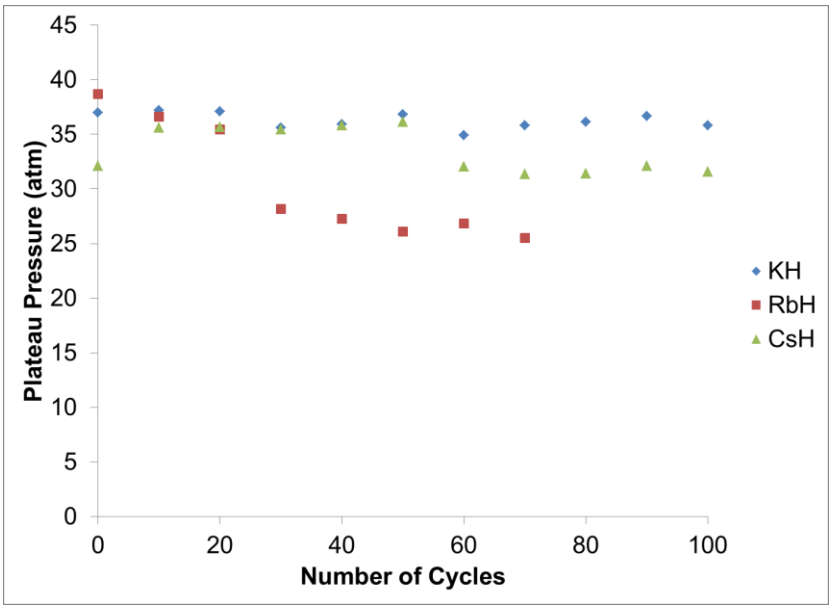

Figure 7.4 Desorption plateau pressures during absorption/desorption cycling studies at 200 °C . A comparative analysis of alkali metal- doped system.

7.3 Kinetic Studies

As was stated in prior chapters, the results representing the rehydriding kinetics of the lithium amide-magnesium doped systems at low temperatures are closer to meeting the criteria for the United States Department of Energy. The temperature of both absorption and desorption reactions were completed at a constant temperature of 180 °C at an N-value of 3. With an N-value that low, it was hypothesized that the reactions would appeared be slower as compared to other research studies conducted and published in the existing literature.[26,78] Absorption kinetics have been demonstrated to be faster as compared to the desorption kinetics for each system. That observation is presented in **Figures 7.5 and 7.6**.

That trend for those results have been determined to be RbH<KH<CsH. That observation is consistent with a trend that was first described by Durojaiye et al.[77] Further, that observation demonstrates that the RbH dopant is more reactive compared to the other metals in Group I in the periodic table.[77]

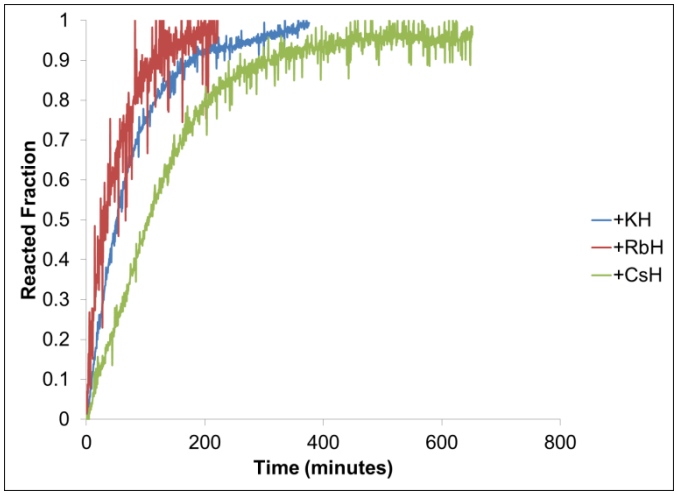

Figure 7.5 Absorption studies of the alkali-metal doped lithium amide-magnesium hydride system at constant temperature 180 °C.

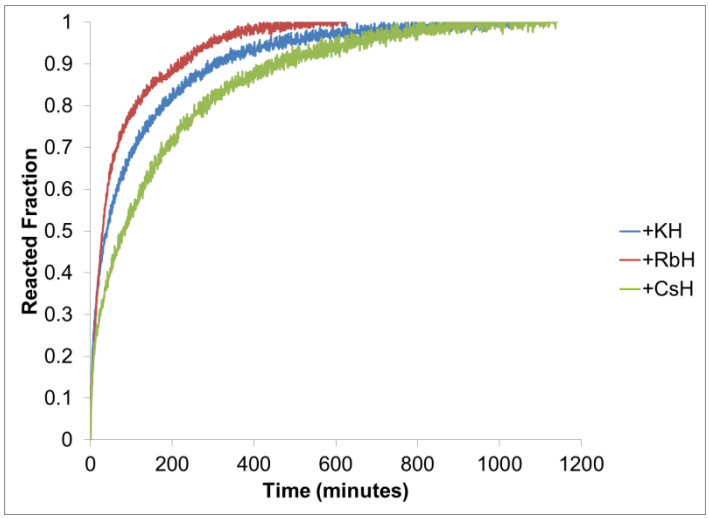

Figure 7.6 Desorption studies of the alkali-metal doped lithium amide-magnesium hydride system at constant temperature 180 °C.

7.4 Activation Energies

Throughout the current dissertation, activation energies have been constructed using two methods: Arrhenius plots and Kissinger plots. Activation energies for absorption studies are introduced for the first time throughout this dissertation. Activation energies for desorption studies have been conducted and compared using the two methods. **Figures 7.7 and 7.8** show the comparisons of Arrhenius plots for absorption and desorption respectively.

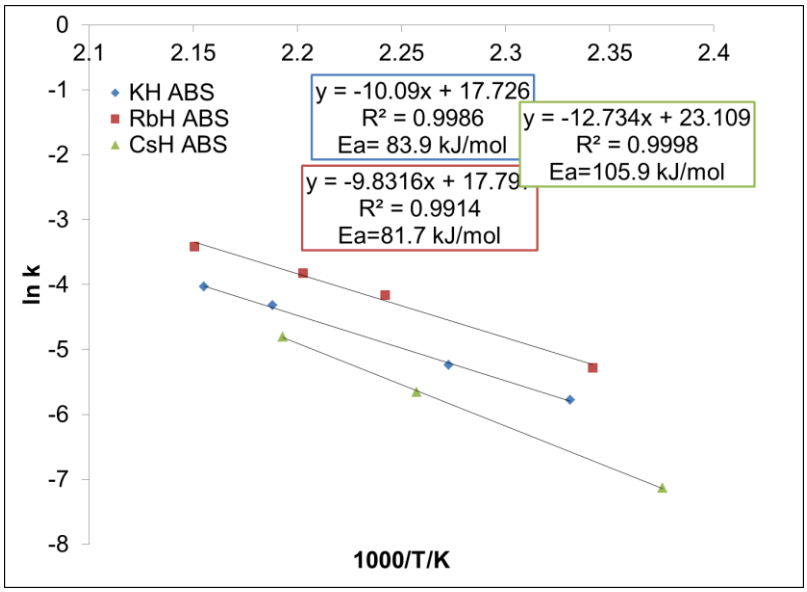

Figure 7.7 Arrhenius plots of absorption studies for the alkali-metal hoped systems.

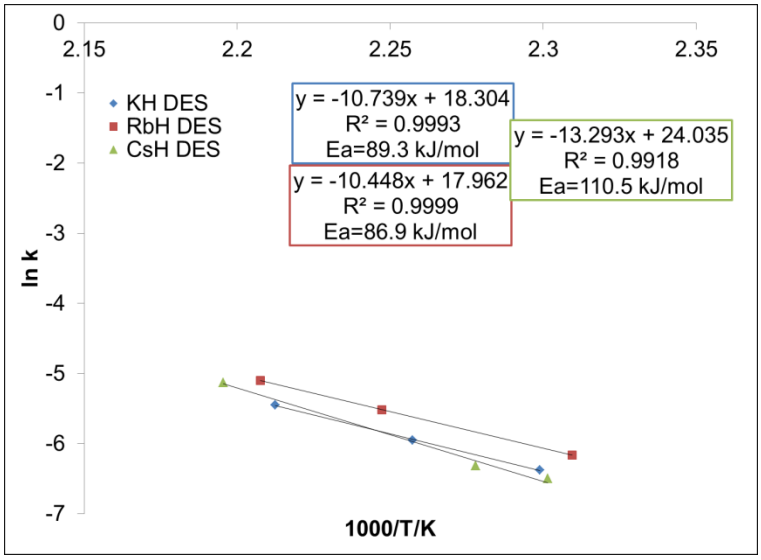

Figure 7.8 Arrhenius plots of desorption studies for the alkali-metal hoped systems.

Based on the parameters presented in **Table 7.1** below, rubidium hydride is the best dopant for the $2LiNH_2/MgH_2$ system. The following trend was observed throughout this current research study: RbH>KH>CsH. Based on the periodic table, cesium hydride was expected to be the best dopant due to lower electronegativity. However, based on results shown, rubidium hydride-doped system was found to be the fastest system at 180 °C. There is no evidence or clear explanation as to why this occurs.

Parameter	KH	RbH	CsH
Abs P_m	32.5	30.2	26.0
Des P_m	25.4	21.5	19.5
Abs ΔH (kJ/mol)	34.3	39.7	40.98
Des ΔH (kJ/mol)	40.9	43.0	46.10
E_a Abs (kJ/mol)	83.9	81.7	105.9
E_a Des (kJ/mol)	89.3	86.9	110.5
E_a Des (kJ/mol)$_{Kiss}$	87.0	89.4	109.1
T_{90} Abs (min)	183	107.5	301
T_{90} Des (min)	297	207	455

Table 7.1 Summary of absorption and desorption parameters for thermodynamics and kinetics results at constant temperature at 180°C.

7.5 Summary

It has been demonstrated that the rubidium-doped system is still by far the best dopant for the lithium amide/magnesium hydride system. Based on the absorption and desorption studies, that system is approximately 1.7 times faster than the KH-doped system and about 2.8 times faster than CsH-doped system. However, that system has produced evidence that it still has some promise that it can operate at a temperature of 180 °C.

CHAPTER 8

CONCLUSION

8.1 Overall Conclusion

The main objective of this research study was focused on the thermodynamic and kinetic studies of the alkali metal dopants (*or destabilizing agents*) and their effects on the $2LiNH_2/MgH_2$ hydrogen storage system. To expand the scientific knowledge in the existing research literature along with broadening the understanding of these theoretical occurrences in the reactions, additional experimental studies were conducted to validate findings of resulting data.

Based on the series of studies that were completed, the following conclusions from those findings can be stated:

- The enthalpy values in the temperature range of 150°C-180°C have remained consistent in the range of $30kJ/mol \leq H \leq 60kJ/mol$ for the alkali-metal doped systems. This indicates that all three systems are suitable materials for hydrogen storage according to various research studies.
    - The trend for enthalpy values for both absorption and desorption is: KH < RbH< CsH
- Cycling studies of each catalyzed system at constant temperature of 200°C have been conducted. Based on the results, the following has been concluded:

- Potassium-doped system had plateau pressures that remained consistent for absorption and desorption studies. The weight capacity however changed over the 100 cycling period.
- Rubidium-doped system created hysteresis over time. The weight percent has also decreased over time as well.
- Cesium hydride –doped system remained consistent in the plateau pressure. However, hydrogen capacity changed significantly each time it was cycled.

- Absorption kinetic studies were introduced in this current research study for the first time regarding experiments for all the alkali metal-doped systems at constant thermodynamic driving force. Desorption kinetic studies were also done under the same conditions.
  - Based on the values discussed in each chapter, absorption studies were faster than desorption studies.
  - Rubidium-doped system was shown to be the fastest system followed by potassium and cesium-doped system respectively. This is presented in **Table 7.1** at constant temperature 180 C.
- Kinetic modeling has been done for both absorption and desorption for the doped systems. The following has been found for the doped systems:
  - Shrinking core model (curve-fitting model)

        - All absorption studies followed reaction-controlled model in the first stages and then diffusion for the latter stages.
        - All desorption studies shows that diffusion model fit best for most of the reactions for each system at different temperatures.
    - Johnson-Mehl-Avarami model (model testing linearity)
        - For absorption studies, it showed that reaction-controlled and diffusion model has linear correlation in the beginning of the plots.
        - Diffusion fit best for desorption experimental studies at different temperatures.
    - Hancock and Sharp (shown diffusion for desorption kinetics)
        - All doped systems showed that diffusion was the rate-determining step according to the slope range of 0.5-0.6 discussed in the Hancock and Sharp paper.
- Activation energies for absorption studies were introduced for the first time for alkali-metal doped systems using the Arrhenius plots discussed throughout the dissertation. Desorption activation energies have also been determined and compared by Arrhenius plots and Kissinger plots.
    - Based on the Arrhenius plots for the absorption studies, RbH-doped system was shown to have the lowest activation energy,

followed by KH- and CsH-doped respectively. **Table 7.1** shows the values of the absorption studies activation energy values.

- For desorption studies, the Arrhenius plot values and Kissinger plot values have shown that the values are similar towards each other.

8.2 Suggestions for future Work

- RbH has been found to have a best effect on the $2LiNH_2/MgH_2$ system thermodynamically and kinetically so far. This knowledge can be applied to the ternary system $LiBH_4/LiNH_2/MgH_2$ as well as other hydrogen storage systems.
- Based on the literature, it has been stated that K and Rb metal has participated in the thermodynamics via temperature desorption and change in structure. This can be investigated by using scanning electron microscopy, x-ray diffraction, and neutron diffraction.
- In a previous study, a dual catalyst of Rb and K has been introduced on the $2LiNH_2/MgH_2$ system and has been studied extensively. This concept can be applied for combining Rb-Cs and/or K-Cs dual catalysts on the $2LiNH_2/MgH_2$ systems.The thermodynamic and kinetic properties and compare the two systems can be compared.

REFERENCES

1. Rand, D.A.J and Dell, R.M. Hydrogen Energy: Challenges and prospects; Royal Society of Chemistry: Cambridge, UK 2008

2. Hoffman, P. Tomorrow's Energy: Hydrogen, Fuel Cells, and Prospects for a Cleaner Planet; MIT Press: Cambridge, Massachusetts 2012

3. US Department of Energy. http://www1.eere.energy.gov/hydrogenandfuelcells/fuelcells/fc_types.html (Accessed April 2014)

4. Wang, Q.; Chen, Y.; Wu, C.; Tao, M.J. *J. Phys. Chem C* **2008,** *112*, 18264.

5. Simpson, A. P and Lutz, A.E. *Int. J. Hydrog. Energ.* **2007,** *32*, 4811.

6. Fujishima, A.; Zhang, X.; Tryk, D.A. *Int. J. Hydrog. Energ.* **2007,** *32*, 2664-2672.

7. Bockris, J.O'M.; Dandafani, B.; Cocke, D.; Ghoroghican, J. *Int. J. Hydrog. Energ.* **1985,** *10*, 179.

8. Aguilar, L.; Zha, S.; Cheng, Z.; Winnick, J.; Liu, M. *J. Power. Sources* **2004,** *135*, 2004.

9. Ibikunle, A.; Goudy, A.J.; Yang, H.; *J. Alloys Compd.* **2011,** *509*, 7143.

10. Chu, H.; Wu, G.; Xiong, Z.; Guo, J.; He, T.; Chen, P. *Chem. Mat.* **2010,** *22*, 6021.

11. Chu,H; Wu,G; Xiong, Z.; Guo, J.; He, T.; Chen, *J. Phys. Chem. C* **2011,** *115*, 18035.

12. Mao,J.; Guo,Z.; Nevirkovets, I.P.; Liu, H.K.; Dou, S.K. *J. Phys. Chem. C* **2012,** *116*, 1596.

13. Vajo, J.J. and Skeith, S.L.; *J. Phys. Chem B Lett.* **2005,** *109*, 3719.

14. Lu, J; Fang, Z.Z.; Sohn, H.Y. *J. Phys. Chem B* **2006,** *110*, 14236.

15. Grochala, W.; Edwards, P.P. *Chem. Rev* **2004,** *104*, 1283.

16. Varin, R.A. and Jang, M. *J. Alloys Compd.* **2011,** *509,* 7143.

17. Saha, D; Wei, Z.; Deng, S. *Sep Pur Technol.* **2009,** *64,* 280.

18. Kim, D.; Kim, J.; Jung, H. J.; Lee, T.B.; Choi, S.B.; Yoon, J.H.; Kim, J; Choi, S-H. *Cat. Today* **2007,** *120,* 317.

19. Luzan, S.M; Jung, H.; Chun, H.; Talyzin, A.V. *Int. J. Hydrogen Energ.* **2009,** *34,* 9754.

20. Darkrim, F.L.; Malbrunot, P.; Tartaglia, G.P. *Int. J. Hydorgen Energ.* **2002,** *27,* 193.

21. Wu, H; Wexler, D.; Liu, H. *Int J. Hydrogen Energ.* **2012,** *37,* 5686.

22. Gayathri, V.; Devi, N.R.; Geetha, R. *Int J. Hydrogen Energ.* **2010,** *35,* 1313.

23. Wu, H; Wexler, D.; Ranjbartoreh, A.R.; Liu, H; Wang, G. *Int. J. Hydrogen Energ.* **2010,** *35,* 6345.

24. Rosi, N.L.; Eckhert, J.; Eddaoudi, M.; Vodak, D.T.; Kim, J.; O'Keefe, M.; Yaghi, O.M. *Science* 2003, *300,* 1127.

25. Walker, G. Solid-state hydrogen storage; Woodhead Publishing Limited: Cambridge, England, UK 2008.

26. Koh, J.T.; Goudy, A.J.; Huang, P.; and Zhou, G. *J. Less-Comm Met.* **1989,** *153,* 89-100.

27. Dehouche, Z.; Djaozandry, R.; Huot, J.; Boily, S.; Goyette, J.; Bose, T.K.; and Schulz, R. *J Alloy Compd* **2000,** *305,* 264.

28. Durojaiye, T.; Ibikunle, A.; and Goudy, A.J. *Int J Hydrog Energ* **2010,** *35,* 10329-10333.

29. Newhouse, R.; Stavila, V.; Hwang, S.J.; Klenbanoff, L.E.; Zhang, J.Z. *J. Phys Chem C* **2010,** *114,* 5224-5232.

30. Rassat, SD; Aardahl, CL.; Aubrey, T.; Smith, RS. *Energ. Fuels* **2010,** 2596.

31. Hwang, H.T.; Al-Kukhun, A.; and Varma, A. *Ind. Eng. Chem. Res* **2010,***49,* 10994-11000

32. Dumar, S. and Ozkar, S. *Int. J. Hydrog. Energ.***2013,** *38,* 180.

33. Chen, P.; Xiong, Z.; Luo, J.; Lin, J.; Tan, K.L. *Nature* **2002,** *420,* 302.

34. Liang, C.; Liu, Y.; Gao, M.; Pan,H. *J. Mater. Chem. A* **2013,** *1,* 5031.

35. Lamb, J.; Chandra, G.; Chien, W.M.; Phanon, D.; Penin, N.; Cerny, R.; Yvon, K. *J. Phys. Chem C* **2011,** *115,* 14386 .

36. Aguey-Zinsou, K.F.; Yao, J.; Guo, Z.X. *J. Phys. Chem B* **2007,** *111,* 12531.

37. Cao,H.; Zhang, Y.; Wang, J.; Xiong, Z.; Wu, G.; Chen,P. *Prog. Nat. Sci.: Mat. Int.* **2012,** *22,* 550.

38. Xiong, Z.; Wu, G.; Chen, P. *Adv. Mat.* **2004,** *16,* 1522.

39. Markmaitree, T.; Osborn, W.; Shaw, L.L. *Int. J. Hydrog. Energ.* **2008,** *33,* 3915.

40. Chen, P.; Xiong, Z.; Luo, J.; Lin, J.; Tan, K.L. *J. Phys Chem B* **2003,** *107,* 10967.

41. Durojaiye, T.; Hayes, J.; and Goudy, A. *J.Phys. Chem. C* **2013,** *117,*6554

42. Durojaiye, T. and Goudy, A.J. *Int. J. Hydrogen Energ.* **2012,** *37,* 3298

43. Luo, W.; Stavila, V.; Klebanoff, L. *Int. J. Hydrogen Energ.* **2012,** *37,* 6646

44. Jacobs, H.; Birkenbeul, J.; and Kockelkorn, J. *J. Less-Comm Met.* **1984,** *95,* 205-214

45. Hirscher, M.; Panella, B.; Schmitz, B.; *Micro Meso Mat.* **2010,** *129,* 335

46. http://pubs.rsc.org/en/content/articlelanding/2009/cs/b800312m/unauth#!divAbstract

47. Li, C.; Liu, Y.; Gu, Y.; Gao, M.; Pan, H. *Chem Asian. J.* **2013,***8,* 2136.

48. Li, C.; Liu, Y.; Ma, R.; Zhang, X.; Li, Y.; Gao, M.; Pan, H. *Appld. Mat. Interfaces* **2014,** *6,* 17024.

49. Li, C.; Liu, Y.; Yang, Y.; Gao, M.; Pan, H. *J. Mater. Chem A* **2014,** *2,* 7345.

50. Elansari, L.; Antoine, L.; Janot, R. ; Gachon, J.C.; Kuntz, J.J..; Guerard, D. *J. Alloys Compd.* **2001,** *329,* L5-L8.

51. Sabitu, S.T. and Goudy, A.J. *Metals* **2012,** *2,* 219.

52. Pendersen, A.S.; Kjoller, J.; Larsen, B.; Vigeholm, B.; and Jensen, J.A. *Int. J. Hydrog. Energ.* **1983,** *9,*799.

53. Yang, H.; Ojo, A.; Ogaro, P.; and Goudy, A.J. *J. Phys. Chem C* **2009,** *113,*14512.

54. Zidan, R.A. Takara, S.; Hee, A.G.; Jensen, C.M.; *J. Alloys Compd.* **1999,** *285,* 119-122.

55. Chalk, S.G. and Miller, J.F. *Power Sources* **2006,** *159,* 73.

56. Zhang, W.; Ciamto, J.; Goudy, A.J. *J. Alloys Compd* **1993,** *201,* 175.

57. Brouwers, H.J.H and vanEijk, R.J. *Concrete Sci Eng* **2002,** *4,* 106.

58. Engel, T. and Reid, P. *Thermodynamics, Statistical Thermodynamics, and Kinetics*, 2nd ed.; Prentice Hall: New Jersey, 2010.

59. Hsu, W-L.; Lin, M-J.; and Hsu, J-P. *Int J Bio. Eng.* **2009,** *2,* 205.

60. Hancock, J.D. and Sharp, J.H. *J. Am. Cerem. Soc.* **1972,** *55,* 74.

61. Kumar, S. and Krishnamurthy, N. *Int. J. Hydrog. Energ.* **2012,** *37,* 13429.

62. Rijissenbeek J, Gao Y, Hanson J, Huang Q, Jones C, Toby B. *J Alloys Compd* **2008,** *454,* 233.

63. Jacobs H, Birkenbeul J, Schmitz D. *J Less Comm Met* **1982**, *85,* 79.

64. Luo, W. *J. Alloys Compd* **2004,** *381,*284.

65. General Motors Hydrogen-Fuel Vehicle - http://www.cnet.com/news/with-toyota-in-its-rear-view-mirror-gm-talks-fuel-cell-car-technology/ (Accessed February 10, 2015)

66. Toyota Hydrogen-Fuel Vehicle- http://www.usatoday.com/story/money/cars/2015/01/25/toyota-fuel-cell-mirai/22308863/ (Accessed February 10, 2015)

67. Honda Hydrogen-Fuel Vehicle - http://www.nytimes.com/2015/01/14/business/honda-introduces-vehicle-powered-by-hydrogen.html?_r=0 (Accessed February 10, 2015)

68. Ford Hydrogen-Fuel Vehicle - http://www.popularmechanics.com/cars/a2017/4220281/ (Accessed February 10, 2015)

69. Lutz, A.E.; Bradshaw, R.W.; Keller, J.O.; Witmer, D.E. *Int. J. Hydrog. Energ.* **2003,** *28,* 159.

70. Carmo, M.; Fritz, D.L.; Mergel, J.; Stolten, D. *Int. J. Hydrog. Energ.* **2013,** *38,* 4901.

71. Zyzdiak, N.; Huber, C.; Bruns, M.; Barner-Kowollik, C. *Macromolec.* **2011,** *44,* 3374.

72. Zhang, S.; Liu, W.K.; Ruoff, R.S. *Nano Lett.* **2004,***4,*293.

73. Murugan, E. and Gopi, V. *J. Phys Chem C* **2011,** *115,*19897.

74. Bogdanovic, B. and Schwickardi, M. *J. Alloy Compd* **1997,** *253-254,* 1-9.

75. Dathar, G.K.P and Mainardi, D.S. *J. Phys Chem C* **2010,** *114,* 8026.

76. Zhao, J.; Wang, A.; Green, M.A. *Appl. Phys. Chem Lett.* **1998,** *71,* 1991.

77. Durojaiye, T.; Hayes, J., Goudy, A. *Int J. Hydrog. Energ* **2014,** In press.

78. Hayes, J.; Durojaiye, T.; Goudy, A. *Int J. Hydrog. Energ* **2014,** In press.

79. Kissinger, H.E. *Anal Chem* **1957,** *29.* 1702.

80. Griffiths, P.R. and Haseth, J.A. Fourier Transfer Infrared Spectroscopy. John Wiley &Sons 2007.

81. Hayes, J. and Goudy, A. *Int. J. Hydrog. Energ.* **2015,** Under Review.

82. Symes, D.; Maillard, J.G.; Courtney, J.; Watton, J.; Meadowcroft, A.; Chandan, A.S.; Gurley, L.; Priestly, R.; Serdaroglu, G. *Int J. Hydrog. Energ* **2014,** *39,* 7460.

83. Taxak, M. and Krishnamurthy, N. *J. Alloy Compd* **2015,** *623,* 121.

84. Anand, N.S.; Pati, S.; Jat, R.A.; Parida, S.C.; Mukerjee, S.K. *Int J. Hydrog. Energ* **2015,** *40,* 444.

85. Chen, Z.I.; Si, T.Z.; and Zhang, Q.A. *J. Alloy Compd* **2015,** *621,* 42.

86. Zhang, X.; Liu, Y.; Wang, K.; Go, M.; Pan, H. *Nano Res.* **2014,** In press.

87. Yao, Y.; Yong, X.; Tse, J.S.; Greschner, M.J. *J. Phys Chem C* **2014,** In press.

88. Tokoyoda, K.; Ichikawa, T.; Miyaoka, H. *Int J. Hydrog. Energ* **2014,** In press.

89. David, W.F.; Makepeace, J.W.; Callear, S.K.; Hunter, H.M.A. Taylor, J.D.; Wood, T.J.; Jones, M.O. *J. Am. Chem. Soc.* **2014,** *136,* 1404.

90. Kim, T. *Int. J. Hydrog. Energ* **2011,** *36,* 1404.

91. Li, C.; Liu, Y.; Pang, Y.; Gu, Y.; Gao, M.; and Pan, H. *Dalton Trans.* **2014,** *43,* 2369.

92. Andreasen, A.; Vegge, T.; and Pendersen, A.S. *J. Phys. Chem B* **2005,** *109,* 3340.

93. Tang, W.S.; Chotard, J.N.; Raybaud, P.; and Janot, R. *J. Phys Chem C* **2014,** *118,* 3409.

94. Andrew Goudy, "Hydrogen Solubility in Rare Earth Intermetallic Compounds: A Dissertation", University of Pittsburg, 1976

95. Tolu Durojaiye, "Thermodynamics and Kinetics Enhancement of $LiNH_2$-MgH_2 Systems using Alkali Metal Hydride Dopants for Hydrogen Storage: A Dissertation, Delaware State University, Spring 2013

96. Adeola Ibikunle, " Destabilized Borohydride as Potential Hydrogen Storage Materials: A Dissertation, Delaware State University, Fall 2012

97. Sakintuna, B .; Lamari-Darkrim, F.; Hirscher, M. *Int. J. Hydrog. Energ.* **2007,** *32,*1121.

98. Crosby, K. and Shaw, L.L. *Int. J. Hydrog. Energ.* **2010,** *35,* 7519.

99. Inomata, A.; Aoki, H.; Miura, T. *Int. J. Hydrog. Energ.* **1992,** *17,* 139.

100. Wang, X.-L. and Suda, S. *Int. J. Hydrog. Energ.* **1992,** *17,* 139.

101. Luo, W. and Gross, K.J. *J. Alloy Compd.* **2004,** *385,* 224.

102. Chou, K-C. and Xu, K. *Intermetallics* **2007,** *15,* 767.

103. Mellouli, S.; Dhao,H.; Askri, F.; Jemni, A.; Nasrallah, S.B. *Int. J. Hydrog. Energ.* **2009,** *34,* 9393.

104. Nakamori, Y.; Kitahara, G.; Ninomiya, A.; Aoki, M.; Noritake, T.; Towata, S.; Orimo, S.0. *Mater. Trans.* **2005,** *46,* 2093.

105. Leng, H.Y.; Ichikawa, T.; Hino, S.; Hanada, N.; Isobe, S.; Fujii, H. *J. Phys. Chem B* **2004,** *108,* 8763.

106. Srinivasan, S.S. and Sharma, P.C. *Catalysis* **2012,** *2,* 434.

107. Yan, M.; Sun, F.; Liu, X.; Ye, J.; Wang, S.; Jiang, L. *J. Alloy Compd.* **2015,** *628,* 63.

108. Davies, R.A.; Hewett, D.R.; Anderson, P.A. *Adv. Nat. Sci.: Nanosci. Nanotechnol.* **2015,** *6,* 1.

109. Bhuiya, M.M.H.; Kumar, A.; Kim, K.J.; *Int. J. Hydrog. Energ.* **2015,** *40,* 2231.

110. Charlas, B.; Kneib, F.; Gillia, O.; Imbault, D.; Doremus, P. *Int. J. Hydrog. Energ.* **2015,** *40,* 2231.

111. Sakintuna, B.; Lamari-Darkrim, F.; Hirscher, M. *Int. J. Hydrog. Energ.* **2007,** *32,* 1121.

112. Bhattacharyya, R. and Mohan, S. *Renew. Sus. Energ. Rev.* **2015,** *41,*872.

113. Zuttel, A. *Mater. Today* **2003,** *6,* 24.

114. Zhou, L. *Renew. Sus. Energ. Rev.* **2005,** *9,* 395

115. Hirscher, M. *Handbook of Hydrogen Storage: New Materials for Future Energy Storage.* **2010,** Wiley Publishing.

116. Chen, P. and Zhu, M. *Mater. Today,* **2008,** *11,* 36.

117. Satyapal, S.; Petrovic, J.; Read, C.; Thomas, G.; Ordaz, G. *Cat. Today* **2007,** *120,* 246.

118. Momirlan, M. and Veziroglu, T.N. *Renew. Sus. Energ. Rev.* **2002,** *6,* 141.

119. Momirlan, M. and Veziroglu, T.N. *Int. J. Hydrog. Energ.* **2005,** *30,* 795.

120. Dunn, S. *Int. J. Hydrog. Energ.* **2002,** *27,* 235.

121. Zeaiter, A.; Chapelle, D.; Nardin, P. *J. Alloy Compd* **2015,** In press.

122. Zhang, B. and Wu, Y. *Int. J. Hydrog. Energ.* **2014,** *39,* 13603.

123. Leng, H.; Pan, Y.; Li, Q.; Chou, K. *Int. J. Hydrog. Energ.* **2014,** *39,* 13622.

124. McWhorter, S.; Read, C.; Ordaz, G.; Stetson, N. *Current Opinion in Solid State and Material Science* **2011,** *15,* 29-38.

125. Hu, J. and Fitchner, M. *Chem Mater.* **2009,** *21,* 3485-3490.

Jalaal Aqil Hayes

Ph.D. Candidate

United States Department of Energy Doctoral Fellow

Permanent Address
1635 West Diamond Street
Philadelphia, PA 19121

Phone: 215-858-2270
Email: jalaal.hayes@gmail.com

Education

Delaware State University, Dover, DE

- Ph.D. in Applied Chemistry

Dissertation entitled, "Thermodynamics and Kinetic Properties of Alkali Metal-doped $2LiNH_2/MgH_2$ Hydrogen Storage Systems"
Expected graduation – August 2015,

Lincoln University of Pennsylvania, Lincoln University, PA

- B.S. in General Science and History majors and Mathematics minor

May 2011, Cum Laude

Northeast Preparatory School, Philadelphia, PA

- High School Diploma, Finished in 2 years

August 2008, GPA: 4.0

Computer Programming Skills and Software Experience

Java, C++, HTML Java, Javascript, Proficient in LabView, Pyris Software, Microsoft Office Suite, and Statsoft Software

Statistical Inference and Methodology

Statistical Methods Used: Descriptive Statistics, t Test, Chi Square Test of Independence, ANOVA, Multiple Linear Regression, Times Series Analysis

Knowledge of Other Statistical Methods: Chi Goodness of Fit Test, Logistics Regression, Discriminant Functional Analysis, Cluster Analysis, MANOVA, Repeated Measures ANOVA, Monte Carlo Simulation.

Laboratory Research Instrumentation and Associated Tools

- X-Ray Diffractometer

- Fourier Transform Infrared Spectroscopy
- PCI machine from Advanced Materials
- Thermogravimetric/ Differential Analyzer
- Gas Chromatogr
- Liquid Chromatogram
- Mass Spectrometer
- Fluorescence Spectroscopy

Research Experience

Doctoral Research: Delaware State University's Center for Hydrogen Storage Research, Department of Chemistry, Delaware State University, 2011 - Present
(Research advisor: Dr. Andrew Goudy)

- Currently working on research regarding enhancing chemisorption properties of intermetallic systems of hydrogen storage through kinetics and thermodynamic forces.
- Analysis of thermodynamic and kinetic results for lightweight storage materials specifically metal amide systems using X-ray diffraction, Fourier Transform Infrared Spectroscopy, Seivert's apparatus, Thermogravimetric analysis, and many more.
- Discovered novel catalytic additives that would improve on hydrogen storage system for on-board storage applications Rubidium-hydride doped system has been patented as the most effective system for the lithium amide-magnesium hydride system

*Summer Undergraduate Research Intern***:** Howard University NASA URC Beltsville Center for Climate Observation Systems **,** Department of Physics, Howard University June 2011- August 2011 (research advisor: Dr. Everett Joseph, Principal Investigator)

- Worked on research dealing with chemical composition of aerosols and measuring air quality for NASA's DISCOVER-AQ campaign and Maryland Department for Environment.
- Read and analyzed weather patterns and seasonal variations for operations in capturing ozone concentration.
- Manage the inventory of supplies for each environmental agency in the state of Maryland.
-

Undergraduate Research Assistant: Lincoln University Great Center for Health Disparities, Department of Chemistry, Lincoln University of Pennsylvania Spring 2011 (Principal Investigator: Dr. Derrick Swinton)

- Worked on Liquid Chromatography/Mass Spectroscopy to determine the levels of nicotine and its major metabolites in the urine of African Americans participating in smoking cessation clinics.

- Learned instrumentation such as centrifugation and fluorescence spectroscopy to separate and analyze urine samples collected by subjects respectively.

Undergraduate Research Assistant: Department of History and Political Science, Lincoln University of Pennsylvania Fall 2008 – Spring 2011

- Assist the chairman of the department with gathering research materials and compiling data for reports and articles.

Other Research Interests

- Conducting research in environmental science attributes.
  I am interested in collecting and analyzing the concentration of aerosols, particular matter, and other contaminants in the air. After collection of such data, the data will be analyzed and innovations will arise to limit the productions of the aerosols. Another interest for environmental science attributes will understanding policies and procedures as it relates to research and development.
- Working and analyzing solid-state hydrogen storage materials.
  For the four years in my doctoral study, I have studied lithium amide-magnesium hydride hydrogen storage materials. Although these materials show promise, discovering materials that are cost-feasible and can reach the goals specified by Department of Energy. I have shown to use the necessary instrumentation to study such materials and am willing to learn more throughout my career.
- Analyzing and characterizing semiconductor materials for photovoltaic devices and applications
  Solar energy has been of great interest other than hydrogen storage. Photovoltaic devices are a great application that I would like to explore in research and development. According to various studies, photovoltaic devices are shown to evolve and help the energy crisis that is of great interest to me. I specifically would like to study more materials or improve the current materials to increase the efficiency of the materials absorbing the sun or any photons that are in the area.
- Research and analyze of alternative energy sources and their chemical properties.
  Based on the descriptions of hydrogen storage and solar energy, I am interested in learning the world of alternative energy. The specific interests in alternative energy are geothermal energy and biodiesel fuel. The creation of building geothermal wells and limiting the pollution of the wells will show alternative ways to produce direct and the interest of creating clean biodiesel fuel for automotive applications and other mobile applications will be of promising research as well.

- Health-related research such as cancer or revolutionary medical discoveries
  Ebola, HIV/AIDS, and other infectious diseases have shown to be very detrimental to the health of the human race. To treat these diseases, there have been numerous vaccines produced in the world so far. However, there are still opportunities that can design drugs or even code genetic information in the body to make the individual life better and effective to fight over the diseases in the future. I would like to take part in those interests.

Patent, Presentations and Refereed Publications

Patent

Andrew Goudy, Tolulope Durojaiye, and Jalaal Hayes. A Rubidium Hydride Catalyzed Lithium Amide/Magnesium Hydride System for Hydrogen Storage Applications. United States Patent Publication Number US2014/0326920 – *Published November 6, 2014*.

Presentations

Presenter, *Effects of KH and RbH on the $2LiNH_2/MgH_2$ Hydrogen Storage System,* 2013 Graduate Symposium, Delaware State University, Dover, DE- April 24, 2013

Invited as a Poster Presenter, *Effects of Alkali Metal Hydrides on 2LiNH2/MgH2 System***,** Gordon Research Conferences, Barga, Italy - Summer 2013

Invited as a Presenter, *Effects of Alkali Metal Hydrides on $2LiNH_2/MgH_2$ System,* Gordon Research Seminar, Barga, Italy - Summer 2013

Invited as a Poster Presenter, *Hydriding and Dehydriding Kinetics of RbH- Doped $2LiNH_2/MgH_2$ Hydrogen Storage System***,** Metal Hydrogen Conference 2014, University of Salford, Manchester, UK - Summer 2014

Invited as a Poster Presenter, *Comparative Analysis of Alkali Hydride Metal Dopants on $2LiNH_2$-MgH_2 Hydrogen Storage System***,** Gordon Research Conferences 2015, Stonehill College, Easton, MA - Summer 2015

Refereed Publications

Jalaal Hayes and Andrew Goudy, *"Thermodynamic, Kinetic and Modeling Studies of KH, RbH, and CsH-doped $2LiNH_2/MgH_2$ Hydrogen Storage System"* Under Review

Tolulope Durojaiye, Jalaal Hayes, and Andrew Goudy, *International Journal of Hydrogen Energy, "Potassium, Rubidium and Cesium Hydrides as Dehydrogenation Catalysts for the Lithium Amide/Magnesium Hydride System.* February 9, 2015;

Pages 2266-2273.

Jalaal Hayes, Tolulope Durojaiye, and Andrew Goudy, *Journal of Alloys and Compound, "Hydriding and Dehydring Kinetics of RbH-Doped $2LiNH_2/MgH_2$ Hydrogen Storage System"* December 23, 2014, In press

Tolulope Durojaiye, Jalaal Hayes, and Andrew Goudy. *Journal of Physical Chemistry C, "Rubidium Hydride: An Exceptional Dehydrogenation Catalyst for the Lithium Amide/Magnesium Hydride System".* March 11, 2013; Pages 6554-6560.

University Involvements

Delaware State University

Graduate Advisor, The God Brothers, 2015
Sergeant-at-Arms, Gamma Sigma Epsilon Chemistry Honors Society 2013 - 2015
Member, Delaware State University Collegiate Entrepreneurs Organization 2013 -2014
Member, Future Leaders in Progress, 2013-2014
Member, American Chemical Society Club at Delaware State University 2013 – Present

Lincoln University of Pennsylvania

Member, Chemistry Club, Lincoln University of Pennsylvania 2008- 2011
Member, Horace Mann Bond Honors Program, Lincoln University of Pennsylvania 2008-2011
Member, History Club at Lincoln University of Pennsylvania 2009-2011
Member, International Students Association at Lincoln University of Pennsylvania 2009-2010
Member, NAACP Lincoln University Chapter 2010-2011

Professional Memberships

American Chemical Society (ACS) 2012-Present
Gamma Sigma Epsilon Chemistry Honors Society 2013-Present

Honors

Horace Mann Bond Honors Program at Lincoln University
Phi Alpha Theta History Honors Society at Lincoln University
Gamma Sigma Epsilon Chemistry Honors Society

References

Furnished upon Request